LAPPEENRANTA
UNIVERSITY OF TECHNOLOGY

MASTER'S THESIS

Mikko Linnala 2008

LAPPEENRANTA UNIVERSITY OF TECHNOLOGY
Faculty of Technology
Department of Chemical Technology

Mikko Linnala

Characterisation of pigment particles by scanning electron microscope and image analysis programs

Examiners: Professor Isko Kajanto
M.Sc. (tech.) Sami Turunen

Supervisors: M.Sc. Anna-Liisa Mäkelä
Professor Isko Kajanto

ABSTRACT

Lappeenranta University of Technology
Faculty of Technology
Department of Chemical Technology

Mikko Linnala

Characterisation of pigment particles by scanning electron microscope and image analysis programs

Master's thesis 2008

106 pages, 112 figures, 17 tables and 4 appendices.

Examiners: Professor Isko Kajanto
M.Sc.(tech.) Sami Turunen

Keywords: particle size, particle shape, particle analysis, sample preparation, scanning electron microscope, image analysis

Coating and filler pigments have strong influence to the properties of the paper. Filler content can be even over 30 % and pigment content in coating is about 85-95 weight percent. The physical and chemical properties of the pigments are different and the knowledge of these properties is important for optimising of optical and printing properties of the paper. The size and shape of pigment particles can be measured by different analysers which can be based on sedimentation, laser diffraction, changes in electric field etc.

In this master's thesis was researched particle properties especially by scanning electron microscope (SEM) and image analysis programs. Research included nine pigments with different particle size and shape. Pigments were analysed by two image analysis programs (INCA Feature and Poikki), Coulter LS230 (laser diffraction) and SediGraph 5100 (sedimentation). The results were compared to perceive the effect of particle shape to the performance of the analysers. Only image analysis programs gave parameters of the particle shape. One part of research was also the sample preparation for SEM. Individual particles should be separated and distinct in ideal sample.

Analysing methods gave different results but results from image analysis programs corresponded even to sedimentation or to laser diffraction depending on the particle shape. Detailed analysis of the particle shape required high magnification in SEM, but measured parameters described very well the shape of the particles. Large particles (ecd~1 µm) could be used also in 3D-modelling which enabled the measurement of the thickness of the particles. Scanning electron microscope and image analysis programs were effective and multifunctional tools for particle analyses. Development and experience will devise the usability of analysing method in routine use.

TIIVISTELMÄ

Lappeenrannan teknillinen yliopisto
Teknillinen tiedekunta
Kemiantekniikan osasto

Mikko Linnala

Pigmenttipartikkelien luokittelu elektronimikroskoopin ja kuva-analyysiohjelmien avulla

Diplomityö 2008

106 sivua, 112 kuvaa, 17 taulukkoa ja 4 liitettä.

Tarkastajat: Professori Isko Kajanto
DI, tutkija Sami Turunen

Hakusanat: partikkelikoko, partikkelimuoto, partikkelianalyysi, näytteenvalmistus, elektronimikroskooppi, kuva-analyysi

Päällystys- ja täyteainepigmenteillä on suuri merkitys paperin ominaisuuksiin. Paperin täyteainepitoisuus voi olla jopa yli 30 % ja päällystyspastassa pigmenttien osuus on noin 85–95 painoprosenttia. Pigmenttien fysikaaliset ja kemialliset ominaisuudet poikkeavat pigmenttien välillä ja näiden ominaisuuksien tunteminen on tärkeää erityisesti paperin optisten ja painatusominaisuuksien optimoimiseksi. Pigmenttien partikkelikoon ja –muodon mittaamiseen on olemassa erilaisia mittalaitteita, joiden toiminta voi perustua muun muassa sedimentaatioon, laserdiffraktioon tai sähkökentän muutokseen.
Tässä diplomityössä partikkeliominaisuuksien tutkimiseen käytettiin pääasiassa elektronimikroskooppia ja kuva-analyysiohjelmia. Tutkimuksen kohteena oli yhdeksän pigmenttiä, joiden partikkelikoko ja –muoto vaihtelivat. Tutkittavat pigmentit analysoitiin kahdella kuva-analyysiohjelmalla (INCA Feature ja Poikki), Coulter LS230:lla (laserdiffraktio) ja SediGraph 5100:lla (sedimentaatio). Eri analyysimenetelmien tuloksia verrattiin keskenään, jotta partikkelimuodon vaikutus analysaattorien toimintaan havaittiin. Käytetyistä laitteista ainoastaan kuva-analyysiohjelmat ilmoittivat tuloksissaan myös partikkelimuotoon liittyviä tunnuslukuja. Kuva-analyysiohjelmien käyttöön liittyvänä tutkimuskohteena oli myös pigmenttinäytteen valmistus elektronimikroskoopilla kuvattavaan muotoon. Analysoitavassa näytteessä yksittäisten partikkelien tulee olla irrallaan ja selkeästi rajattavissa.
Eri mittausmenetelmät antoivat erilaisia tuloksia, mutta kuva-analyysien tulokset vastasivat joko sedimentaation tai laserdiffraktion tuloksia riippuen partikkelimuodosta. Partikkelimuodon yksityiskohtainen määritys vaati suurta suurennosta kuvattaessa, mutta mitatut tunnusluvut kuvasivat hyvin partikkelin muotoa. Isommista (ecd~1 µm) partikkeleista oli mahdollista tehdä myös 3D-malli, jolloin myös paksuusdimensio pystyttiin mittaamaan. Elektronimikroskooppi ja kuva-analyysiohjelmat olivat kaiken kaikkiaan tehokkaita ja monipuolisia välineitä partikkelianalyysien tekemiseen. Kehityksen ja kokemuksen kautta menetelmästä on mahdollista saada vieläkin toimivampi.

TABLE OF CONTENTS

ABBREVIATIONS:

A	area of the particle or absorbance
a	particle radius
B	structuring element
$\check{B}$	reflected structuring element
BE	backscattered electrons
BSE	backscattered electrons
C	circularity
CPM	convex perimeter
D_a	equivalent circular area diameter
D_p	equivalent circular perimeter diameter
d	thickness or diameter of the particle
d_I	the intermediate dimension of the particle
d_L	the longest dimension of the particle
d_l	length mean diameter
d_S	the shortest dimension of the particle
d_s	surface mean diameter
d_v	volume mean diameter
ECAD	equivalent circular area diameter
ECPD	equivalent circular perimeter diameter
EDS	energy dispersive X-ray spectroscopy
F	Feret's diameter
f	shape factor
F_{max}	maximum Feret's diameter
FL	fibre length
FW	fibre width
f	class frequency or grey level of the point in original image
f_T	respective point in thresholded image
g	gravitation constant
GFD	greatest Feret's diameter
HFD	horizontal Feret's diameter
HMD	horizontal Martin's diameter
I, I_0	intensity of incident light

I_s	intensity of scattered light
i	aperture current
K_B	Boltzmann's constant
k	number of statistical classes
k_0	wave vector of incident light
k_s	wave vector of scattered light
L	length or width of the particle
l	distance that the light travels in sample
LBC	the least bounding circle
LBRL	the least bounding rectangle length
LBRW	the least bounding rectangle width
LFD	the least Feret's diameter
Md	sample median
m	relative refractive index
m_1	refractive index of particle
m_2	refractive index of medium
n	statistical number of units
P	perimeter of the particle
p	Van de Hulst parameter
PSD	particle size distribution
R	aperture radius
r	distance from scattering centre
S	sphericity
s	standard deviation
s^2	variance
SE	secondary electrons
SEM	scanning electron microscope
SF	shape factor
T	temperature or threshold or mean deviation
t	time
U	amplitude of the voltage pulse
VFD	vertical Feret's diameter
VMD	vertical Martin's diameter
v	sedimentation velocity

W	width of the particle, statistical population
w	statistical unit
X	statistical property
x	realized observation of property X
$\bar{x}$	mean value of observations
$\bar{y}$	mean value of classified observations
y	middle point of class
α	statistical risk level or polarizability of the particle or absorption coefficient
η	viscosity of fluid or medium
θ	scattering angle
λ	wavelength of light
ρ	density
ρ_0	electrolyte resistivity
φ	azimuthal angle of scattering
ψ	angle between incident and scattered light

1 Introduction

Particle size and shape and their distributions are critical properties of coating and filler pigments. Particle size can be measured by many different methods, but particle shape is more difficult to measure. Particle analyses by a microscope enable a forming of images of the particles. The images can be analysed by image processing programs and particle size and shape can be measured with many parameters. Measuring of particle shape with other analysing methods is also evolved, but the methods are not comparable because they base on different techniques as measuring of particle size too.

The main targets of this master's thesis are development of particle shape analysing methods with scanning electron microscope and image analysis programs and comparison of results from different particle analysers.

Literary part

2 Pigments

The pigments constitute the largest part (80-95 weight percent) of coating and therefore their effects on the properties of coating are very significant. The physical and chemical properties of the pigment influence also on the application of the pigment. Therefore there are many different pigments for the different paper and process types. Table I shows the most important physical properties of coating pigments [Lehtinen[1]]. Pigments are also used as filler and filler content can vary between 0-35 percent depending of the grade of paper. The content of cheaper main pigments is usually about 20-35 % when the content of expensive speciality pigments is only 5-10 % [Krogerus[2]]. The term pigment is usually connected to the coating, but in this paper term pigment contains also the filler pigments.

Table I: Physical properties of the most common coating pigments [Lehtinen[1]].

Pigment	Chemical composition	Most particles [µm]	Particle shape	Density [kg/dm^3]	Refractive index	ISO-brightness
Clay	$Al_2O_3 \cdot 2SiO_2 \cdot 2H_2O$	0.3-5	hexagonal platy	2.58	1.56	80-90
Talc	$MgO \cdot 4SiO_2 \cdot H_2O$	0.3-5	platy	2.7	1.57	85-90
GCC[1]	$CaCO_3$, $MgCO_3$ (2-3 %)	0.7-2	cubic, prismatic, platy	2.7	1.56-1.65	87-97
PCC[2]	$CaCO_3$	0.1-1.0	variable, usually rodlike	2.7	1.59	96-99
Calcined clay	$Al_2O_3 \cdot 2SiO_2$	0.7 (median)	aggregated plates	2.69	1.56	93
Titanium dioxide						
-anatase	TiO_2	0.2-0.5	rodlike	3.9	2.55	98-99
-rutile	TiO_2	0.2-0.5	roundish	4.2	2.70	97-98
Gypsum	$CaSO_4 \cdot 2H_2O$	0.2-2	roundish	2.3	1.52	92-94
Plastic pigments	polystyrene most common					
-solid		0.1-0.5	spherical	1.05	1.59	93-94
-hollow		0.4-1.0	spherical	0.6-0.9	1.59	93-94
ATH[3]	$Al(OH)_3$	0.2-2	platy	2.42	1.57	98-100

1: Ground calcium carbonate, 2: Precipitated calcium carbonate, 3: Alumina trihydrate

The fillers and the coating pigments have similar mineralogical properties, but the particle size and shape and the optical properties differ. The coating pigments have usually smaller particle size and their color is whiter. The coverage and the optical properties as light-scattering are more significant in the coating and therefore the coating pigments are better classified and their prices are higher than the filler pigments [Krogerus[2]]. The use of filler pigments in the paper making has two reasons. As long as the fillers are cheaper than fibres the economy will improve. The mineral fillers also modify the technical properties of the paper; printing and optical properties improve but strength properties become weaker, what borders the upper limit of the filler content (about 35 %) [Velho[3]].

2.1 Main pigments

The main pigments are clay, talc and calcium carbonates. They are natural minerals and quite easy to product and use. They all are used as both coating pigment and filler in paper production. [Lehtinen[1]]

2.1.1 Clay

Clay is very old mineral in the paper industry; it is used as filler as early as 18th century and in the paper coating on 19th century. The most important clay deposits are in southwest England (primary deposit), in the middle Georgia in The United States (secondary deposit) and in Brazil (secondary deposit) [Drage and Tamms[4]]. Figure 1 shows a scanning electron microscope (SEM) image of Brazilian clay. The primary clay is formed in place where founded but the secondary clays are formed some where else and transported by water to present sites like the estuaries of rivers. Because of the difference in origin, the primary and the secondary clays have different properties like colour and particle size [Eklund and Lindström[5]]. All clays have very platy particle shape. The primary clays have aspect ratios (plate diameter : plate thickness) between 10 and 80. The secondary clays are little less platy and have the aspect ratios between 6 and 25. Clays can be grounded also to finer particle size. [Drage and Tamms[4]]

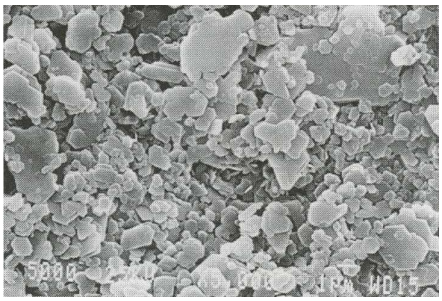

Figure 1. SEM image of the Brazilian clay particles [Drage and Tamms[4]].

2.1.2 Talc

Talc is used as filler in the European paper industry first time in the beginning of the 20th century. In the coating applications it is widely used since 1982 and nowadays it is produced all over the world. Talc has also platy particle shape; its aspect ratio is about 30, but it is however very variable on naturally talcs. Average particle size of talcs is usually little higher than the other platy pigments because it is used in the coating applications which desires good coverage or a matte effect [Likitalo[6]]. Figure 2 shows the SEM image of talc pigment. Talc has oleophilic character and therefore it is commonly used also to pitch control. The resin particles form agglomerates with talc and leave the paper machine with the paper. [Eklund and Lindström[5]]

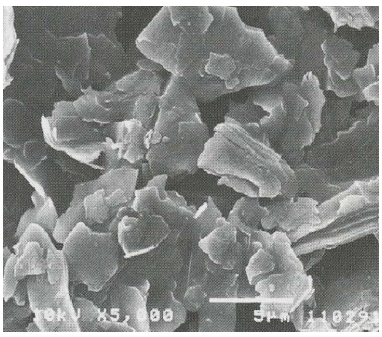

Figure 2. SEM image of talc particles [Likitalo[6]].

2.1.3 Ground calcium carbonate

Ground calcium carbonate (GCC) is used as filler and coating pigment in the Europe since 1960s. There are about 40 GCC production sites in the Europe and more than 90 around the world. Calcium carbonate occurs as calcite in rock forms chalk, limestone and marble [Huggenberger *et al.*[7]]. It has two remarkable crystalline polymorphs in the nature; calcite and aragonite. Valerite is third but unstable form and it has no importance in technology [Eklund and Lindström[5]]. The particle shape of ground calcium carbonate is rhombohedral. The particle size in the coating applications is mainly under 2 µm (40-98 %). [Huggenberger *et al.*[7]]

2.1.4 Precipitated calcium carbonate

Calcium carbonate has three different mineralogical forms which each has the different properties. Calcium carbonate for the paper industry can be also made by a controlled synthesis; it is called precipitated calcium carbonate (PCC) [Lehtinen[1]]. Precipitated calcium carbonate can be in calcite or in aragonite form and particle size and shape can also differ as figure 3 shows [Eklund and Lindström[5]]. Usually the particle size distribution of calcium carbonate is narrow. The needle-like particle shape of aragonite has been seen suitable for the coating [Imppola[8]]. Brightness of PCC is higher than talc's and kaolin's (96-99 ISO) [Lehtinen[1]].

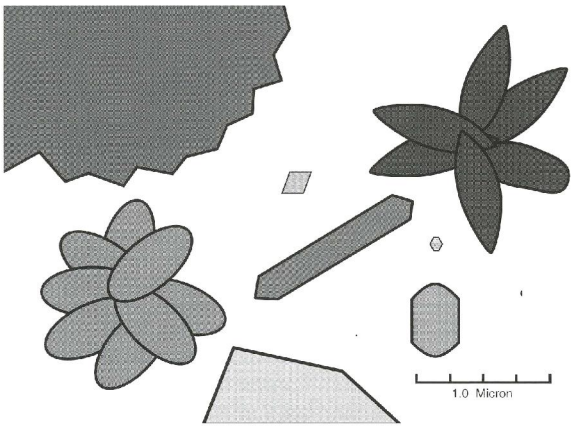

Figure 3. Different shapes and sizes of PCC particles [Imppola[8]].

2.2 Additional pigments

There are many additional pigments besides the main pigments. They are used in the special applications to improve the optical and printing properties of coated paper [Lehtinen[1]]. The price of synthetically produced pigments is usually higher than the common pigments and fibres. Therefore they are used also in smaller quantities [Eklund and Lindström[5]].

2.2.1 Calcined clay

Calcined clay is aggregated by thermally or chemically. The purpose of aggregation is to increase light-scattering coefficient and to form intra-particle pores. These properties improve brightness and opacity of the coating layer. Particle size and particle size distribution can be modified also by the aggregation process. Figure 4 shows the SEM image of calcined clay. [Drage and Tamms[4]]

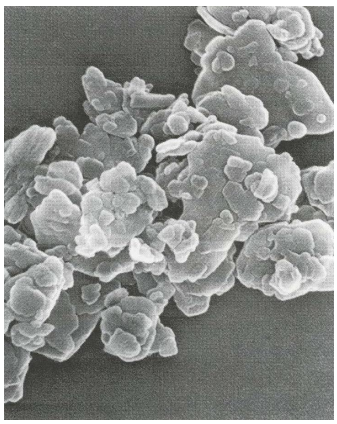

Figure 4. SEM image of calcined clay [Drage and Tamms[4]].

2.2.2 Titanium dioxide

Titanium dioxide is used as pigment since 1920s. TiO_2 is produced around the world but two-thirds of the capacity is located in North America and Western Europe. TiO_2 is very good pigment because it has high brightness (97-99 ISO), small particle size (mainly 0.2-0.5 µm) and very high refractive index (2.5-2.7). [Alatalo and Heikkilä[9]]

2.2.3 Other additional pigments

In addition of the pigments mentioned above there are few additional pigments which are used for some special purpose. For example gypsum, aluminium trihydrate, plastic pigments (figure 5), satin white and silicate belong in that group. These pigments are mainly used in board production because they have different cost/benefit ratio than the other pigments. [Sokka[10]]

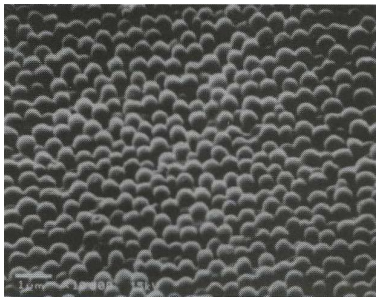

Figure 5. SEM image of plastic pigments [Brown and Kotoye[11]].

3 Physics of light scattering

Particle size analyses by laser diffraction are based on optics and understanding of basic physics is important. Particle size limits differ between the analysers and therefore few various theories are used.

3.1 Basics of optics

Light scattering is a natural phenomenon which can be perceived everywhere. Interaction between light and atoms, molecules, particles etc. has been studied scientifically already in 19th century. The characterising of scatterers bases on experimental data, but understanding the effects between the properties of scatterer (size, shape, refractive index) and the distribution of scattered light has not been so easy [Kerker[12]]. Figure 6 shows a geometrical model of light scattering where θ is scattering angle, k_0 and k_s are wave vectors, I_0 is the intensity of incident light and I_s the intensity of scattered light. Azimuthal angle φ is usually assumed to be 90° [Xu[13]].

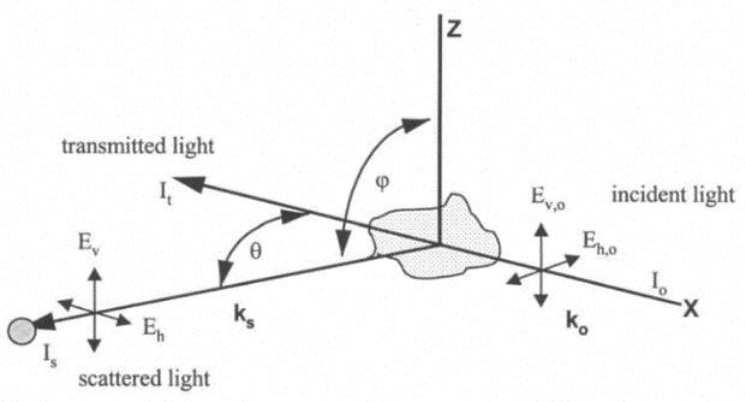

Figure 6. Geometrical model of light scattering [Xu[13]].

Theory of light scattering originates in Maxwell's equations of electromagnetism and Lorenz-Mie theory is great achievement of applying theories. Used theory of the light scattering depends on particle size, refractive indexes of the particle and the medium and observation angle. Rayleigh theory is adjusted when particles diameter d is very small compared to the wavelength of light λ ($d < \lambda/10$). When the particles diameter is about the same than the wavelength ($d \approx \lambda$), Lorenz-Mie theory is used. If the particles diameter is higher than the wavelength ($d > 4\lambda$) then Fraunhofer diffraction theory is used. [Brittain[14]]

Van de Hulst has created an equation which caters for both the particle size and the refractive indexes (equation 1). With the Van de Hulst parameter p use of different theories can be separated more effectively. [Brittain[14]]

$$p = \frac{2\pi d|m-1|}{\lambda} \tag{1}$$

where
	p	Van de Hulst parameter
	d	diameter of particle
	m	relative refractive index m_1/m_2
	m_1	refractive index of particle
	m_2	refractive index of medium
	λ	wavelength of light

Use of the different theories can be separated as follows:

$p < 0.3$	Rayleigh theory is valid
$p \approx 1$	Lorenz-Mie theory is valid
$p > 30$	Fraunhofer theory is valid

3.2 Rayleigh theory

As seen Rayleigh theory demands that the particle size is much smaller than the wavelength of incident light. In that case the whole particle behaves similarly in a homogeneous electric field. The incident light penetrates the particle due to the polarizability α of the particle. The penetration time is short compared to the period of incident light. Induced dipole moment is formed when electric charges of nonpolar particle are forced apart by subjecting the particle to electromagnetic wave. Like so, the polarized particle is created. The electric field and the dipole moment oscillate synchronously and the axis of the dipole moment is downright to the incident light as in figure 7 which also describes the intensity of scattering to different directions. [Xu[13]]

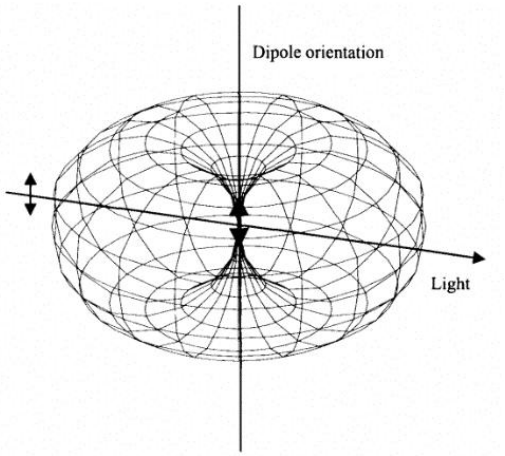

Figure 7. Three dimensional model of scattering from a dipole [Xu[13]].

The polarizability α is a tensor, but all three perpendicular components are the same in case of optically isotropic materials. Although α is a function of particle volume and particle shape and effects to the intensity of scattering light, all particles scatter light without defined structure. Rayleigh theory for the natural light can be defined as in equation 2. [Xu[13]]

$$I = \left(1+\cos^2\theta\right) k_0{}^4 |\alpha|^2 I_0 / 2r^2 \tag{2}$$

where
- I intensity of scattered light
- θ scattering angle
- k_0 wave vector of incident light
- α polarizability of the particle
- I_0 intensity of incident light
- r distance from scattering centre

The scattered light is linearly polarized if the particle is isotropic, optically inactive and the incident light is also linearly polarized. The intensity of scattered light is rotational symmetry as saw in figure 7 [Xu[13]]. For small particles the formula of Rayleigh theory can be represented also as in equation 3 [Kerker[12]].

$$I = \frac{16\pi^4 a^6}{r^2\lambda^4}\left(\frac{m^2-1}{m^2+2}\right)^2 \sin^2\psi \tag{3}$$

where
- I intensity of scattered light
- a radius of the particle
- r distance from scattering centre
- λ wavelength of incident light
- m relative refractive index
- ψ angle between incident and scattered light

3.3 Lorenz-Mie theory

Lorenz-Mie theory (or Mie theory) is more detailed and wider theory of the light scattering than Rayleigh theory. It can be used for spherical particles which can be small, large, transparent or opaque. According to Lorenz-Mie theory the intensity of scattering from the surface of the particle (primary scattering) can be predicted with the refractive indexes of the particle and the medium. Lorenz-Mie theory also caters the light refraction with the particle (secondary scattering) which is very important when particle diameter is below 50 µm. This is also mentioned in the standard for laser diffraction measurements (ISO 13320-1) [Kippax[15]]. According to Lorenz-Mie theory the scattering patterns of spheres are symmetric with axis of the incident light. Scattering minima and maxima are in different angles if the properties of the particles vary. Figure 8 shows the diffraction patterns of two particles with different sizes. [Xu[13]]

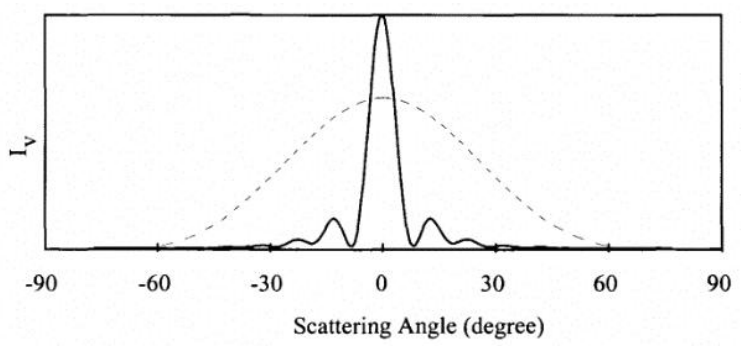

Figure 8. Scattering patterns of two particles of a different size [Xu[13]].

With large particle (solid line) the peak of intensity is stronger than with small particle (dashed line) and the intensity minimum is much closer to axis of the incident light. The intensity peaks are in the same locations in the both positive and negative angles because the symmetrical nature of scattering. Very illustrative way of displaying the intensity distribution is also a radial graph as in figure 9. The bold trace describes the intensity of scattered light in different angles. [Xu[13]]

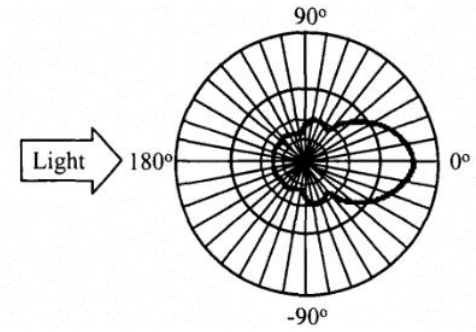

Figure 9. Intensity of scattered light presented in the radial graph form [Xu[13]].

3.4 Fraunhofer theory

Fraunhofer theory covers the light diffraction in the aperture which is described in Fresnel-Kirchoff diffraction integral [Brittain[14]]. Fresnel diffraction and Fraunhofer diffraction are quite similar. In Fresnel diffraction (near-field diffraction) distances from the point source and the screen to the obstacle forming the diffraction pattern are relatively short. In Fraunhofer diffraction (far-field diffraction) the distances are much longer and all lines from the source to the obstacle and forward to the screen can be considered parallel. Figure 10 shows contrast between Fresnel diffraction and Fraunhofer diffraction. In figure 10c the lens forms smaller image of the same diffraction pattern which would be formed on the screen extremely far without the lens [Young and Freedman[16]].

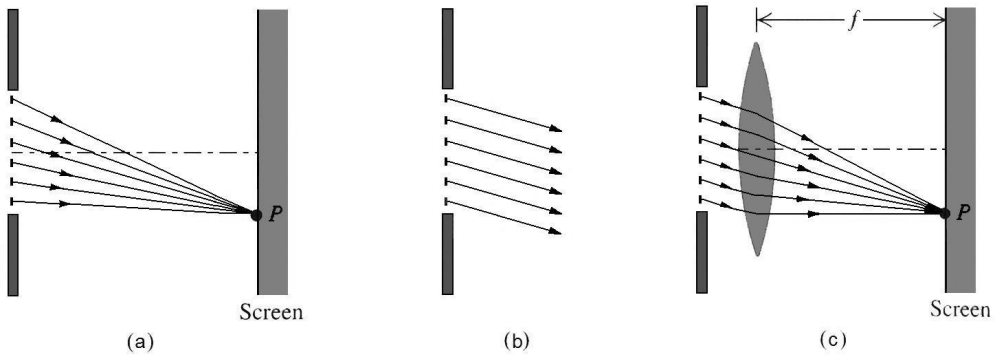

Figure 10. Principles of Fresnel diffraction (a) and Fraunhofer diffraction (b and c) [Young and Freedman[16] modified by Linnala].

Fraunhofer diffraction applies only if the diffraction is caused by the edges of aperture. Babinet's theorem enables to replace the aperture with the opaque object which has the same size and shape as the aperture because the diffraction patterns are similar this way. That enables to estimate the particle sizes if they are comparable with the size of aperture. [Brittain[14]]

Fraunhofer theory is used in the first diffraction analysers. It assumes that the measured particles are opaque and scatter light at narrow angles. Therefore it is applied only with the large particles and gives incorrect results with the fine particles. [Kippax[15]]

4 Particle size and shape

Particle size and shape are significant characteristics because they have influence to the light scattering. Theoretically optimal particle size of the spherical particle with high refractive index should be half of the light wavelength, 0.2-0.3 µm. Pigments have normally low refractive index and therefore the particle size is about 0.4-0.5 µm. The correlation between particle size and refractive index of the particle is defined also in equation 1. Particle size of the pigments is distributed and particle shape can differ also. [Krogerus[2]]

4.1 Particle size

The irregular shape of the particle presents a problem in particle size analyses. Sphere is the only particle shape which size can be described by a single number (diameter). An equivalent particle size is therefore used in representations of the particle sizes and the particle size distributions [Kippax[15]]. The equivalent particle size can be represented by few ways. Equivalent circular area diameter D_a (as ECAD in fig. 12) as in equation 4 is the most widely used in image analysis. The equivalent circle has the same projected area as the particle [Li *et al.*[17]].

$$D_a = 2\sqrt{\frac{A}{\pi}} \tag{4}$$

where D_a equivalent circular area diameter
A area of the particle

Another definition is equivalent circular perimeter diameter D_p as in equation 5. In this case the equivalent circle has the same perimeter as the silhouette of the particle. [Li *et al.*[17]]

$$D_p = \frac{P}{\pi} \tag{5}$$

where D_p equivalent circular perimeter diameter
P perimeter of the particle

The different methods of the particle size analyses measure different dimensions of the particle and the results are not comparable when irregular particles are measured. Figure 11 shows an example of different results of particle size measurement. [Kippax[15]]

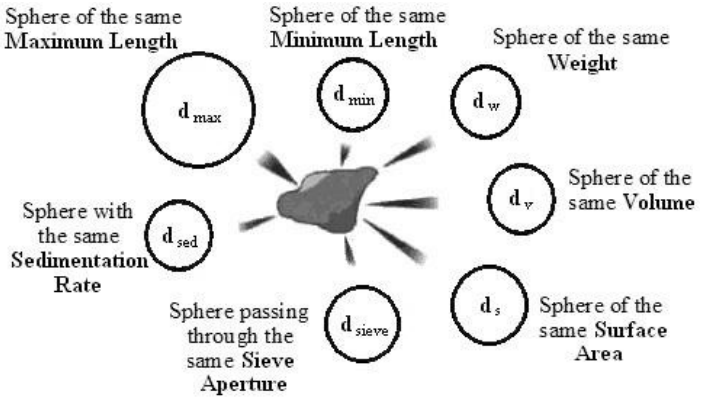

Figure 11. Equivalent particle sizes measured by different methods [Kippax[15] modified by Linnala].

The methods can be based on measuring of diameter, volume, surface area or surface area per unit volume, settling velocity or projected area. Because the particle shape is irregular, the results depend also on particle orientation during the measurement. Figure 12 shows common two-dimensional parameters used in the particle size and shape analyses. [Backhurst *et al.*[18]]

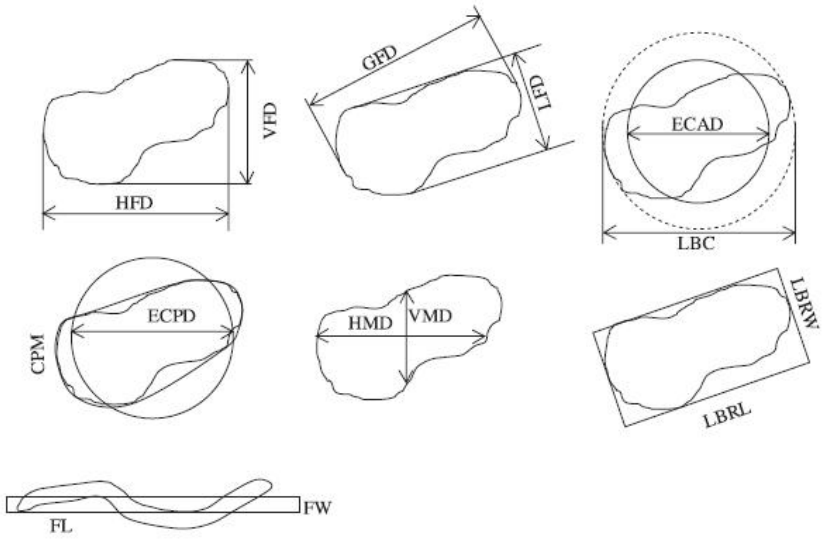

Figure 12. Common two-dimensional particle parameters. HFD: horizontal Feret's diameter, VFD: vertical Feret's diameter, LFD: least Feret's diameter (Feret's width), GFD: greatest Feret's diameter (Feret's length), ECAD: equivalent circular area diameter (Heywood's diameter), LBC: least bounding circle, ECPD: equivalent circular perimeter diameter, CPM: convex perimeter, HMD: horizontal Martin's diameter, VMD: vertical Martin's diameter, LBRW: least bounding rectangle width, LBRL: least bounding rectangle length, FL: fiber length, FW: fiber width. [Xu and Di Guida[19]]

The particle size of needle-like particles can be represented by the length of the particle L and the width of the particle W. The length of the particle is estimated from maximum Feret's diameter F_{max} (GFD in figure 12) which responds the longest dimension of particle. The width of the particle is then defined from rectangle which length is L and the area is same as the area of the particle A as in equation 6. [Li *et al.*[17]]

$$W = \frac{A}{L} = \frac{A}{F_{\max}} \tag{6}$$

Where W width of the particle
A area of the particle
L length of the particle
F_{max} maximum Feret's diameter

4.2 Particle shape

Particle shape is a very important property of the pigment because it has significant affects to the optical and the printing properties of the paper [KnowPap[20]]. Each particle has some shape; the simplest form can be spherical or

cubical. The spherical particle is unique because anyone other particle shape doesn't have the same properties than the sphere. It is symmetric, looks the same from all directions and behaves in the same way irrespective of its alignment [Backhurst *et al.*[18]].

In image analyses the particle shape is usually defined as sphericity S (equation 7), which is the ratio between the areas of the particle and the circle with diameter D_p (showed in equation 5) [Li *et al.*[17]]. The value of sphericity for sphere is 1 and for square 0.78.

$$S = \frac{4\pi A}{P^2} = \left(\frac{D_a}{D_p} \right)^2 \tag{7}$$

where S sphericity
A area of the particle
P perimeter of the particle
D_a equivalent circular area diameter
D_p equivalent circular perimeter diameter

In three-dimensional analysis the sphericity is defined as in equation 8 [Backhurst *et al.*[18]].

$$S = \frac{\text{surface area of sphere of same volume as particle}}{\text{surface area of particle}} \tag{8}$$

If the all three dimensions (the longest, the intermediate and the shortest) of the particle can be measured, then the sphericity S can be calculated using equation 9 and shape factor SF using equation 10 [Xu and Di Guida[19]]. The values of sphericity and shape factor for sphere are also 1.

$$S = \sqrt[3]{\frac{d_S d_I}{d_L^2}} \tag{9}$$

where S sphericity
d_S the shortest dimension of the particle
d_I the intermediate dimension of the particle
d_L the longest dimension of the particle

$$SF = \frac{d_S}{\sqrt{d_L d_I}} \tag{10}$$

where SF shape factor
d_S the shortest dimension of the particle
d_I the intermediate dimension of the particle
d_L the longest dimension of the particle

The particle shape is defined also as circularity *C*, which is the ratio between the area of the particle *A* and the area of the circle with diameter F_{max} [Li *et al.*[17]]. Another used term is roundness which is an inverse of sphericity (showed in equation 7) [Biagini *et al.*[21]].

$$C = \frac{4A}{\pi F_{\max}^2} \tag{11}$$

where C circularity
A area of the particle
F_{max} maximum Feret's diameter

Aspect ratio can be informed many ways like a ratio of particle perimeter to particle area or a maximum dimension to minimum dimension [Lieberman[22]]. With the pigments the aspect ratio means typically a ratio of the particle width *L*, to the particle thickness *d* as in figure 13 [Turku[23]]. The higher aspect ratio, the platier particle [Sokka[10]].

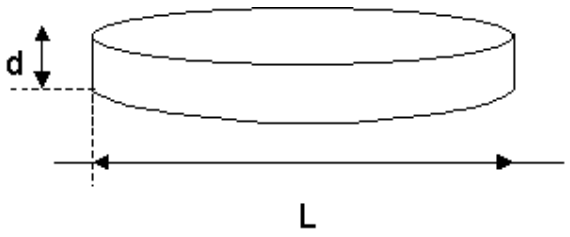

Figure 13. Aspect ratio of platy particle. *d*: particle thickness, *L*: particle width [Turku[23] modified by Linnala].

With needle-like particles the aspect ratio means the ratio of the particle length *L* to the particle thickness *d* as in figure 14 [Turku[23]].

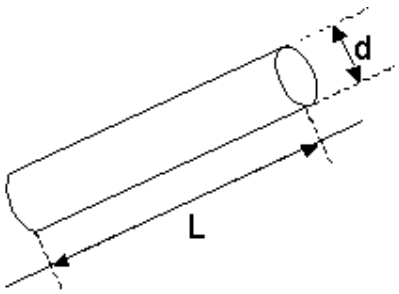

Figure 14. Aspect ratio of needle-like particle. *d*: particle thickness, *L*: particle length [Turku[23] modified by Linnala].

5 Methods of particle analysis

There are many methods to analyse particle size and shape. They can be based for example on mechanical, optical or electronic sorting or interact with light or sound. [Backhurst *et al.*[18]]. Two the most widely used techniques are electric sensing zone and laser diffraction [Xu and Di Guida[19]].

5.1 Sieving

Sieving is simple way to classify particles and measure the particle size distribution. The lower particle size limit in sieving is about 50 µm. Sieving is performed using a pile of sieves; the sieves on the top of the pile have larger apertures than lower sieves. The aperture size of the sieves can follow a few standard sieve series; for example British, French and Americans have their own standards. Sieving can be performed either dry or wet; both methods have advantages and disadvantages. In wet sieving part of the small particles are washed out, but the apertures stay open. In dry sieving all particles stay in the sieve series, but the small particles can form a thin layer over the sieves because the attractive forces between the particles become higher when the particle size shrinks. [Backhurst *et al.*[18]]

5.2 Sedimentation

Sedimentation method is based on the different settling velocity of the particles with the different particle size; larger particles settle faster than smaller particles. The lower particle size limit in the gravitational sedimentation is about 1 µm but if the gravitation is replaced by the centrifugal forces then the lower particle size limit is even 0.05 µm. The settling velocity can be measured at intervals of time either from the suspension samples or the weight changes. Isolating of the

particles is very important in the sedimentation analyses because agglomeration of the particles affects to the settling velocity. Temperature control must be specific also (± 0.1 K) to avoid convection currents [Backhurst *et al.*[18]]. Non-spherical particle shape is a problem in the sedimentation method. All the six different pigment particles in figure 15 have the same equivalent spherical diameter 0.5 µm when measured by sedimentation. [Nikki and Nutbeem[24]]

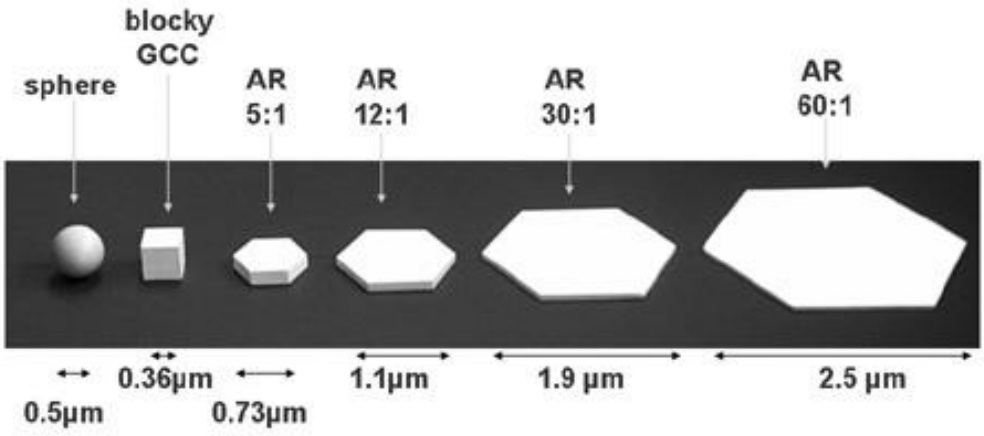

Figure 15. The effect of particle shape to equivalent spherical diameter measured by sedimentation [Nikki and Nutbeem[24] modified by Linnala].

Sedigraph™ is the particle size analyser which consists of sedimentation and photon absorption. Terminal settling velocity of the particles is measured and converted to the particle size of equivalent sphere with Stoke's law as in equation 12. [Anon.[25]]

$$v = \frac{g d_p^2 \left(\rho_p - \rho_m\right)}{18\eta} \tag{12}$$

where
v sedimentation velocity
g gravitation constant
d_p diameter of spherical particle
ρ_p density of particle
ρ_m density of medium
η viscosity of medium

Relative mass concentration for each particle size class is measured by absorption of low-power X-ray. Narrow collimated X-ray beam is projected through the sample suspension continuously during settling. With Beer-Lambert-Bouguer law

the absorption of X-ray can be converted to the mass concentration as in equation 13. [Anon.[25]]

$$A = \alpha l c = \log_{10}\left(\frac{I_0}{I_1}\right) \tag{13}$$

where A absorbance of the sample
α absorption coefficient of the absorber
l distance that the light travels through the sample
c concentration of absorbing species in the sample
I_0 intensity of the incident light
I_1 intensity after passing through the sample

The particle size can be measured between 0.1 and 300 µm. Data can be handled many ways and combining the data from the other analysers the particle size can vary between 0.1 µm and 125 mm when reporting. [Anon.[25]]

5.3 Electronic particle counters

Electronic particle counters use electrodes to cause an electric current. Conductive particle suspension flows through the orifice which has the electric current. When the particle is in orifice, the volume of a conductive medium is decreased and the voltage must be raised to achieve constant electric current. Each particle causes an electric pulse which is measured and classified. The pulse amplitude is depending on the particle volumetric size which is the same as the volume of displaced medium in orifice. The particle size distribution can be formed from the classified electric pulses [Backhurst *et al.*[18], Strickland[26]]. The correlation between the amplitude of the pulse and the particle volume can be defined as in equation 14. [Xu[13]]

$$U = \frac{V\rho_0 if}{\pi^2 R^4} \tag{14}$$

where U amplitude of the voltage pulse
V particle volume
ρ_0 electrolyte resistivity
i aperture current
f shape factor of the particle
R aperture radius

The electronic particle counters assume that the particle shape is sphere. Results may be reported as equivalent spherical diameter or the diameter of sphere which

have the same volume as the particle. The electric pulses differ between the particle shapes. When the spherical and the rod-like particle have the same volume, the generated electric pulses have the same area but different width. Reporting of particle shapes could be possible also with that method, but it still needs much development. [Strickland[26]]

The *Coulter Counter*® is one example of the electronic particle counters. It can measure up to 3000 particles per second. The lowest particle size limit is below 0.5 µm and the highest particle size limit is about 1200 µm and above. The Coulter Counter uses platinum electrodes to cause the electric current. The amplitudes can be classified into 16 size interval channels. [Kinsman[27]]

5.4 Laser diffraction

Particle size analysis by laser diffraction bases on the optical properties of the particles. Particle suspension flows through the beam of collimated laser light and the scattered light is collected by the photo detectors as in figure 16 [Backhurst *et al.*[18]]. The wavelength of used light affects to the measured particle size; long wavelength is used with large particles and short wavelength is required for small particles. The particle size affects to the angle of scattering and also to the intensity of scattered light. Small particles scatter the low intensity light at wide angles and large particles scatter the high intensity light at narrow angles. With the modern analysers the light scattering can be detected between angles 0.02 and 140 degrees [Kippax[15]]. To provide the particle size distribution the scattered light distribution is processed and compared to the scattering models. The lowest particle size limit in laser diffraction is about 0.1 µm but when the particle size is already less than 1 µm data processing requires care. The maximum particle size in laser diffraction is about 600 µm. [Backhurst *et al.*[18]]

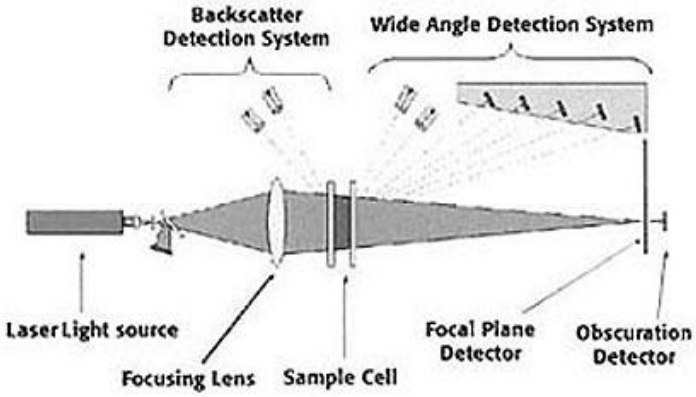

Figure 16. Principle of laser diffraction apparatus [Kippax[15] modified by Linnala].

Coulter LS 230™ is analyser which bases on laser diffraction. The efficiency of particle size analysing of the small particles is intensified with a method called Polarization Intensity Differential Scattering (PIDS). PIDS bases on the differential light scattering property of a vertically polarized light and a horizontal polarized light. With these two methods LS 230 overtakes minimum particle size 40 nm and maximum particle size 2000 µm. [Anon.[28]]

Another laser basis particle measuring application is Nanoparticle Tracking Analysis (NTA, NanoSight). A horizontal laser beam is focused through the sample suspension which is injected onto the special optical flat. Scattering of the laser light is observed by optical microscope equipped with video camera. Figure 17 shows the basis of NTA. [Carr *et al.*[29]]

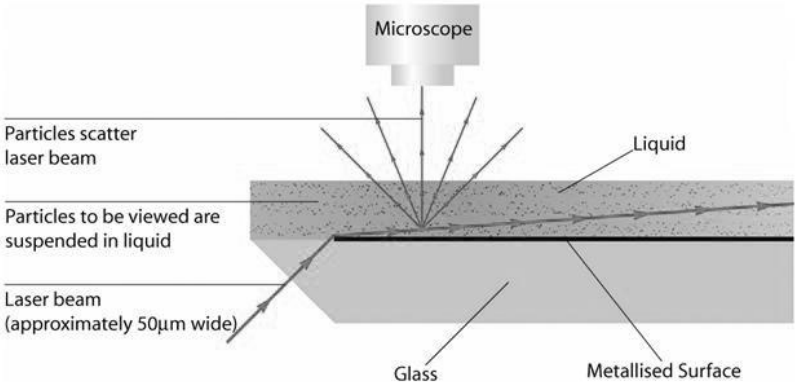

Figure 17. The basis of Nanoparticle Tracking Analysis [Anon.[30] modified by Linnala].

Particles can be perceived as individual light sources which move under Brownian motion. The displacement of the particle is inversely proportional to the particle size as represented in equation 15. [Carr *et al.*[29]]

$$\overline{(x, y, z)}^2 = \frac{2TK_B t}{\pi \eta d} \tag{15}$$

where
- x x-directional displacement
- y y-directional displacement
- z z-directional displacement
- T temperature
- K_B Boltzmann's constant
- t time
- η viscosity
- d particle diameter

The intensity of scattered light is also proportional to the particle size as showed in equation 3. The observing of these two properties is visualised in figure 18.

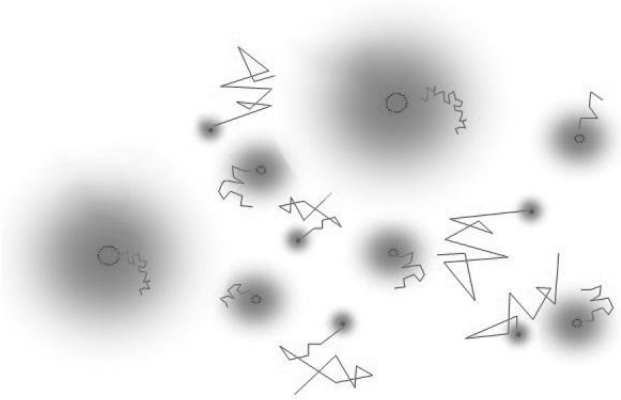

Figure 18. Principle of NTA measurement [Anon.[30] modified by Linnala].

NTA has a couple of limitations of measured particles. The lowest limit of particle size (~10 nm) can be overtaken only by the particles with high refractive index such as colloidal silver. For the particles with slightly lower refractive index (metal oxides, TiO_2) the lowest limit is over 20 nm. E.g. polymers and biological materials have even lower refractive index and therefore the minimum visible particle size is about 50-75 nm. The second limitation is particle shape. The calculation method of particle size turns complicated when particles are non-spherical. Therefore the aspect ratio of examined particles should be below 2-3. [Carr *et al.*[29]]

5.5 Optical methods

Optical methods are based on microscopy. The lowest particle size limit in the traditional microscopy is about 1 µm but in the electron microscopy the resolution is only few (<5) nanometres depending on the hardware and operating conditions. The particle size measurement can be done in two dimensions and with the special image processing programs even in three dimensions. The particle size can be compared to the gauge circles of eyepiece or measured by automatic image analysis programs. [Backhurst *et al.*[18], Goodhew and Humphreys[31]]

6 Scanning Electron Microscope (SEM)

Scanning electron microscopes operational principle is like the conventional light microscopes but the light is replaced with the electrons. Resolution, magnification and the depth of field are based on the same properties but the technology between the light microscope and the electron microscope is different because of the different nature of light and electrons. [Goodhew and Humphreys[31]]

6.1 Construction of scanning electron microscope

The scanning electron microscope has two main parts. *The electronics* are used to control electron beam to specimen, identify and analyse signals, form image and do other functions to control the microscope. *The electron column* creates electrons including the group of lenses that focus the electron beam exactly to the specimen. Figure 19 shows the features of the scanning electron microscope. [Lyman *et al.*[32]]

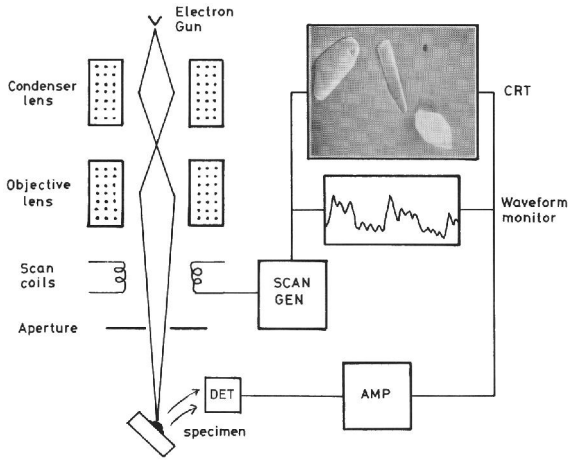

Figure 19. The main components of SEM [Goodhew and Humphreys[31]].

Electron gun is the source of primary electrons. The electron gun usually uses heated filament (F in figure 20) to thermionic emission. The filament is usually made of tungsten, but if high brightness of the electron beam is required then LaB_6 filament can be used. Figure 20 shows the features of electron gun. [Goodhew and Humphreys[30]].

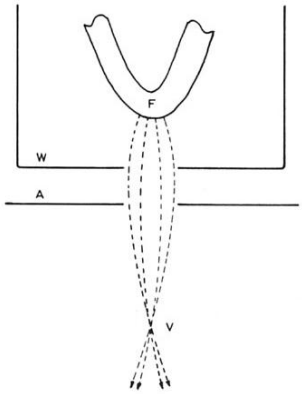

Figure 20. The features of electron gun. F: filament, W: Wehnelt cap, A: anode, V: focus. [Goodhew and Humphreys[31]]

Magnetic lenses are used to deflection of electrons. The lenses cause magnetic field almost parallel to the direction of electrons. Electrons move in a helix and can be exactly focused because the magnetic field strength has two components; radial and axial. [Goodhew and Humphreys[31]] SEM has two or three magnetic lenses and with them the electron beam diameter is reduced to 5-50 nm. [Lyman *et al.*[32]]. In addition of the magnetic lenses the most microscopes have dozen or more coils which can be used to optimize the position of the electron beam. Figure 21 shows the construction of lens and coil system. [Goodhew and Humphreys[31]].

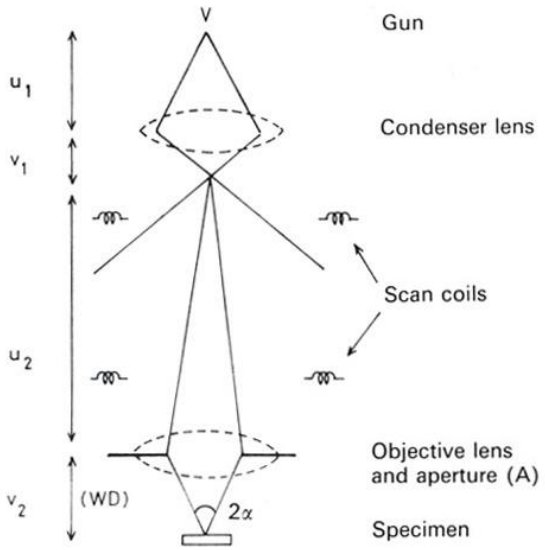

Figure 21. Two lens system of scanning electron microscope [Goodhew and Humphreys[31]].

Inside the objective lens is located an objective aperture. It is very small gap (diameter about 100 µm) in a platinum disk. It reduces aberration effects of the lens and improves the depth of field by limiting the angular width of the electron beam. [Lyman *et al.*[32]]

Sample chamber is located below the electron gun and consist of a signal detectors for the backscattered and the secondary electrons, an X-ray detector and a moving stage for the samples. The sample chamber is evacuated as the electron gun because the electrons travel in the air only very short distances. [Lyman *et al.*[32]]

6.2 Image forming

When the sample is bombed by the primary electrons even same or different electrons are collected from different regions as represented in figure 22. These secondary (SE) and backscattered (BE or BSE) electrons are detected as in figure 23 and used to form image. [Goodhew and Humphreys[31]]

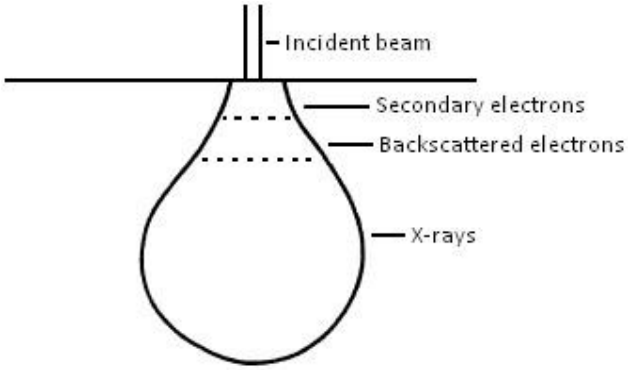

Figure 22. The regions from which the different electrons and the X-rays can be detected [Goodhew and Humphreys[31] modified by Linnala].

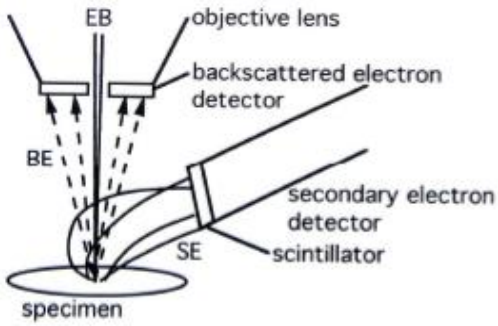

Figure 23. The detectors of secondary and backscattered electrons. EB: electron beam, BE: backscattered electrons, SE: secondary electrons. [Banerjee and Conners[33]]

Secondary electrons are escaped from the sample with energy below 50 eV. The term is not very accurate because "secondary" electron can be also the primary electron which has lost the most of its energy. More likely they are electrons which have got small amount of energy in short distance of the sample surface. The ratio between the number of emitted secondary electrons and the primary electrons is called the yield of secondary electrons which can be as high as one. [Goodhew and Humphreys[31]]

Backscattered electrons are the primary electrons which have left the sample before they have lost all of their energy. The backscattered electrons have high energies but they are not as numerous as the secondary electrons. [Goodhew and Humphreys[31]]

7 Basics of image analysis

Particle analysis with microscopy is based on a digital images and use of an image processing programs. Image processing is critical part of the particle analysis because if it has been done careless the results will be false.

7.1 Imaging

The sample can be examined with the light microscope or if higher accuracy is required then the scanning electron microscope is needed. Imaging can be done with a digital camera in case of the light microscopy. Today the quality of the digital cameras is advanced and therefore the camera is not the most critical part of the image analysis [Niemistö[34]]. With the scanning electron microscope the image forming can be done without separate digital camera because the same image as on the CRT can be stored into the computers hard drive. Images can be gathered up with slow scan rate to get better image quality and processed later. This is an advantage for sensitive samples which don't stand the conditions of SEM [Goodhew and Humphreys[31]].

7.2 Image processing

After the digital images are stored they can be processed by many ways. Basic image properties like contrast, brightness and gamma can be optimised. For particle analysis the most important property is the grey level of the image which can be segmented to reduce different shades. [Niemistö[34]]

7.2.1 Segmentation

Segmentation is the most important but also the most difficult step in the image analysis. Segmentation means the separation of different parts of the image; a foreground objects like particles from a background of image. In the particle size and shape analysis segmentation has to be done with very high accuracy because the area of the particle is dependent of the accuracy of segmentation and the results of analysis have to be reliable. [Niemistö[34]]

Segmentation can base on either discontinuity or similarity of intensity values. Discontinuity methods find abrupt changes in the intensity and separate various regions on that way. Methods of similarity needs predefined criteria of the

intensity value and separate regions based on that. Thresholding, clustering, region growing, region merging and region splitting are methods which are included in the category of similarity methods. [Niemistö[34]]

Thresholding is a central method of segmentation due to its simple and intuitive properties. It separates bright foreground objects on a dark background and can be defined as in equation 16:

$$f_T(x) = \begin{cases} 1 & \text{if } f(\mathrm{x}) > T \\ 0 & \text{if } f(\mathrm{x}) \leq T \end{cases} \tag{16}$$

where $f(\mathrm{x})$ grey level of the point x
$f_T(\mathrm{x})$ the respective point in the thresholded image
T threshold

If a pixel in f_T gets value 1 it is called a foreground or object point and if it gets value 0 it is called a background. In some cases the background is bright and the objects are dark, then the roles of 1 and 0 are swapped. Threshold T can be the same for the whole image (global threshold) or there can be different thresholds in different parts of the image (local threshold). [Niemistö[34]]

It is usually very difficult to select optimal threshold. The transition between the object point and the background may be so unsteady that a human can't decide where the borders between the object and the background exactly go. The task is not any easier for computers and that’s why there is no satisfactory general solution for the thresholding problem. Many papers are published on the automatic selection of the threshold since 1960's. The most commonly used method is created by Otsu. That method maximizes the between-class variance of the grey levels of the objects and the background and minimizes the intra-class variance. Usually threshold is selected from a histogram of the image. If the histogram is bimodal threshold should be selected between the modes because supposedly a one mode represents the foreground and the other one represents the background. Otsu's method can be used if the histogram has even one or two modes. Figure 24 shows an example of thresholding. [Niemistö[34]]

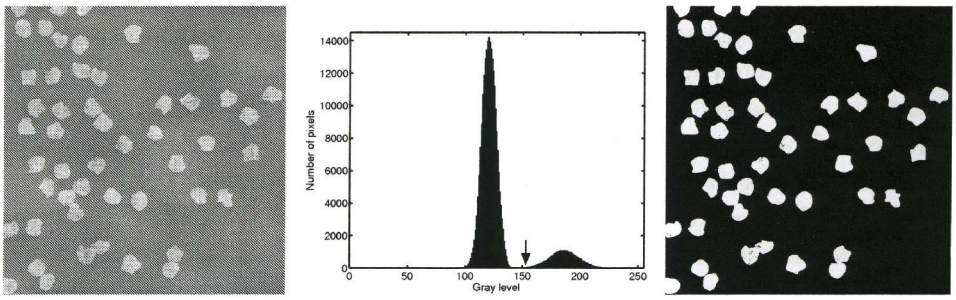

Figure 24. An example of thresholding. Left: original image, middle: the histogram of the original image, the threshold T=153 (the arrow) obtained with Otsu's method, right: the thresholded image [Niemistö[34]].

Clustering methods are used in complicated situations. The simplest segmentation case has only two classes; the object and the background. But there may be need for more threshold classes which represent different types of objects. Clustering collects together patterns which are similar. Each cluster has patterns which differ from patterns in the other clusters. Clustering can be used in situations in which the results from the thresholding are incorrect. It can be used also with colour images when different types of the objects can have different colours. [Niemistö[34]]

Region growing bases on predefined criteria of the pixels what is used to segmentation. Method needs a set of seed points to start. The neighbouring pixels of the seed points are added one by one to the growing region if they have similar properties than the pixels in the growing region. This continues until the neighbouring pixels have too different properties and can't be added to the growing region. Usually the similarity criterion is the similarity of the grey levels of the neighbouring pixels. One popular region growing method is a watershed transformation. The idea of the watershed method is analogy to flooding water when water rises from topography regional minima and the watersheds are built to prevent the merging of water areas. The image with different intensities corresponds with a topographic map and the watershed method uses a new intensity layer in the each iteration. The gradient of the image is used for the watershed transformation rather than the image itself because the lowest values of the gradient image correlate well with the foreground and also with the background. Respectively the largest values of the gradient image are the borders between the objects and the background. [Niemistö[34]]

Region merging is usually used as a post-processing step. With that method two regions which average intensity levels are similar or the gradient of the border between them is low are combined to one object. This method can be also used if a minimum area of object is defined. Then all objects which are smaller than that have to be combined with some of the neighbouring objects. Properties of the neighbouring objects are compared as mentioned above and the best is chosen to combine with. [Niemistö[34]]

Region splitting is also a post-processing step and is often needed after the segmentation. The foreground objects may be clustered together although they should be individual objects. Splitting can be divided two parts; in the first step the clustered objects are detected and in the second step they are separated. The advantage of the two-step method is that the splitting of correctly segmented objects can be avoided so the targets of splitting can be controlled [Niemistö[34]].

7.2.2 Morphological filtering

Morphological filtering bases on two fundamental operations: *erosion* and *dilation*. These operations compare the properties between a structuring element *B* and a sliding window. The structuring element is a binary-valued mapping and each cell has value even 1 or 0 as represented in figure 25. [Niemistö[34]]

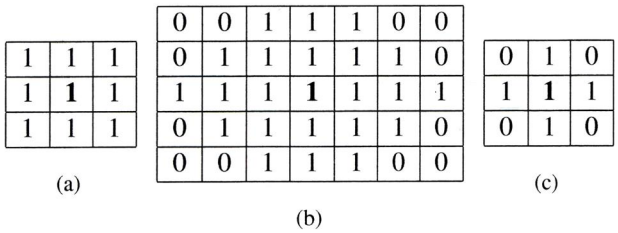

Figure 25. Examples of the structuring elements [Niemistö[34]].

If the image is eroded by the structuring element as in figure 26(a) the equivalent minimum filter is a 3x3 sliding window. When the morphological filtering is used with binary images as usual, the result of erosion is zero unless all the cells of sliding window have value one. Respectively the result of dilation is one unless all the cells of sliding window have value zero. Simpler, erosion shrinks the foreground and expands the background. Respectively dilation expands the

foreground and shrinks the background. Figure 26 shows an example of erosion and dilation. [Niemistö[34]]

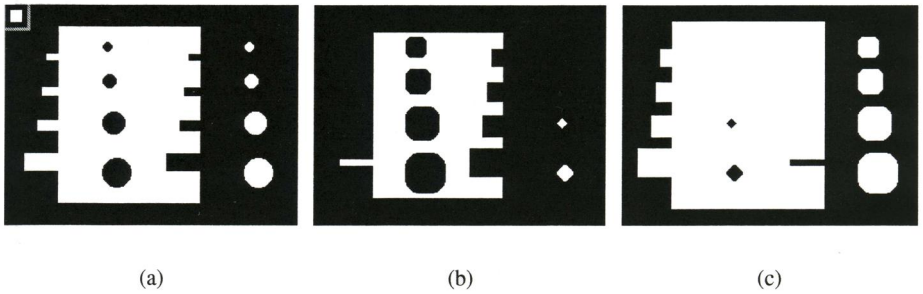

Figure 26. An example of erosion and dilation. (a) An original binary image with a structuring element in top left corner, (b) erosion of the original image, (c) dilation of the original image [Niemistö[34] modified by Linnala].

The morphological *opening* and *closing* are operations which combine erosion and dilation operations. The morphological opening completes first erosion by the structural element B and then dilation by the reflected structuring element $\check{B}$. Erosion shrinks objects which can contain the structural element and removes other objects. If some object is removed in erosion it is not recovered in dilation. Opening operation can be used to remove small foreground objects and to smooth the larger objects. The morphological closing completes first the dilation by the structural element B and then the erosion by $\check{B}$. Dilation expands all the foreground objects and fills the background structure if it is smaller than the structural element. Therefore the closing operation can be used to fill small holes and to smooth the objects. Examples of the opening and closing operations are showed in figure 27. [Niemistö[34]]

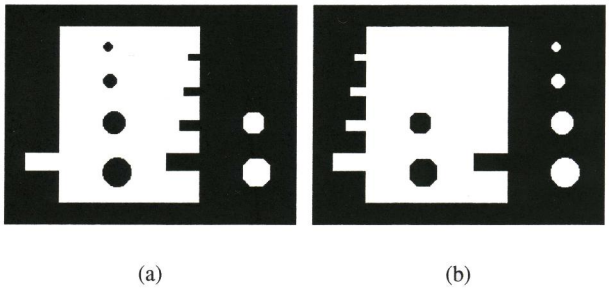

Figure 27. Examples of morphological opening (a) and closing (b) operations. Original image and structural element are the same as in figure 26(a). [Niemistö[34] modified by Linnala]

8 Sample preparation

Sampling and the sample preparation are the most difficult part of the particle analysis with SEM as with the other analyse methods.

8.1 Sampling

The particle size of pigments used in paper industry is usually below two micrometers and the particle size analyses use only few thousands particles. Situation is that the measuring of the whole lot of the pigment particles is impossible and the sampling is essential. The sampling is critical point of the research chain, usually the weakest link. The sample should be representative, but problem is that scientific definition of representative sample is very difficult because it needs understanding of many definitions like selection and sampling. Few definitions of sampling are widely used; the sampling can be even probable when all particles have some probability to be taken to the sample or non-probable if some particle has zero probability to be selected to the sample. The sampling must be probable and reliable to get a correct sample. Correctly selected sample consists of the particles which all have an equal probability to get selected and are not altered in any way. In an incorrect selection at least one of these two defines is not valid. Only correctly selected sample is structurally faithful. [Gy[35]]

Homogenization is a method to get a sample which is correctly selected. When correlations between the position of the particles and the physical properties (density, size, shape) of the particles are eliminated the distributional heterogeneity of the sample is minimal. Unfortunately the heterogeneity is only minimised, it can't ever be eliminated. The pigment sample includes particles with different sizes and therefore it can't be ever homogenised and the results of the particle analyses are only estimations of the lot of the pigment particles. [Gy[35]]

8.2 Sample preparation for particle analysis

Most particle analysing methods require that particles are suspended into a liquid. The concentration of the suspension has to be low enough to avoid aggregates and interactions between the particles. For example, if two particles go through the orifice of electric particle counter too near of each other, the results will be incorrect. Respectively in laser diffraction the scattered light may interact with

another particle before reaching the detector if the sample concentration is too high. [Xu and Di Guida[19], Webb and Orr[36]] Of course when measuring the shape of the particles they can't be clustered either.

8.3 General demands of sample preparation for SEM

Scanning electron microscope is very useful tool for analysing different materials and samples. SEM has some requirements on sample type and sample preparation. The sample has to be clean and dry, it can't be volatile or include dissolved gas which could be released [Neijssen and Roussel[37]]. The conductivity of the sample is also important because a nonconductive material causes charging which weakens the quality of the image. That is why the samples must be coated with a thin layer of carbon, gold or gold-palladium mixture. [Lyman *et al*.[32]]. Figure 28 shows a principle of the prepared paper sample on the specimen stub.

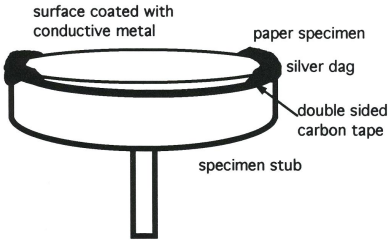

Figure 28. Paper sample prepared on the specimen stub [Banerjee and Connors[33]].

8.4 Special demands for particle character analysis with SEM

The particle and fibre analyses with SEM need special attention deriving the small size of particles. The particle is not mechanically stable on the stub because the particle shape prevents large contact area. But if the particle size is below 40 µm the attractive force between the particle and the stub is strong enough to keep the particles in place and a separate fixing is not required. The particle shape causes also problems with the primary electrons. The electrons penetrate the platy particle and interact with the stub and other surrounding material which generate incorrect signals. The pigment particles are also nonconductive material and therefore the risk of the particle charging in electron microscope exists. [Lyman *et al.*[32]]

8.5 Sample preparation techniques

The greatest problem in the particle analyses with SEM is to get all the particles separated and still get sufficient number of the particles analysed. One method is making of suspension which particle concentration is about 0.1-1 % depending on the particle size. Liquid phase can be purified water or better option is fast evaporating solvent like the alcohols. The suspension is properly mixed for example with ultrasound and one drop of the suspension is applied onto a carbon tape on the stub. The evaporation of the liquid phase can be accelerated with a heat lamp. Fast evaporation of the liquid will reduce the aggregation of the particles. After the sample is completely dry, it should be coated with carbon or gold. [Lyman *et al.*[32], Kaur *et al.*[38], Xu[39]]

Other commonly used method bases on the filtration. The particles are suspended into the purified water or the alcohol and small amount of the suspension is filtered onto a polycarbonate filter which aperture size depends on the particle size. The concentration of the suspension is changed to achieve optimal number and settling of the particles on the filter. Effective mixing is important also before the filtration. When the sample is dried a piece of it is fixed onto the stub and the sample is coated. [Huffman *et al.*[40], Turner *et al.*[41], Linnala[42]]

The particle suspension could be also sprayed onto different materials. Polycarbonate membrane, polypropylene foil, sandpaper and adhesive tape have been examined. Spraying causes aggregation of the particles because they move with the liquid phase if it can't be evaporated fast enough. The shapes of base material also gather up the particles. Sandpapers abrasive particles are minerals and them can't be separated from the pigment particles in the SEM images. [Linnala[42]]

Freeze drying is method to avoid the move of the particles with liquid phase. The moisture is removed dipping the sample into liquid nitrogen. The volume of water did not expand when the freezing is rapid and forming ice is non-crystal. Drying happens under high vacuum. When the air pressure goes below the vapour pressure of ice in the sample, the moisture removes by sublimation [Shi *et al.*[43]]. Few conditions are required for the freeze drying. The sample must be solidly frozen, the condensing surface must be at or below 233 K, the absolute pressure of

vacuum chamber is 5 to 26 µm of Hg and the heat system must keep the optimal temperature for sublimation (controlled 233-338 K). Figure 29 shows the principle of the freeze drying machine. [Banerjee and Conners[33]]

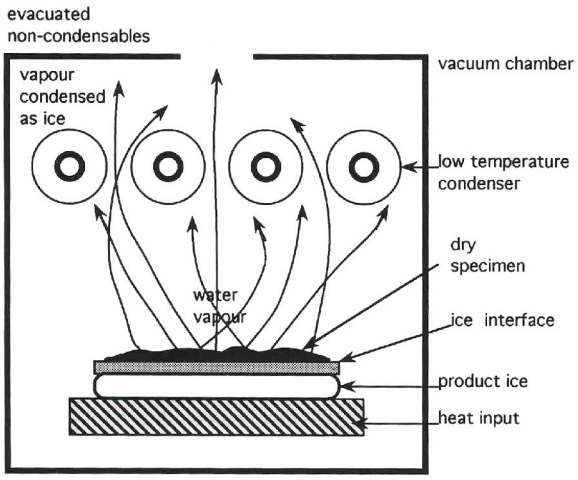

Figure 29. Diagram of freeze drying technique [Banerjee and Conners[33]].

9 Statistics

Statistics are used to classifying and analysing the particle sizes and the particle size distributions. The regularity of quality and reliability of the sampling can also be adjusted by the statistical analysis.

9.1 Basics of statistics

All researches have some examination material which is called population *W*. The population has units *w*, whose property *X* is examined. Usually in practice it is not possible to examine all the units of the population and therefore sampling must do exactly to get a representative sample of the population. The sample consist of *n* units which property *X* is realized to observations $x_1,\ldots,x_n$. The results of the sample examination are generalised to cover the whole population which is called statistical inference [Laininen[44]]. This is also the method of the pigment sampling and analysing. The population can be several tons and the final examined sample is just hundreds or thousands particles.

9.2 Describing of observation material

The observational data consist of the realisations x_n from units' examination and can be represented on nominal scale, ordinal scale, interval scale or on ratio scale.

The nominal scale is used for classifying of the units and the classes can be represented by letters or numbers. The ordinal scale classifies the units and also orders them. The interval scale addition of the previous scales also notifies numerically the magnitude differences between the classes. The interval scale demands the unit of measurement and a zero point (for example Celsius-scale). The ratio scale is the most common and like the interval scale, but it has an absolutely zero point (for example length or area scale). [Laininen[44]]

For better impression of the examined material e.g. distribution curve, mean value and standard deviation is calculated. A sample mean value $\bar{x}$ is an arithmetic mean value of the observations $x_1 \ldots x_n$ and can be calculated using equation 17. [Laininen[44]]

$$\bar{x} = \frac{1}{n} \sum_{i=1}^{n} x_i \tag{17}$$

where n number of observations
x_i realisation of point i / observation i

If the observations are classified then the samples mean value $\bar{y}$ can be calculated using equation 18 [Laininen[44]].

$$\bar{y} = \frac{1}{n} \sum_{i=1}^{k} f_i y_i \tag{18}$$

where n number of observations
k number of classes
f_i frequency of class i (number of observations in class i)
y_i middle point of class i

In practice the mean particle size can be calculated basing on volume, weight, surface, or length as represented in equations 19-21. [Backhurst *et al.*[18]]

$$d_v = \frac{\sum\left(n_1 d_1^4\right)}{\sum\left(n_1 d_1^3\right)} \tag{19}$$

where d_v volume mean diameter
n_1 number of particles in class 1
d_1 volume/weight of particle in class 1

$$d_s = \frac{\sum\left(n_1 d_1^3\right)}{\sum\left(n_1 d_1^2\right)} \tag{20}$$

where d_s surface mean diameter
n_1 number of particles in class 1
d_1 surface of particle in class 1

$$d_l = \frac{\sum\left(n_1 d_1^2\right)}{\sum\left(n_1 d_1\right)} \tag{21}$$

where d_l length mean diameter
n_1 number of particles in class 1
d_1 length of particle in class 1

The quartiles Q_r and a sample median Md are percent points. In generally below the x value of the percent point r is r % of the observations $x_1 \ldots x_n$. The most usual quartiles are Q_1 and Q_3 which are equivalent to 25 % and 75 % points. The sample median Md is that x value which below is 50 % of the observations $x_1 \ldots x_n$. The value of sample median can be specified classifying the observations $x_1 \ldots x_n$ in order of the magnitude and calculated using equation 22 if n is odd or using equation 23 if n is even. [Laininen[44]]

$$Md = x_{((n+1)/2)} \tag{22}$$

$$Md = \frac{x_{(n/2)} + x_{(n/2+1)}}{2} \tag{23}$$

The gauges of deviation define how extensively the observations $x_1 \ldots x_n$ are deviated surround the middle point. A sample standard deviation s can be calculated using equation 24 and a sample mean deviation T using equation 25. [Laininen[44]]

$$s = \sqrt{\frac{1}{n-1}\sum_{i=1}^{n}\left(x_i - \bar{x}\right)^2} \tag{24}$$

where s standard deviation
n number of observations
x_i observation i
$\bar{x}$ mean value

$$T = \frac{1}{n}\sum_{i=1}^{n}\left|x_i - \bar{x}\right| \tag{25}$$

where T mean deviation
n number of observations
x_i observation i
$\bar{x}$ mean value

If the observations are classified with the middle points of class's $y_1 \ldots y_k$, the class frequencies $f_1 \ldots f_k$ and the mean value of classified observations is $\bar{y}$ then the standard deviation can be calculated using equation 26 and the mean deviation using equation 27 [Laininen[44]].

$$s = \sqrt{\frac{1}{n-1}\sum_{i=1}^{k} f_i\left(y_i - \bar{y}\right)^2} \tag{26}$$

where s standard deviation
n number of observations
k number of classes
f_i frequency of class i
y_i middle point of class i
$\bar{y}$ mean value of observations

$$T = \frac{1}{n}\sum_{i=1}^{k} f_i\left|y_i - \bar{y}\right| \tag{27}$$

where T mean deviation
n number of observations
k number of classes
f_i frequency of class i
y_i middle point of class i
$\bar{y}$ mean value of observations

A sample variance s^2 can be calculated using equation 28 or if the observations are classified then using equation 29 [Laininen[44]].

$$s^2 = \frac{1}{n-1}\left\{\sum_{i=1}^{n} x_i^2 - \left(\sum_{i=1}^{n} x_i\right)^2 / n\right\} \tag{28}$$

where s^2 variance
n number of observations
x_i observation i

$$s^2 = \frac{1}{n-1}\left\{\sum_{i=1}^{k} f_i y_i^2 - \left(\sum_{i=1}^{k} f_i y_i\right)^2 / n\right\} \tag{29}$$

where s^2 variance
n number of observations
k number of classes
f_i frequency of class i
y_i middle point of class i

A distribution curve is very useful way to visualize the results of particle size analyses. It can be represented even a cumulative or a frequency basis as showed in figure 30. In the cumulative basis distribution curve the proportion of the particles *x*, smaller than size *d*, is plotted as function of the particle size *d*. The frequency basis distribution curve shows which particle size is dominant. In that the mass fraction of the certain particle size d*x*/d*d* is plotted as the function of particle size *d*. The frequency curve has single peak for natural materials, but for mixtures it can have more peaks. [Backhurst *et al.*[18]]

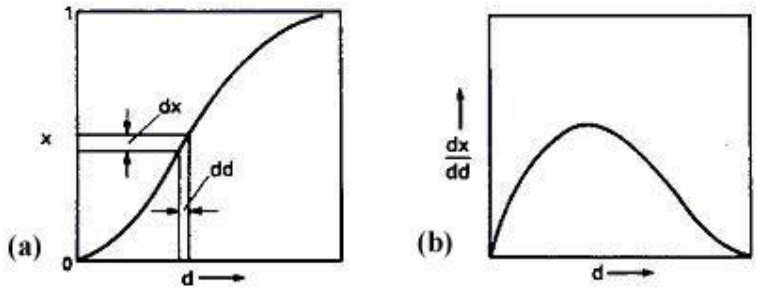

Figure 30. Examples of distribution curves. (a) cumulative basis, (b) frequency basis. [Backhurst *et al.*[18]]

9.3 Statistical testing

Statistical testing of hypotheses is used to testing statements of the population on the grounds of the sample. Testing can be *parametric* if the statements relate some parameter of the sample like the variance or the expectation value. In the other

cases testing is *non-parametric* like testing of the distributions. Testing can be divided five stages as follow: [Anon.[45]]

1. Setting of the hypotheses
2. Choosing of the risk level
3. Choosing of the test variable and identification of the disagreement condition
4. Collecting of the observations and calculation of the values of test variable
5. Making of conclusion

Statistical testing requires two hypotheses; H_0 is a zero hypothesis and H_1 is a counter hypothesis. In parametric testing the hypotheses concern some parameter of the distribution of variable. H_0 and H_1 exclude each other and cover all values of the tested parameter. The counter hypothesis defines aberration from a normal situation (for example effect or change) and the zero hypothesis defines a present situation. [Anon.[45]]

The conclusion can be wrong in two ways. Bias can lead to the disagreement of zero hypothesis even if it is true or the zero hypothesis can be accepted even if it is not true. The risk level or the level of significance α is the highest probability of the disagreement bias. In other words the level of significance is the probability that the zero hypothesis will be disagreement even if it is true. The disagreement bias of the zero hypothesis is more serious and therefore the risk level is chosen in advance. Usually α is 0.05, 0.01 or 0.001. [Anon.[45]]

The conclusion of hypotheses bases on the test variable $T(X_1, X_2,..., X_n)$ which is some sample variable. The values of the test variable are classified into two classes which exclude each other. An approving area of zero hypothesis is marked S_0 and a disagreement area is marked S_1. The critical values are the borders of the disagreement area and when the zero hypothesis is valid then the test variable belongs to the disagreement area at probability α. [Anon.[45]]

The collecting of observations consists of an arrangement of sampling and an examination, sampling and measuring. The values of the test variable are measured from the observations. [Anon.[45]]

The conclusions are comparison of the calculated value of test variable and the critical values. [Anon.[45]]

If $T(x_1, x_2,\ldots,x_n) \in S_0$ H_0 is accepted
If $T(x_1, x_2,\ldots,x_n) \in S_1$ H_0 is abandoned

P-value is the significance level of the test variable. If the zero hypothesis is valid, then the P-value is a probability to get aberration from the value of the zero hypothesis that is the same or higher than the value of the test variable. The P-value is the lowest risk level when the zero hypothesis would be accepted. The statistical software gives the P-value of the test variable and if the risk level α is chosen in advance, the conclusion is made as follow: [Anon.[45]]

If $P < \alpha$ H_0 is abandoned
If $P \geq \alpha$ H_0 is accepted

Parametric testing can be testing or comparison of the expectation value or the variance or the proportion. These tests require that the estimates of expectation values have the normal distribution. Used tests are X^2-test, z_λ-test and t-test. [Laininen[44]]

In the other situations and also if the observations have the nominal or the ordinal scale, testing have to be non-parametric. The middle points of the independent samples can be compared with Mann-Whitney test or Kruskal-Wallis test. The middle points of the dependent samples can be compared with Friedmann test. If the number of observations is high, then the comparison of the distributions can be done with X^2-test. Kolmogorov-Smirnov test is used if the analysing of the observations is made from small samples. [Laininen[44]]

Experimental part

Experimental part was partitioned into two test series; the first test series was as the pre-test and the second test series was wider-ranging.

10 Used materials and equipments

10.1 Used materials and laboratory hardware

Used pigments are represented in table II.

Table II: Specifications of used pigments.

Material	Shape
talc	platy
kaolin 1	platy, AR ~ 25
kaolin 2	platy, AR ~ 40
cubic PCC	cubic
nano PCC	cubic
clustered aragonite	irregular, clustered
aragonite	needle-like
wollastonite	needle-like, irregular
plastic 1	spherical
plastic 2	spherical

Three dispersing agents were used in dispersing test; 100 mol-% acrylic acid, 28000 g/mol. 100 mol-% acrylic acid, 130000 g/mol. 50 mol-% maleic acid, 8000 g/mol.

Sample preparation was made with Badger Air Brush model 100G and used bases were polycarbonate filter (pore size 0.015 and 0.2 µm), mica sheet, laser printable transparency and cellulose film. Examined filters in filtration method were polycarbonate filters with pore size 0.015 µm and 0.2 µm. Used ultrasound baths were both from FinnSonic; model m03 and old, unknown model.

Sample coating was made with Bal-Tec CED 030 Carbon Evaporator and SCD 005 Sputter Coater. Coating materials were carbon and gold-palladium mixture.

Samples were imaged by LEO 1450EP and/or JEOL JSM-5900LV scanning electron microscopes. 3D-modelling was made with MeX (version 5.0) from Alicona Imaging Corporation. More information about MeX-program is available in the reference 46.

10.2 Used image analysis programs

Used image analysis programs were INCA Feature (versions 4.06 and 4.08) from Oxford Instruments and Poikki-program from UPM-Kymmene Oyj / VTT Technical Research Centre of Finland. Feature is a part of INCA program and it is very versatile image analysis program. The most significant differ from Poikki-program is on-line use which means real time connection between SEM and Feature. Analysis starts with determination of analysis area. Area can be point (single field), line, rectangle, quadrilateral or circle. In "line"-mode area is defined by two points (start and end) and in "rectangle"-mode area can be defined by two or four points (angles). After the area is chosen, detection set-up is defined. These set-ups have very high effect to results, so definition needs to be done exactly. Detection set-up contains field set-up (image area in pixels and pass image speeds), feature set-up (magnification, particle size limits) and used filters in grey image and binary image processing. Alternative filters in grey image processing are "median", "smooth", "grid mask", "kernel" or some external user defined filter. "Median" filter equates intensity levels in 3x3 environment. "Smooth" filter performs a 9-point 4:2:1 weighted smooth upon the intensities of the image. "Grid mask" filter creates a user defined grid of small areas of known dimensions and spacing. This grid is used to acquire spectra from grid points of each analysed images. "Kernel" filter replaces each pixel by the sum of neighbouring pixels which each is multiplied by an integer weight. That sum is then divided by a normalising factor. The size of neighbourhood and the weights can be modified in the filter file. In binary image processing possible filters are "erode", "dilate", "hole fill", "open", "close", "separate", "remove edge touching" and external filter. Most of these are represented in chapter 7.2.2. "Hole fill" fills holes of the particles and "remove edge touching" leaves particles which touch edges out of analysis. Next step of analysis is the most critical: threshold in "Feature detection" part. After the threshold value is defined, analysis can be started. Results can be presented in table which can be exported to spreadsheet program. Results includes following parameters of each particle: area, length (max Feret), breadth (min Feret), perimeter, aspect ratio, direction of maximum Feret (degrees from the horizontal), shape, beam X of longest chord, beam Y of longest chord, ECD, spectrum area, mean grey level, stage X-Y-Z (of the centre of the longest chord)

and element %. Reported shape factor is inverse of normal sphericity which is represented in equation 7. More information about INCA Feature is available in the reference 47.

Poikki-program analyses images from hard or network drive because it works off-line. Analysis can be made even in manual or in automatic function. Manual function enables to define more set-ups when automatic function uses specified filters in image processing, but still enables the definition of threshold. "Automate Partikkeli"-function is used in all cases, because it is fast and useful. Grey image processing uses "rank"-filter which means median filtration in 5x5 environment but could be exchanged to some other than 5x5 environment or minimum or maximum filtration. In binary image processing Poikki-program uses "erode" and "dilate" filters which are represented in chapter 7.2.2. It also fills holes and removes edge touching particles. The most visible property for the user is programs language Finnish when Feature is in English. "Automate Partikkeli"-analysis proceeds after the image is opened to threshold when image processing is already done. When binary image is thresholded, user can draw manually to image; e.g. separate particles. After the image is accepted, program makes calculations and prints the results into two text files. Poikki-program reports following parameters for each particle: stage X-Y, area, area-%, diameter and shape. The shape factor of Poikki-program is the same as sphericity in equation 7.

11 Test series I

The test series I included only two pigments; talc and plastic 1. The main targets were examination of the different sample preparation techniques and acquainting to the image analysis programs.

11.1 Execution of work

11.1.1 Sample preparation

The pigments were prepared by filtration, spraying and freeze-drying methods. *Filtration* was made onto a polycarbonate filter whose pore size was 0.2 µm. Volume of filtrated suspension was 5 ml. Concentrations of pigment suspensions were at first 6, 30 and 60 mg/l and were optimised for both pigments. Dilutions were made with purified water. When the filter was dried, two parallel samples

were made by cutting small parts of filter onto the stubs and the one coated with carbon and the other coated with gold-palladium mixture.

In *spraying* method the sample suspension was sprayed by air brush onto the base materials which were polycarbonate membrane (the same as in filtration), mica and laser printable transparency. The polycarbonate membrane was examined also with vacuum, respectively as in filtration method. Sample volume was 0.5 ml which was diluted with purified water and water-ethanol-mixture (50:50). Ethanol was used to achieve faster evaporation of liquid phase, which was accelerated also with infrared-lamp. Sample suspension was diluted with purified water only when vacuum was used, because evaporation was not needed. Examined sample concentration was at first 60 mg/l and was also optimised for both pigments. In all cases the sample was sprayed onto the base from 20 cm distance when the diameter of spout was about 5 cm. Air brush was fixed onto a stand and spraying angle varied from 0° (vertical) to about 30°. After the samples were dried they were coated with carbon and gold-palladium mixture (two parallel samples). Figure 31 shows the principle of spraying method.

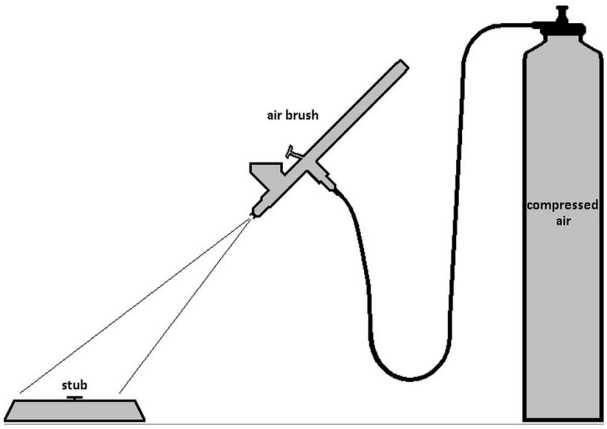

Figure 31. Equipments of the spraying method.

Freeze-drying method connected both freezing and one drop methods. One drop of sample suspension was applied by pipette onto the stub covered by polycarbonate membrane. Examined sample concentrations were 6, 30 and 60 mg/l. The stub was dipped into the liquid nitrogen until the sample was totally frozen. Ice was then evaporated in vacuum chamber and samples were coated with carbon and gold-palladium mixture (two parallel samples).

In all preparation methods the sample suspensions were stirred five minutes in ultrasound bath before preparation. The ultrasound device was old, unknown model from FinnSonic.

11.1.2 Sample imaging and image analysis

All prepared pigment samples were imaged by SEM and sample concentrations were optimised. Sample imaging was made with 15 kV acceleration voltage, spot size and used magnification varied depending on the particle size.

The best preparation methods and sample concentrations were chosen to be used in image analyses. Images were saved on hard drive from which they were used in Poikki-program. INCA Feature used live images and the program imaged the samples each time when it made analysis. In Feature the best settings were found out by experimental examination. The most critical set points were pass image speeds and threshold. First pass image speed was examined between 2 and 10 µs/pix and second pass image speed was examined between 40 and 80 µs/pix. "Automate Partikkeli" function was used in Poikki-program.

The same threshold value was used in all images of the sample, but it varied between the programs. In both programs the agglomerated plastic pigments were deleted manually to find more reliable reference material.

11.2 Results and discussions

11.2.1 Sample preparation

Filtration was the best preparation method for the both pigments of the first test series. The effect of sample concentration became evident easily; higher concentrations, 30 and 60 mg/l, were too high for both pigments. 6 mg/l was too high for plastic 1 but quite good for talc. Concentration was optimised to 3 mg/l for plastic 1 and to 15 mg/l for talc which was however slightly too high. Figure 32 shows the difference between the sample concentrations 6 and 15 mg/l of the talc pigment.

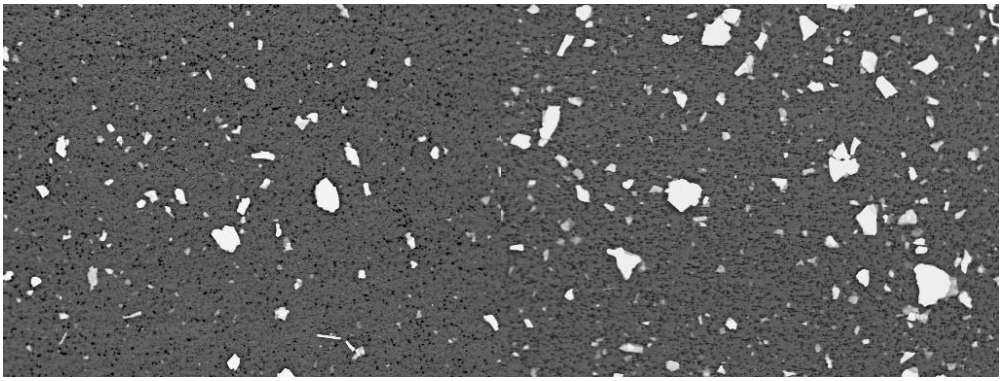

Figure 32. Filtrated talc samples. Left: 6 mg/l, 1000x, BSE, right: 15 mg/l, 1000x, BSE.

Like figure 32 showed, the risk of particle overlapping was higher when sample concentration rose from 6 mg/l to 15 mg/l. Therefore the best sample concentrations were 3 mg/l for plastic pigment and 6 mg/l for talc. The SEM images of analysed samples are showed in figure 33.

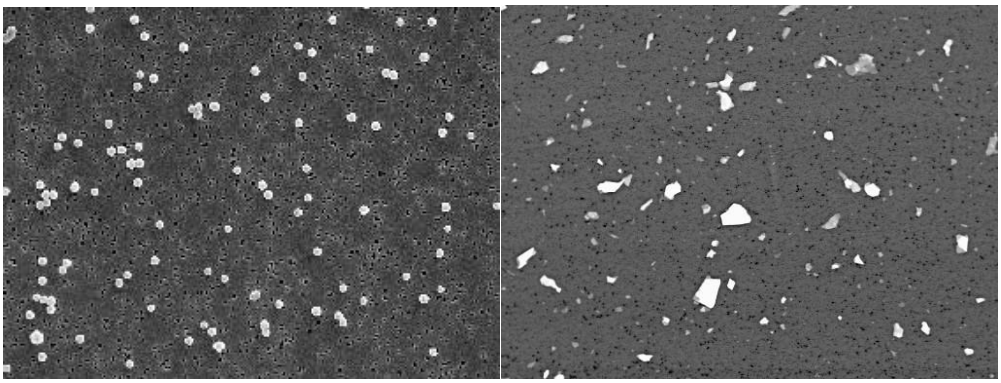

Figure 33. The SEM images of the best filtrated samples. Left: plastic 1, 3 mg/l, 4000x, SE. Right: talc, 6 mg/l, 1000x, BSE.

Spraying method needed the most development, but some signs of functionality were found in the first test series. The best base for spraying was polycarbonate membrane combined with vacuum (figure 34) and that was corresponding to filtration method.

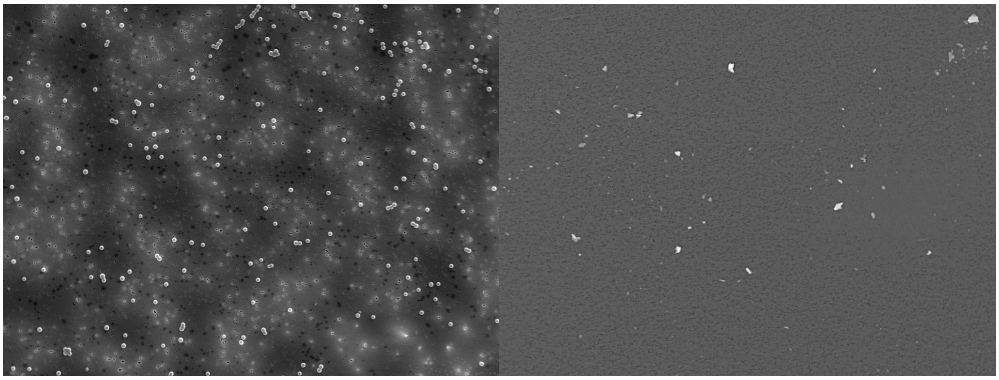

Figure 34. SEM image of pigments sprayed onto the polycarbonate membrane with vacuum. Left: plastic 1, 60 mg/l, 2000x, SE. Right: talc, 60 mg/l, 250x, BSE.

When the base was polycarbonate membrane without vacuum or mica sheet the problem was the migration of particles with liquid phase and agglomeration down to that. Mica sheet was also impractical because its chemical composition was similar to the composition of mineral pigments and deposition of particles was weak in BSE images. Laser printable transparency was surprisingly good base material especially for plastic 1 as showed in figure 35.

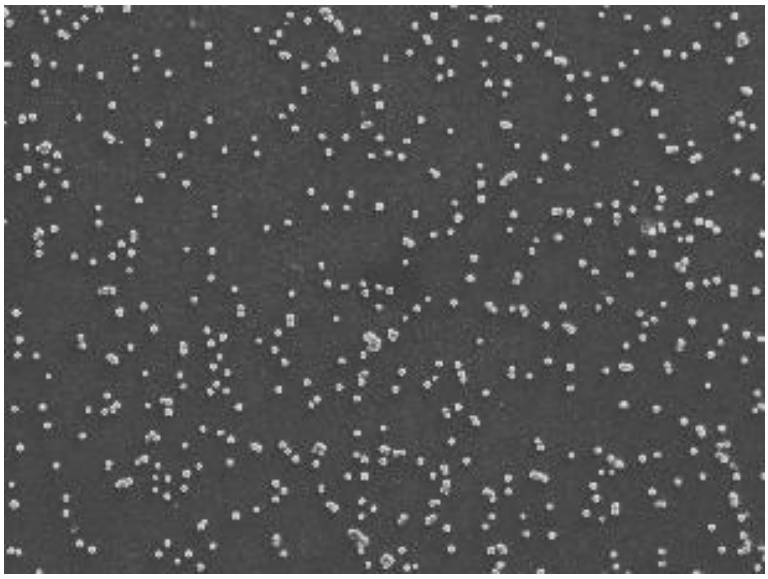

Figure 35. SEM image of plastic 1 sprayed onto the laser printable transparency, 100 mg/l, 2000x, SE.

The problem was still the weak quality of bulk product; transparency had pores and other shapes which incurred interference to the images as showed in figure 36.

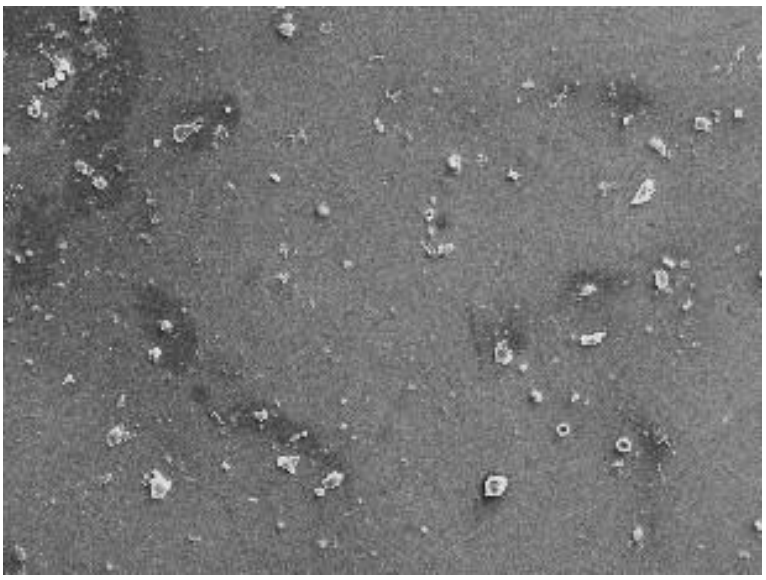

Figure 36. SEM image of talc particles sprayed onto the transparency, 150 mg/l, 250x, SE.

Freeze-drying was the most complicated preparation method. Both pigments were in aggregates which may be caused by too low heat transfer capacity of the used liquid nitrogen, by this way the freezing was too slow. Use of transmitter with higher heat transfer capacity (e.g. 1,1,1,2-tetrafluoroethane) might keep the particles separated. The aggregation was not still the only problem; the plastic particles “melt” to the large accumulations (figure 37) and the talc particles posed in vertical position (figure 38).

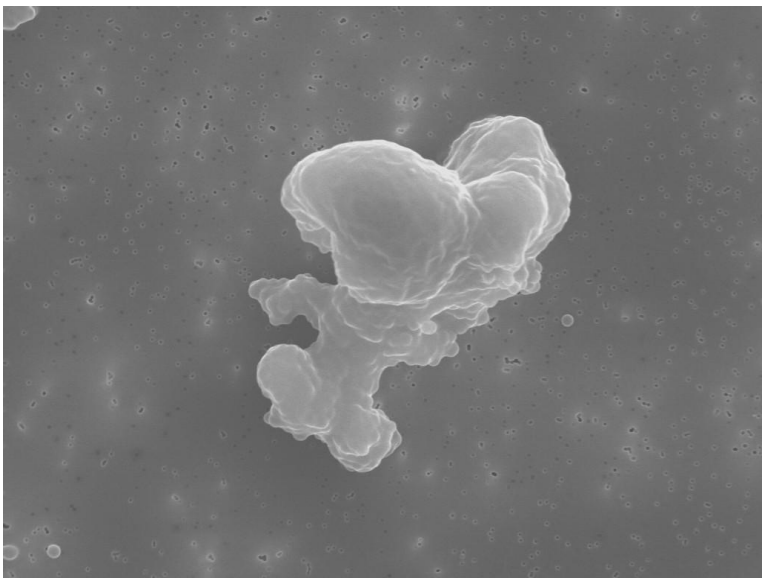

Figure 37. Freeze-dried plastic 1 particles, 6 mg/l, 4000x, SE.

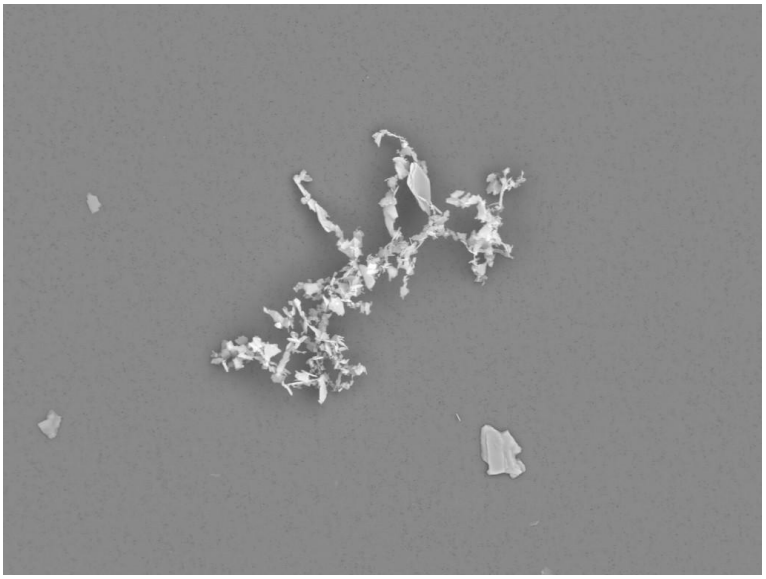

Figure 38. Freeze-dried talc particles, 30 mg/l, 500x, BSE.

As showed in figures 37 and 38, freeze-drying method was not good preparation technique for plastic and platy pigments and therefore it was not used in test series II.

11.2.2 Sample imaging and image analysis

The best samples were used in image analyses. Talc sample (6 mg/l, filtrated) was imaged with 1000x magnification and 1.0 nA spot size whereas plastic pigment sample (3 mg/l, filtrated) was imaged with 4000x magnification and 50 pA spot size. The best image quality of talc particles was attained with BSE detector, but plastic pigments stuck out better with SE detector, which was result from the low molar mass of plastic pigment.

Samples were analysed first with Feature because it is on-line analyser. Used filters were "median" in grey image processing and "erode", "dilate", "hole fill" and "remove edge touching" in binary image processing. These filters corresponded to Poikki-programs filters which enabled the comparison of programs. Feature calculated minimum expected particle size which bases on used magnification. Additional limitation in minimum particle size was ten pixels/particle. In that way the interference from the base material was tried to reduce. In Poikki-program "Automate partikkeli"-function was used and the only

needed setting was threshold. Grey and binary image processing corresponded to Feature's settings except grey image was filtered twice with 5x5 median filter.

11.2.3 Particle characterisation

Both image analysis programs showed the data of each analysed particle and data can be exported into other software. In this case the data was exported into Microsoft Excel where it was used to form particle size distributions (PSD) and statistical parameters. Figure 39 shows the cumulative basis and figure 40 shows the frequency basis particle size distribution of plastic 1. Number of particles in image analyses was 497 in Feature and 629 in Poikki-program. Both programs have measured the particles size quite similarly. Poikki-program's results have more deviation which can be seen as additional peaks in figure 40. Deviation may be caused by different threshold properties between the image analysis programs.

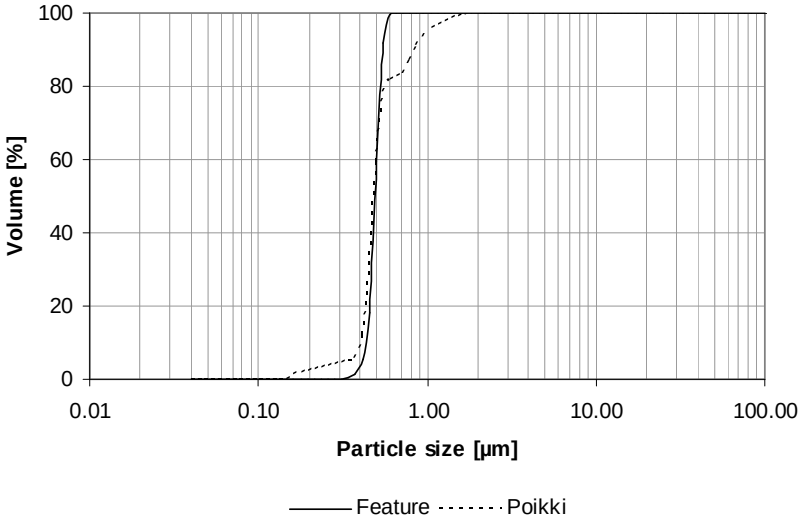

Figure 39. Cumulative basis particle size distribution of plastic 1 (3 mg/l) measured by image analyses.

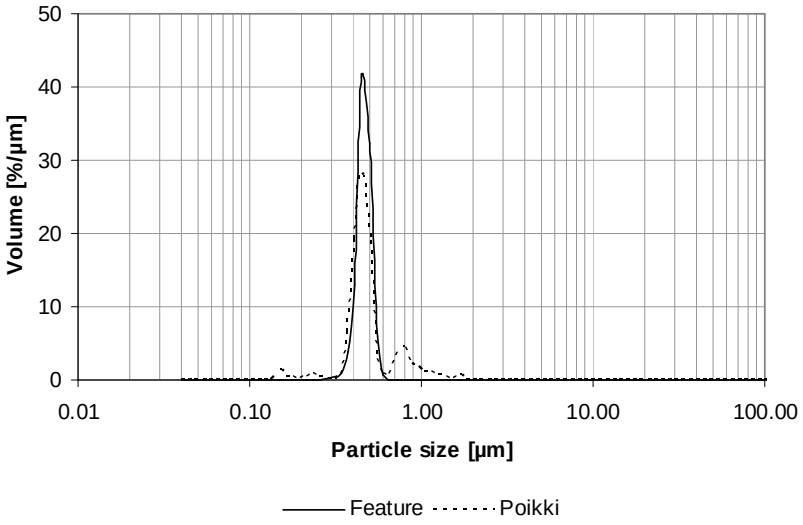

Figure 40. Frequency basis particle size distribution of plastic 1 (3 mg/l) measured by image analyses.

Table III shows some parameters of plastic 1 particle analyses. The particle size of plastic 1 was 450 nm according to pigment's supplier. Both image analysis programs calculated median particle size little larger and mean particle size differed even more from 450 nm in Poikki-programs results. Plastic particles were spherical as mentioned in table II and showed in figures 33-35. Both image analysis programs calculated shape factor; Feature 1.00 and Poikki 1.11, which was too high for spheres. Feature's result 1.00 means perfect sphere and looks very realistic.

Table III: Parameters of plastic 1 particle analyses.

Particle size	**Feature**	**Poikki**
Mean [µm]	0.49	0.55
Median [µm]	0.49	0.48
PSD, steepness		
d20/d50	93	92
d30/d70	92	87
Particle shape		
Aspect Ratio, mean	1.11	-
Shape factor, mean	1.00	1.11

Figures 41 and 42 show the cumulative and the frequency basis particle size distributions of talc pigment. Number of particles in image analyses was 849 in Feature and 839 in Poikki-program. Particle size of platy talc was complicated to specify. In image analysis the particle size was measured from two dimensional

images and it describes ECD of the largest area of the particle. Cumulative particle size distribution of talc was very similar measured by Feature and Poikki. In this case Feature detected more small particles which caused more deviation.

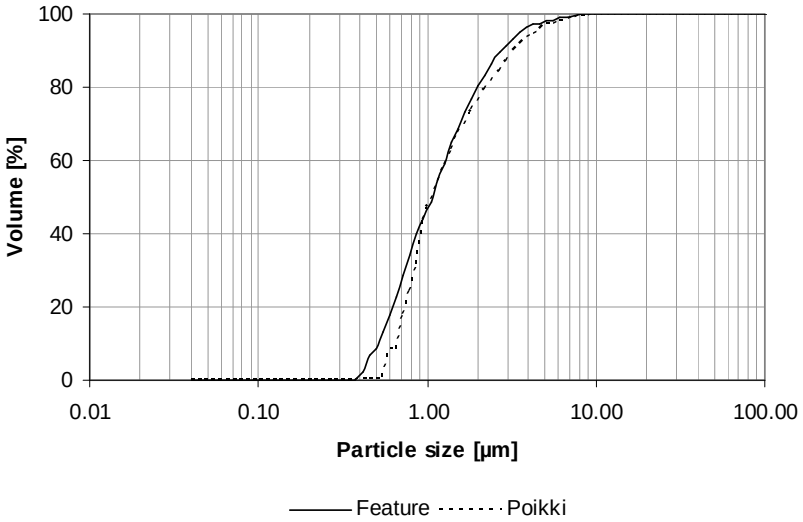

Figure 41. Cumulative basis particle size distribution of talc pigment (6 mg/l) measured by image analyses.

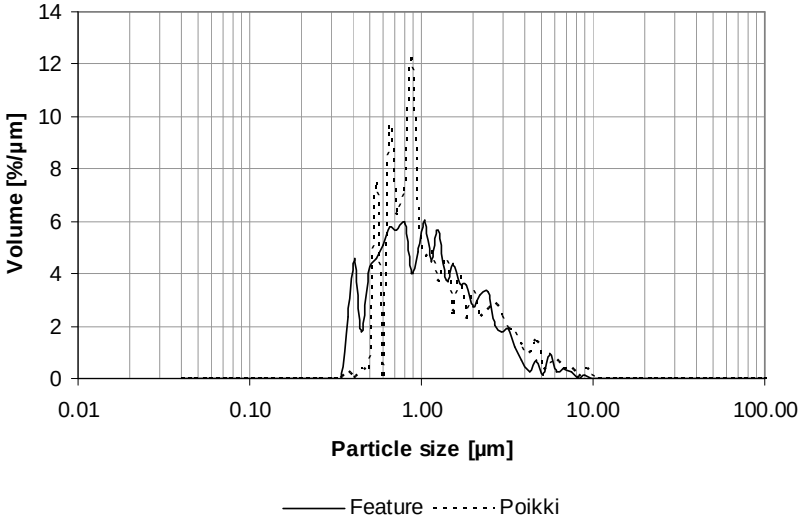

Figure 42. Frequency basis particle size distribution of talc pigment (6 mg/l) measured by image analyses.

Results of image analyses were very similar between the image analysis programs also according the parameters showed in table IV. Both particle size and particle size distribution were very similar. Only the larger number of small particles in Feature caused deviation into the mean particle size. Particle shape differed between the programs. Two parameters (aspect ratio and shape factor) in Feature described better the shape of talc particles than only shape factor in Poikki-program.

Table IV: Parameters of talc particle analyses.

Particle size	**Feature**	**Poikki**
Mean [µm]	1.42	1.60
Median [µm]	1.06	1.05
PSD, steepness		
d20/d50	59	72
d30/d70	47	51
Particle shape		
Aspect Ratio, mean	1.61	-
Shape factor, mean	1.23	1.16

12 Test series II

The second test series included seven pigments which were earlier analysed also by SediGraph 5100 and Coulter LS230.

12.1 Execution of work

12.1.1 Sample preparation

The sample preparation techniques were filtration and spraying. First sample suspension concentrations were estimated by the results of the first test series. Concentration was 15 mg/l for large particles (kaolin, cubic PCC, wollastonite and clustered aragonite), 3 mg/l for small particles (nano PCC and aragonite) and 2 mg/l for very small plastic 2 particles. Almost all pigment samples needed optimising after first inspection by SEM.

Filtration was made the same way as in test series I, but samples were coated only with gold-palladium-mixture for better image quality and faster processing of large number of samples. The most optimal concentrations were found after two

to six dilution experiments; only wollastonite was good enough after the first dilution.

Spraying method was more widely examined in the first test series; test series II examined mainly different base materials. Used base materials were polycarbonate membrane (pore size 0.015 µm), mica and cellulose film. Sample suspension was applied by freehand to control the sprayed volume and evaporation of liquid phase was accelerated with infrared lamp. Only one concentration was chosen for each pigment on the grounds of the results of the first test series.

12.1.2 Dispersing agent test

Dispersing was made with three dispersing agents which were represented in chapter 10. Used pigment was cubic PCC.

pH of used dilution water was adjusted with sodium hydroxide to about nine before addition of dispersing agent and the pigment. Ratio between the pigment and the dispersing agent was 1:1 and 1:10. Suspensions were stirred five minutes in ultrasound bath before filtration. Samples were coated with gold-palladium-mixture and imaged by SEM.

12.1.3 Comparison of ultrasound baths

Clustered aragonite pigment was used for comparison of ultrasound baths because it seemed to break down when stirred with ultrasound. Normally, all pigment samples were stirred five minutes in ultrasound bath before preparation for image analyses and ten minutes before analysing by laser diffraction and sedimentation. The ultrasound devices were different types and therefore their effects to the particles were examined.

The concentrations were 25, 50 and 100 mg/l. One sample of each concentration was stirred ten minutes in the old ultrasound bath (unknown model from FinnSonic) and the other was stirred ten minutes in the model m03 (FinnSonic) ultrasound bath. Stirred samples were filtrated onto the polycarbonate membrane (V=5 ml, pore size 0.2 µm), coated with gold-palladium-mixture and imaged by SEM.

12.1.4 Sample imaging and image analysis

The best samples for image analyses were imaged by LEO 1450EP SEM. The acceleration voltage was 15 kV, magnification and spot size varied between the samples as showed in table V.

Table V: The settings in sample scanning in LEO 1450EP.

Pigment	Magnification	Spot size	Detector	Fields
Kaolin 1	1500x	1.0 nA	BSE	6
Kaolin 2	500x	1.0 nA	BSE	6
Cubic PCC*	1500x	1.0 nA	BSE	7
Aragonite	1500x	50 pA	SE	9
Wollastonite	250x	1.0 nA	BSE	8
Clustered aragonite	750x	244 pA	SE	30
Plastic 2	4000x	50 pA	SE	5
Plastic blend	3500x	50 pA	SE	5

* Dispersed with 8000 g/mol maleic acid.

Particle analyses were made one field (image) at the time, because the same images were analysed by Poikki-program also and needed to be saved in hard drive for that. "Rectangle" and "line" area modes of Feature were examined also. In these cases used electron microscope was JEOL JSM-5900LV.

12.1.5 3D-modelling of pigment particles

3D-modelling was started by imaging the samples by JEOL JSM-5900LV SEM. Imaging was made as normally except the samples were tilted. Table VI shows the used magnifications and tilt angles.

Table VI: Specifications of SEM set-points for 3D-modelling.

Pigment	Magnification	Detector	Tilt
Wollastonite	750x	BSE	-5°, 0°, +5°
Wollastonite	2000x	BSE	-8°, 0°, +8°
Aragonite	9000x	SE	-7°, 0°, +7°
Kaolin 1	7500x	SE	-7°, 0°, +7°
Kaolin 2	4000x	SE	-7°, 0°, +7°

3D-models of wollastonite based on both two and three images. Aragonite and kaolin models were based on three images only. Needed dimensions of pigment particles were measured manually from 3D-models.

12.2 Results and discussions

12.2.1 Sample preparation

The best preparation method for most pigments was *filtration*. Only clustered aragonite and aragonite were analysed from sprayed samples. Filtration was easy to do and repeatability was very good because method did not have any unclear stages. The filters had pore size 0.2 µm which caused interruption when high magnifications (>2000x, depended on particle size) were used. Smaller pore sizes cause less interruption but they have own limitations. Pore sizes 0.015 µm and 0.05 µm were also examined but 0.015 µm was too small because water and ethanol did not penetrate it. Filtration through the 0.05 µm pores was too slow and aggregation happened. Figures 43-45 show the SEM images of pigment samples prepared with filtration.

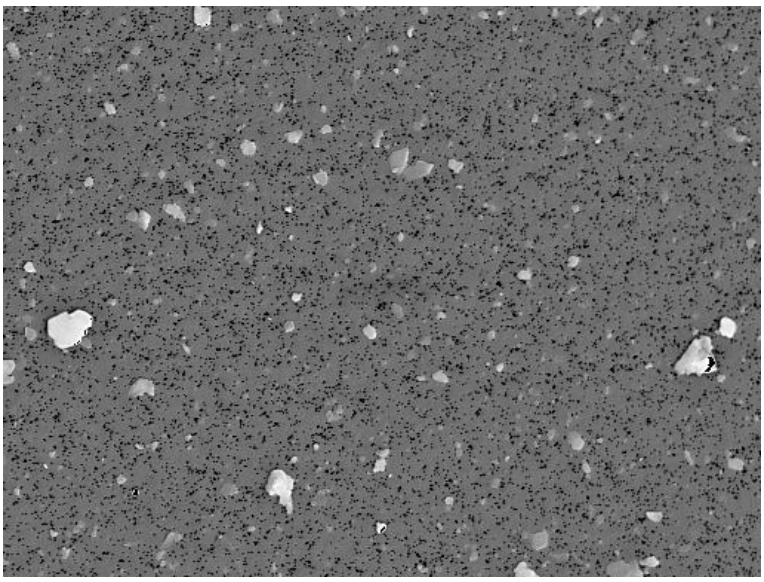

Figure 43. SEM image of kaolin 1 prepared with filtration, 5 mg/l, 1500x BSE.

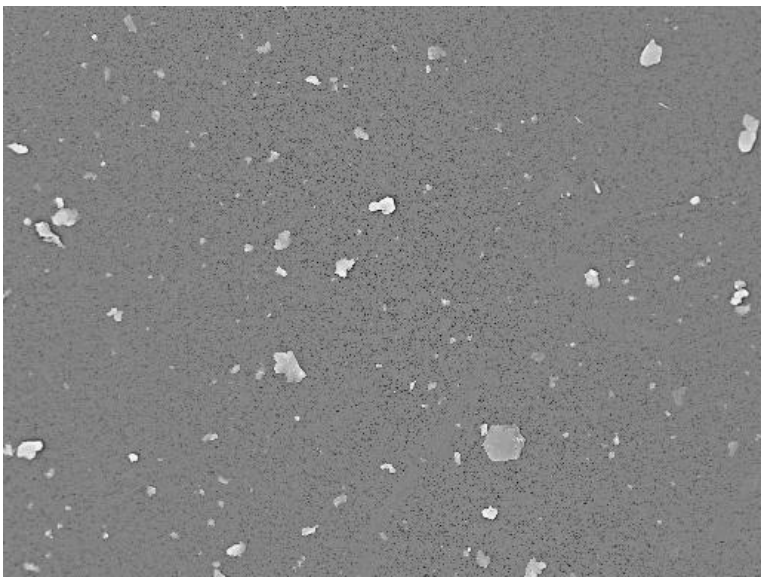

Figure 44. SEM image of kaolin 2 prepared with filtration, 5 mg/l, 500x BSE.

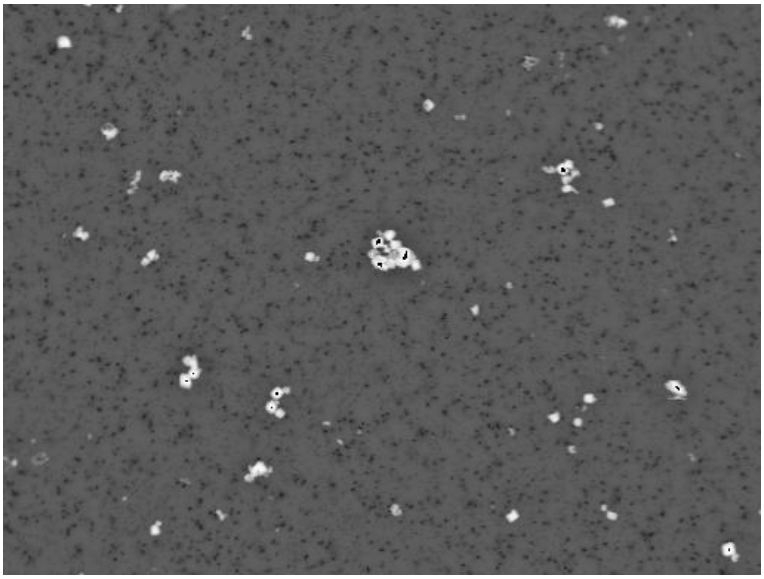

Figure 45. SEM image of cubic PCC (no dispersing agent) prepared with filtration, 15 mg/l, 1500x BSE.

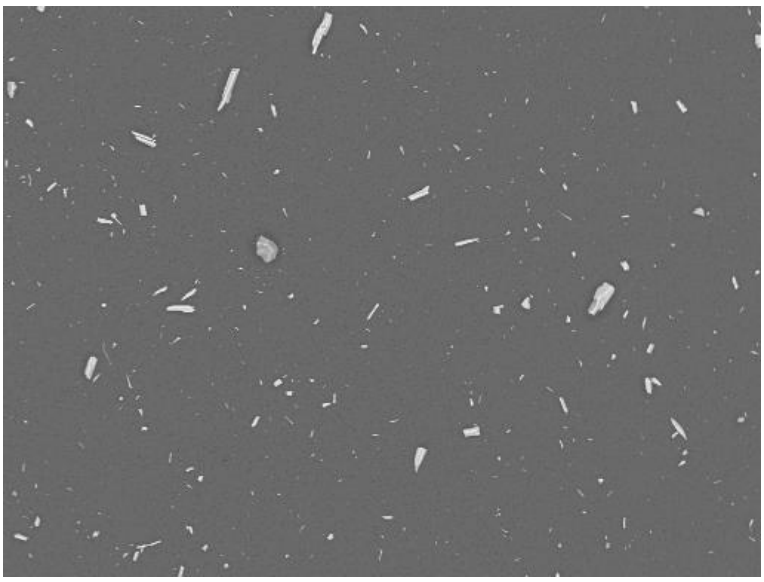

Figure 46. SEM image of wollastonite prepared with filtration, 15 mg/l, 250x BSE.

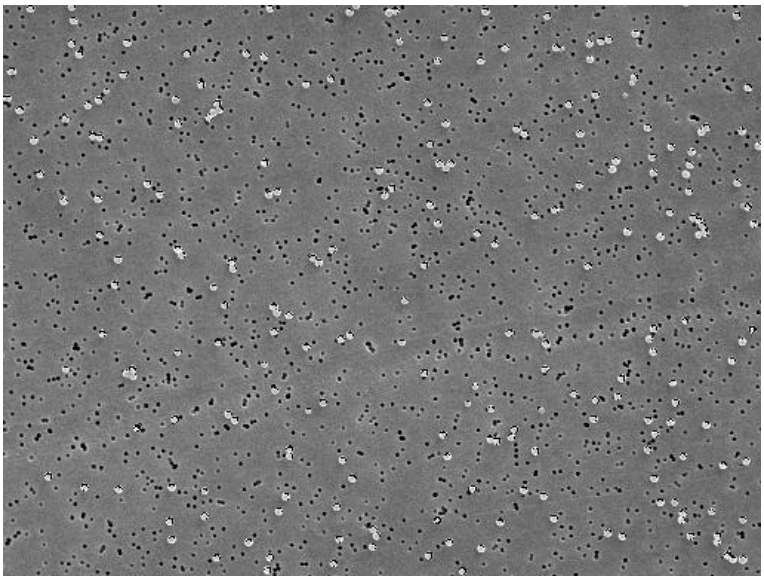

Figure 47. SEM image of plastic 2 prepared with filtration, 1 mg/l, 4000x SE.

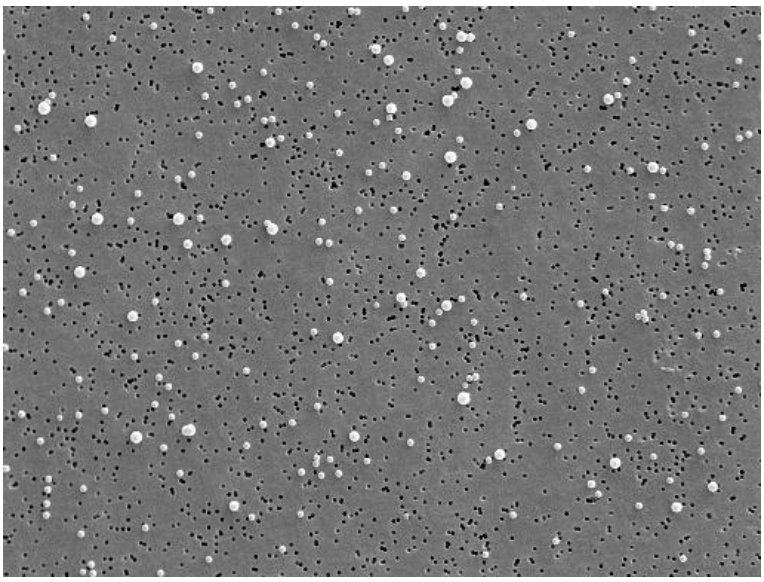

Figure 48. SEM image of plastic blend prepared with filtration, 1 mg/l, 3500x SE.

As figures 43-48 show, filtration method gave very uniform samples without aggregation of the particles. Samples still had some empty areas which disturbed use of "rectangle" and "line" modes in Feature analysis.

Spraying was examined with different base materials; polycarbonate membrane, mica and cellophane. Aragonite stuck out better on the mica layer than on the polycarbonate membrane in filtration. Particles were still aggregated and choosing of analysing area needed to be done very carefully. Figure 49 shows SEM image of sprayed aragonite sample. The best clustered aragonite sample was sprayed onto the polycarbonate membrane. Clustered particles were separated very well and no individual, needle-like particles were visualised as can be seen in figure 50.

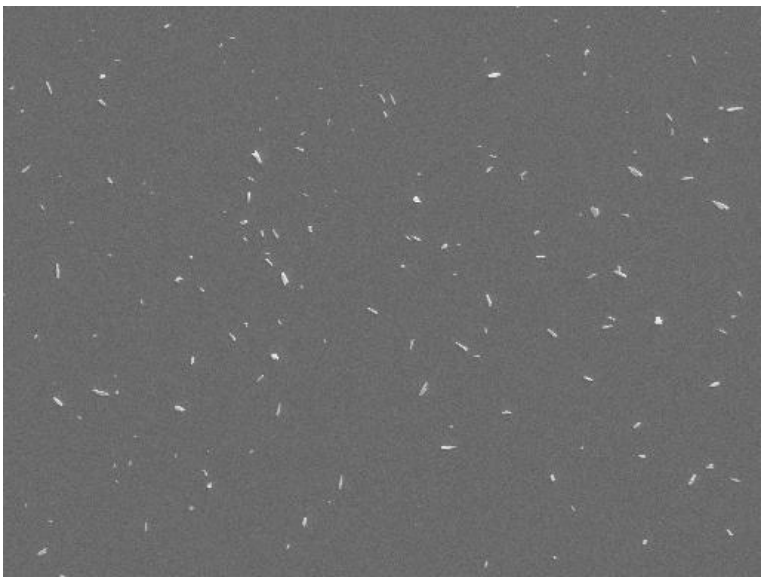

Figure 49. SEM image of aragonite prepared with spraying, 100 mg/l, 1500x SE.

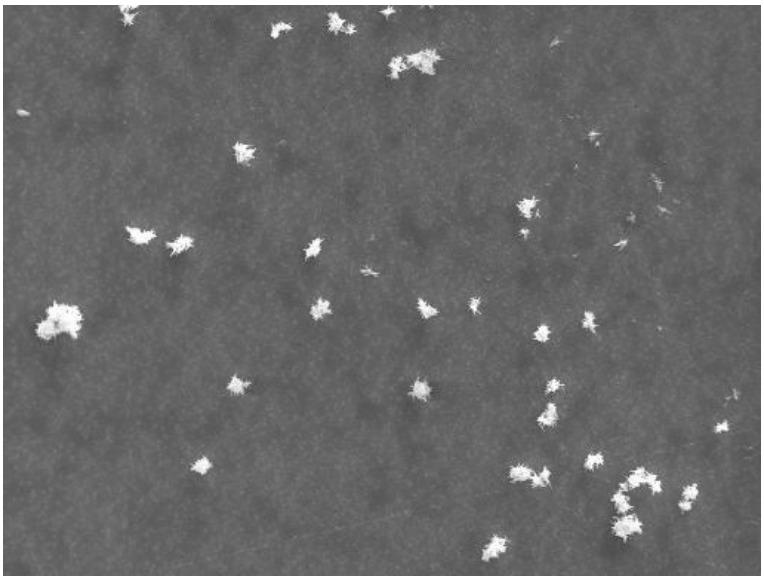

Figure 50. SEM image of clustered aragonite prepared with spraying, 150 mg/l, 750x SE.

Dispersing agent test was made with cubic PCC (15 mg/l) which seemed to be aggregated if any dispersing agent was not used as in figure 51.

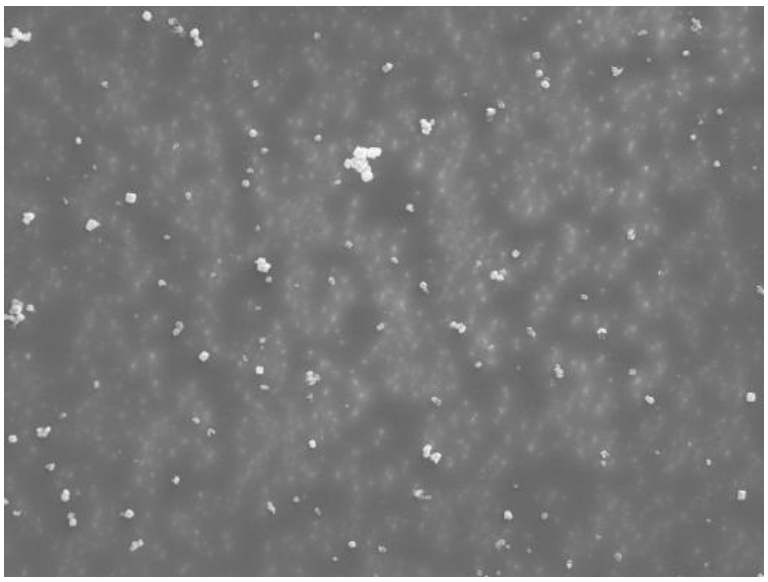

Figure 51. SEM image of cubic PCC without dispersing, 1000x SE.

Figures 52-57 show the SEM images of dispersed samples.

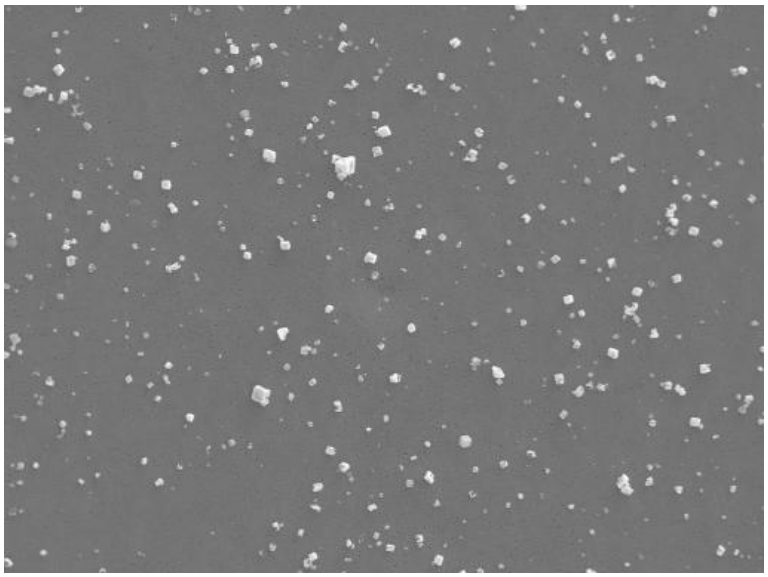

Figure 52. SEM image of cubic PCC dispersed with 28000 g/mol acrylic acid, 1:1, 1000x SE.

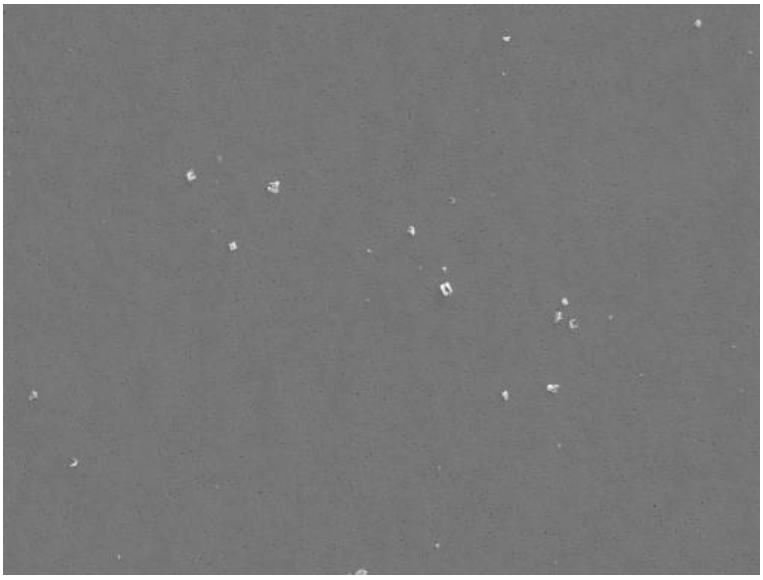

Figure 53. SEM image of cubic PCC dispersed with 28000 g/mol acrylic acid, 1:10, 1000x SE.

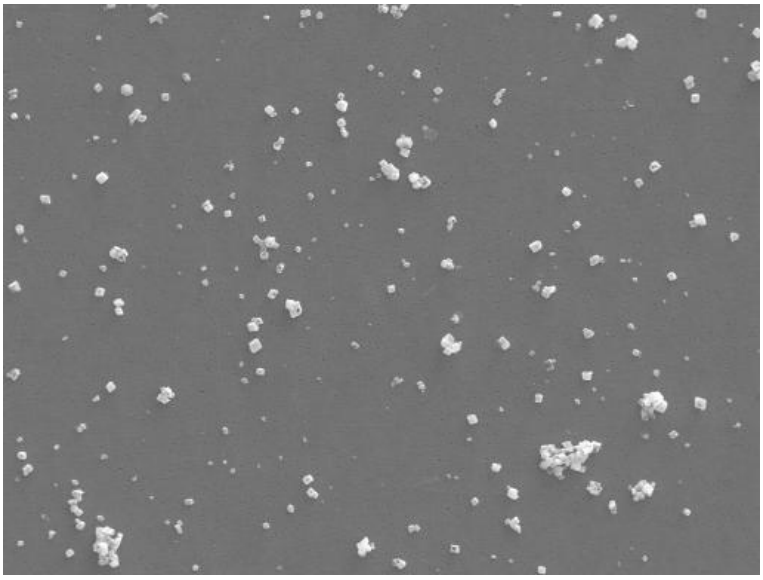

Figure 54. SEM image of cubic PCC dispersed with 130000 g/mol acrylic acid, 1:1, 1000x SE.

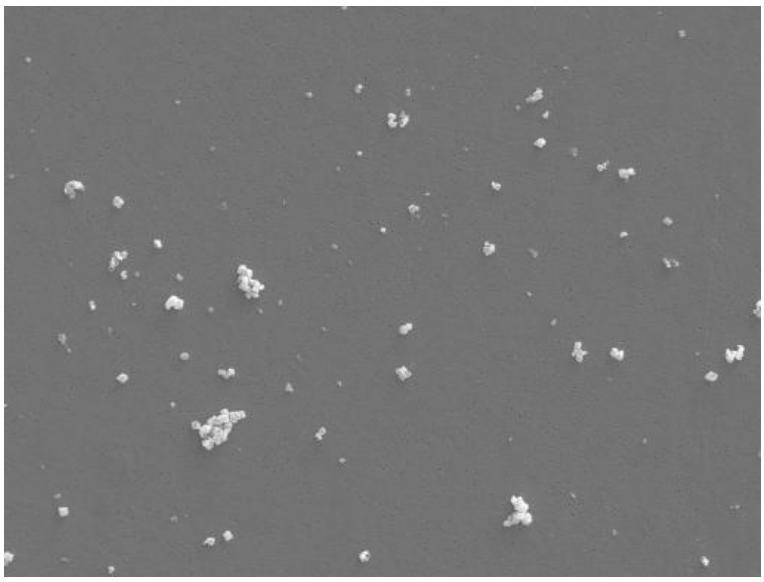

Figure 55. SEM image of cubic PCC dispersed with 130000 g/mol acrylic acid, 1:10, 1000x SE.

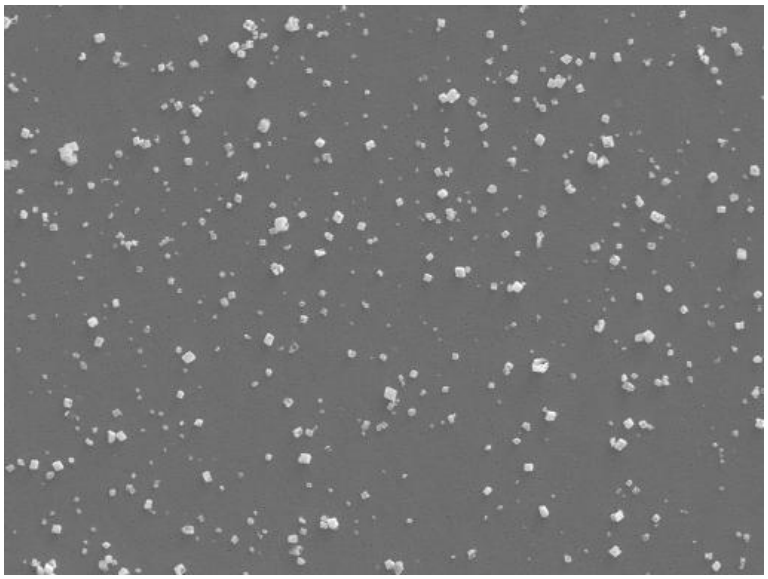

Figure 56. SEM image of cubic PCC dispersed with 8000 g/mol maleic acid, 1:1, 1000x SE.

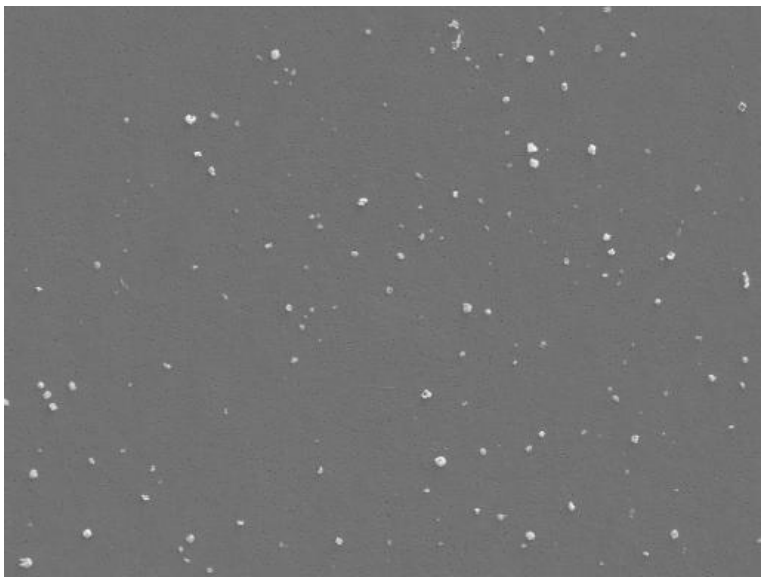

Figure 57. SEM image of KPCC-87 dispersed with 8000 g/mol maleic acid, 1:10, 1000x SE.

According to visualisation of dispersed samples (figures 52-57), all three dispersing agents had a very similar effect. Number of particles in one field (image) seemed to be increased when pigment-dispersing agent ratio was 1:1. Ratio 1:10 was too high because the number of particles seemed to be even lower than without any dispersing. The best sample was dispersed with 8000 g/mol maleic acid (figure 56) and it was used in image analyses whose results are shown in figures 58 and 59 and in table VI. The figures and the table include also results of image analyses of cubic PCC without any dispersing agent.

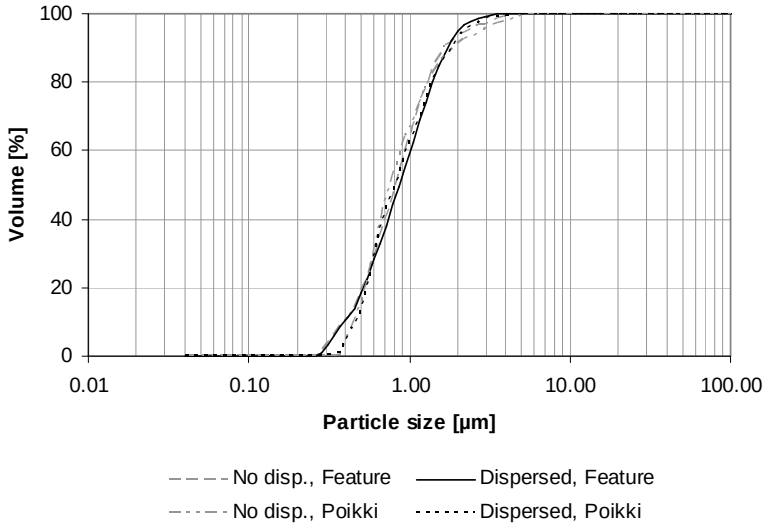

Figure 58. Cumulative basis particle size distribution of cubic PCC measured by image analyses.

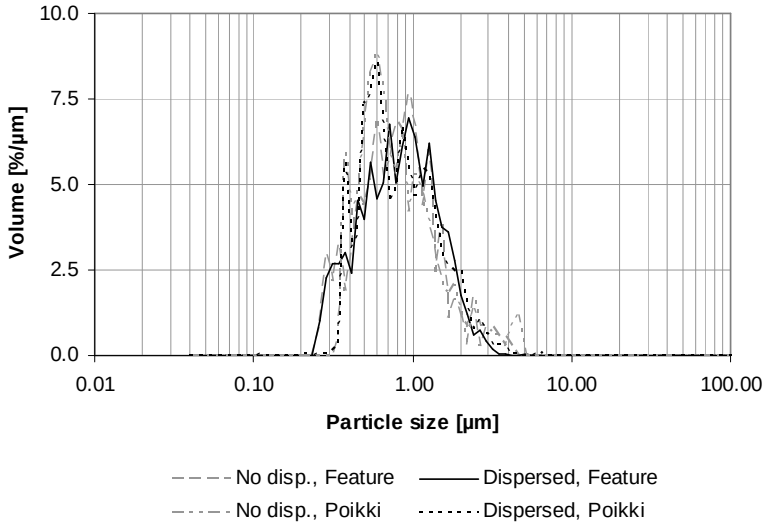

Figure 59. Frequency basis particle size distribution of cubic PCC measured by image analyses.

Table VII: Results of cubic PCC image analyses.

	No dispersing agent		8000 g/mol mal. acid	
Particle size	**Feature**	**Poikki**	**Feature**	**Poikki**
Mean [µm]	0.98	1.04	0.99	1.01
Median [µm]	0.85	0.77	0.87	0.82
PSD, steepness				
d20/d50	61	69	59	66
d30/d70	57	54	53	53
Particle shape				
Aspect Ratio, mean	1.44	-	1.41	-
Shape factor, mean	1.23	1.16	1.22	1.13

As figures 58 and 59 show, the particle size distribution of cubic PCC was similar regardless of the use of dispersing agent. The particle shape was also similar in both cases although the number of measured particles increased from 365 to 1407 in Feature and from 338 to 1310 in Poikki-program when dispersing agent was used. Therefore the only benefit of dispersing was that less measurement points were needed in image analysis.

Ultrasound baths were compared with clustered aragonite. All filtrated samples were scanned by SEM to analyse the effect of ultrasound to clustered particles. Figures 60-62 show the SEM images of clustered aragonite which concentration was 25 mg/l.

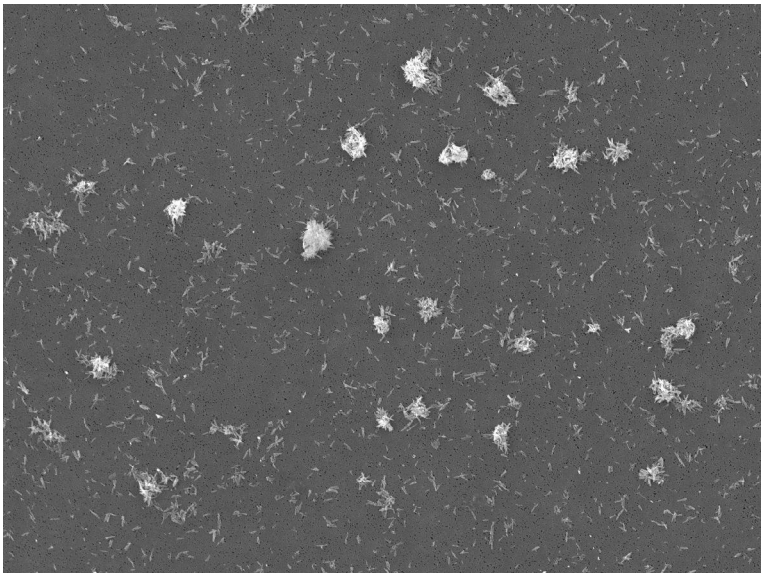

Figure 60. SEM image of clustered aragonite, 25 mg/l, no ultrasound, 1000x SE.

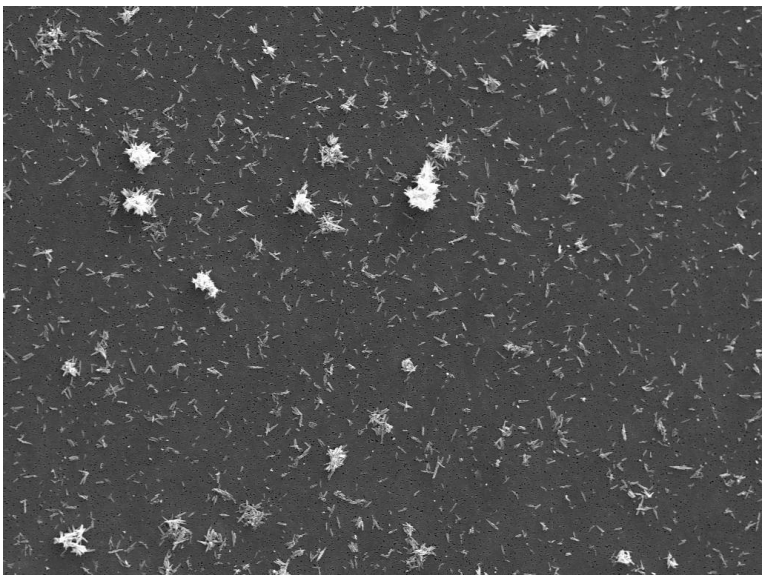

Figure 61. SEM image of clustered aragonite, 25 mg/l, "old" ultrasound, 1000x SE.

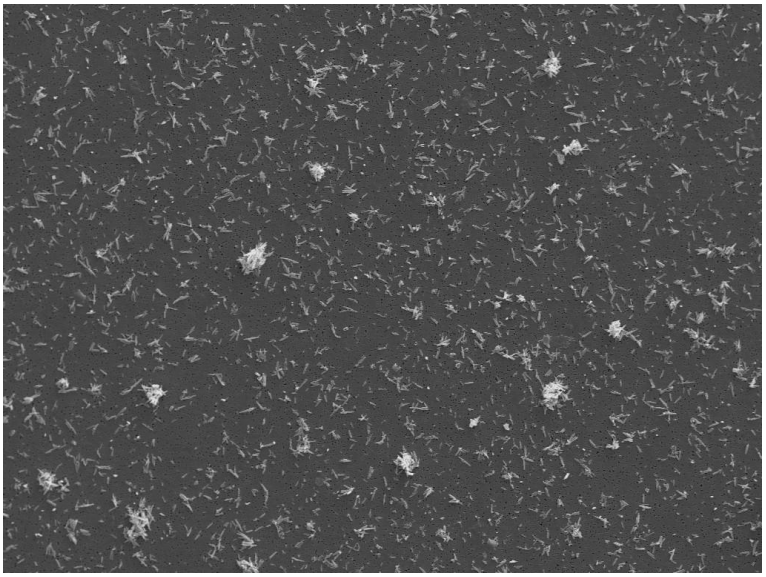

Figure 62. SEM image of clustered aragonite, 25 mg/l, m03 ultrasound, 1000x SE.

Clustered aragonite included individual, needle-like particles already before ultrasound bath as can be seen in figure 60. The old ultrasound device broke clusters slightly and m03 device broke even more. Figures 63-65 show SEM images of clustered aragonite which concentration was 50 mg/l.

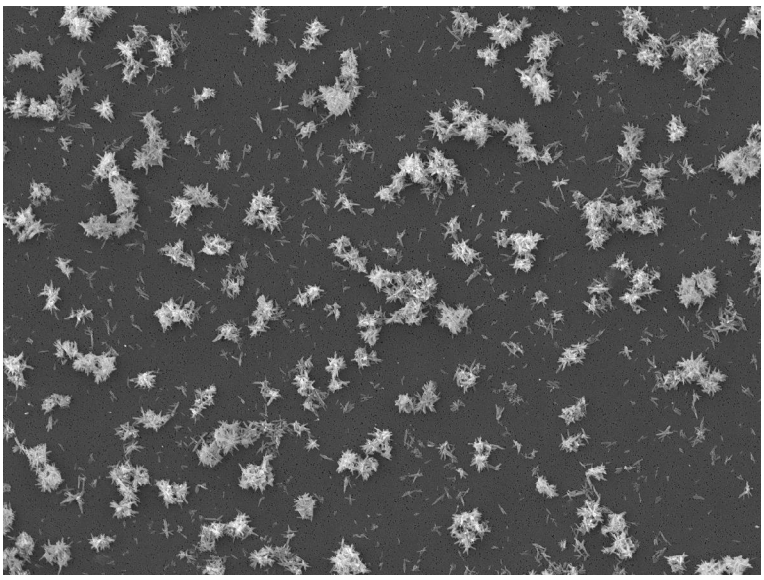

Figure 63. SEM image of clustered aragonite, 50 mg/l, no ultrasound, 1000x SE.

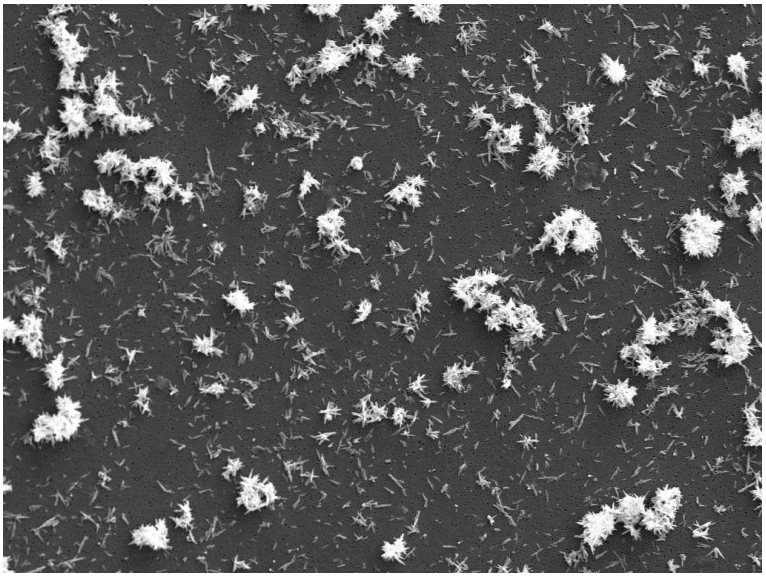

Figure 64. SEM image of clustered aragonite, 50 mg/l, "old" ultrasound, 1000x SE.

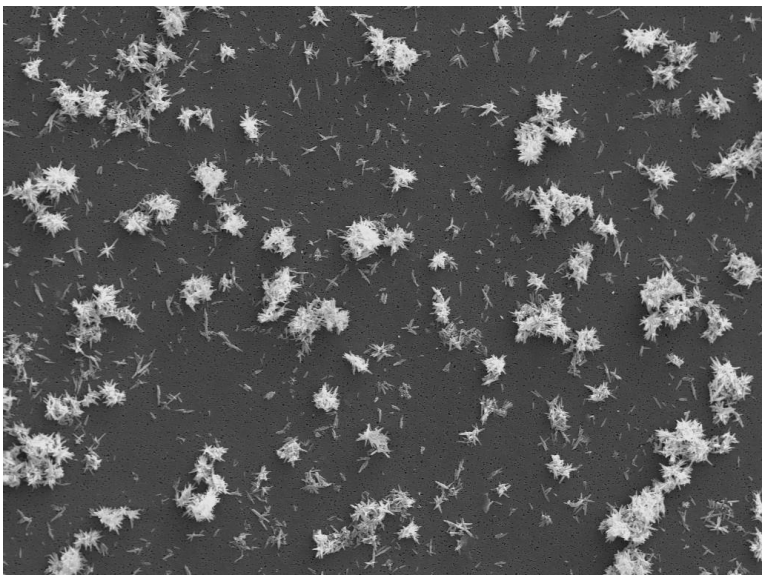

Figure 65. SEM image of clustered aragonite, 50 mg/l, m03 ultrasound, 1000x SE.

When sample concentration increased from 25 mg/l to 50 mg/l, the effect of ultrasound devices inversed. The old ultrasound device seemed to break clusters more than m03 ultrasound. The number of individual particles was almost the same without ultrasound and after ten minutes stirring in m03 ultrasound device, but much more numerous when the old ultrasound device was used. The highest concentration was 100 mg/l which SEM images are showed in figures 66-68.

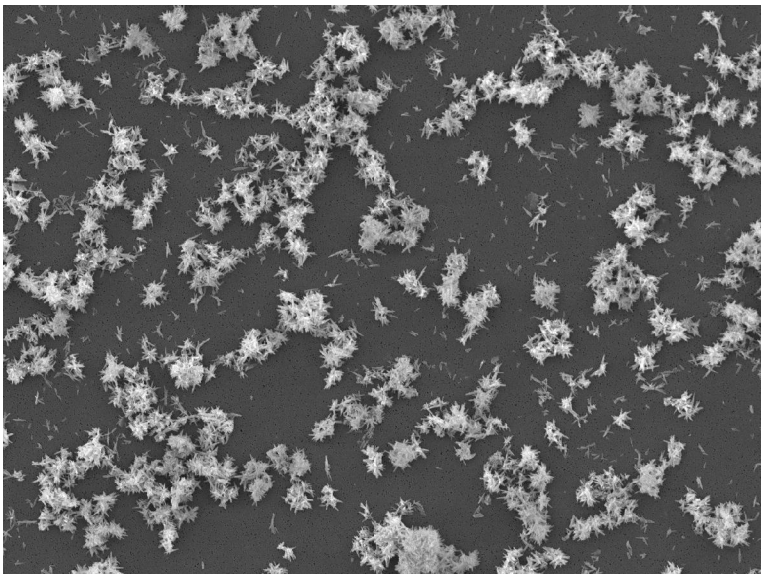

Figure 66. SEM image of clustered aragonite, 100 mg/l, no ultrasound, 1000x SE.

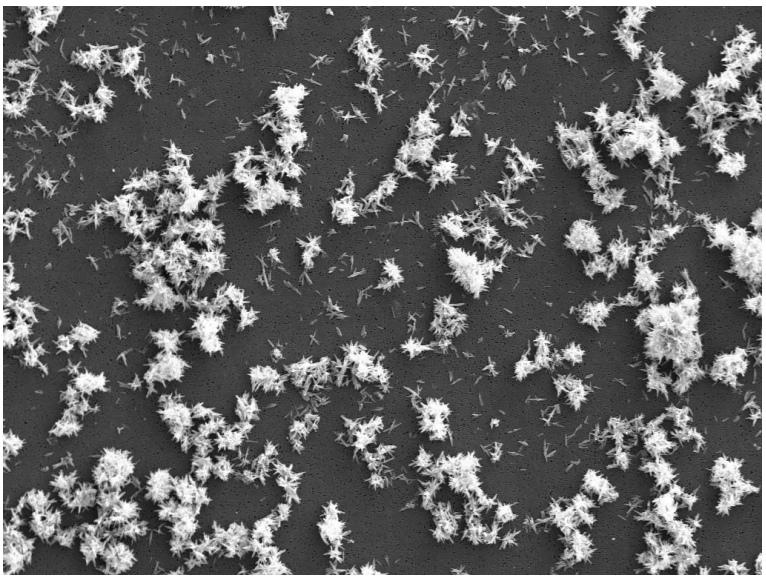

Figure 67. SEM image of clustered aragonite, 100 mg/l, "old" ultrasound, 1000x SE.

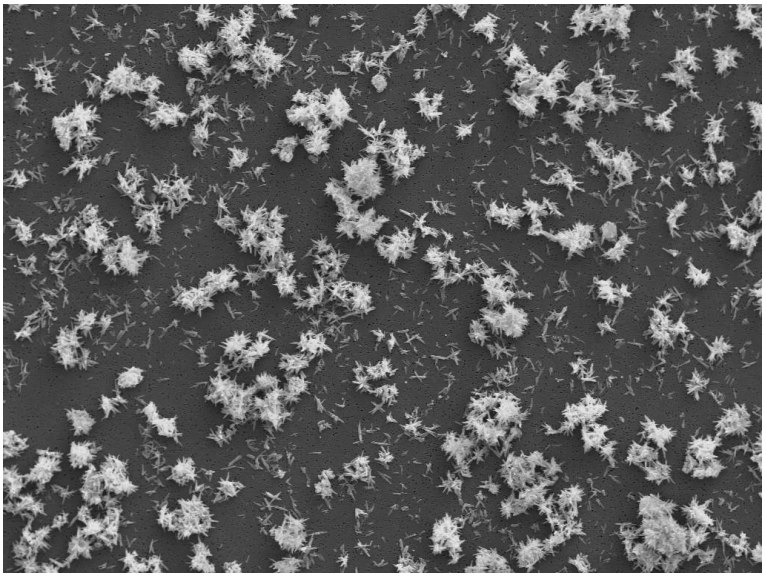

Figure 68. SEM image of clustered aragonite, 100 mg/l, m03 ultrasound, 1000x SE.

When sample concentration was 100 mg/l, aragonite clusters seemed to be broken once again more when m03 ultrasound device was used. To be base on figures 60-68 it is very difficult to notice which one of ultrasound devices broke particles more. When different sample concentrations are compared, it seems that higher concentrations have less individual, needle-like particles than the lowest concentration. Individual particles may be aggregated to already clustered particles or large clusters hide them in SEM images. Image analysis needs very low concentration when individual, needle-like particles cause deviation to results but laser diffraction and sedimentation are carried out in higher concentrations when influence to results may be smaller. The observations of ultrasound bath comparison base on visualisation of SEM images and image analysis was not made because concentrations were so high that results would have been unreliable.

12.2.2 Sample imaging

Different analysing areas were examined with wollastonite sample. Rectangle (based on 2 and 4 defined angles) and line modes were good ways to analyse larger number of particles. Line mode was better because the analysing area could be visualised before analysis and empty areas could be avoided that way. Analyses of larger areas needed uniform sample which can be prepared by filtration. The most important target of analysing area tests was possible differences in results depending on number of test points. Four point rectangle area was defined so that the total number of fields was 91, but analysis needed to stop after 19 fields because the running time was over nine hours. Normally, image analysis of one pigment takes about four hours including sample preparation. The number of particles in normal analysis was 976 and in rectangle test 3517. Figures 69 and 70 show the particle size distribution of wollastonite analysed with different sample sizes. Table VIII shows the parameters of particle analyses of wollastonite.

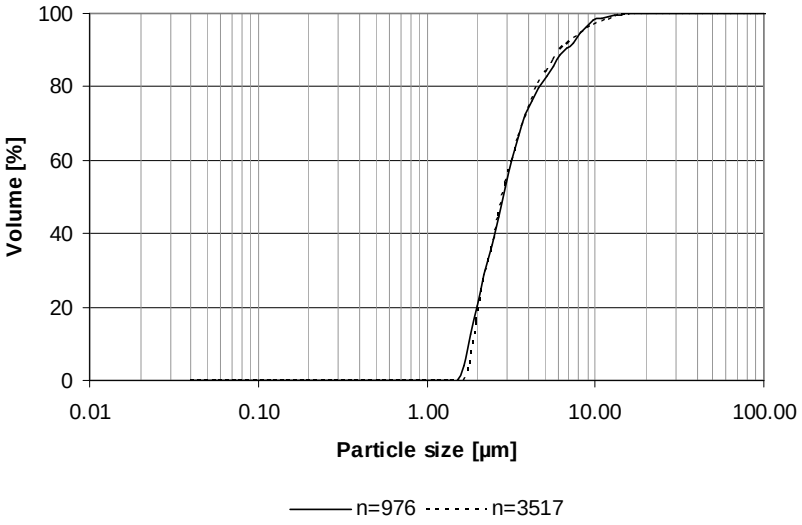

Figure 69. Cumulative basis particle size distribution of wollastonite (15 mg/l) analysed with different sample sizes.

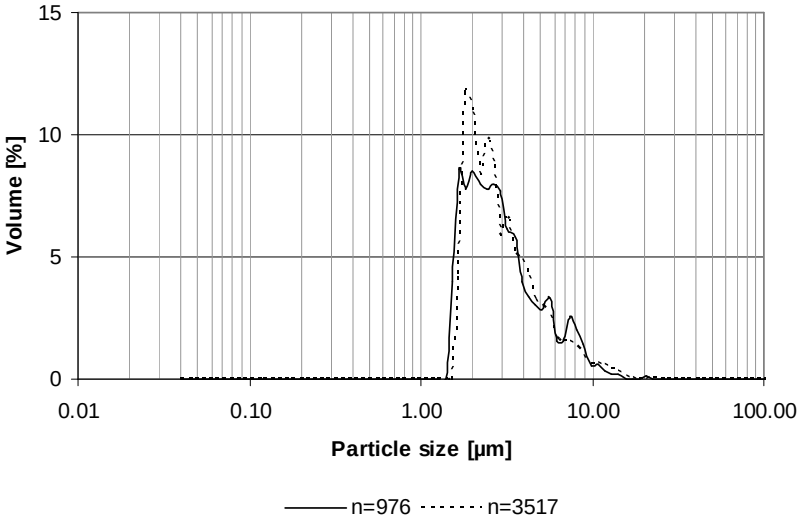

Figure 70. Frequency basis particle size distribution of wollastonite (15 mg/l) analysed with different sample sizes.

Table VIII: The parameters of particle analyses of wollastonite with different sample sizes.

	n = 976	**n = 3517**
Mean particle size	3.57 µm	3.62 µm
Median particle size	2.79 µm	2.81 µm
Aspect ratio, mean	2.19	2.08
Sd	0.91	0.96
Shape, mean	1.42	1.40
Sd	0.48	0.69

Particle size distributions and the parameters of particle analyses showed that the differences in results between the sample sizes were small. Figure 71 shows differences in standard deviation of particle size and in mean particle size when sample size differed between 500 and 3000 particles.

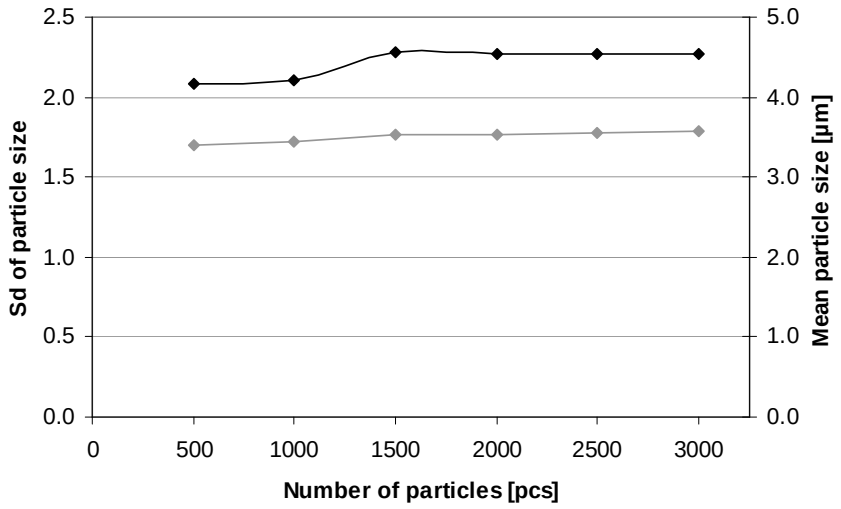

Figure 71. Effect of sample size to standard deviation of particle size and to mean particle size of wollastonite pigment.

Standard deviation increased a little when sample size rose from 1000 to 1500 particles and stayed stable until sample size was 3000 particles. Mean particle size rose until sample size was 1500 particles and after that the rising slowed down substantially. According to results of particle analyses and figure 71, about 1500 particles are enough in image analysis to get reliable results.

12.2.3 Particle characterisation by different methods

The best samples were used for image analyses in Feature and Poikki programs. The number of particles in image analyses varied between the pigments as table IX shows.

Table IX: The number of particles in image analyses.

	Number of particles	
	Feature	**Poikki**
Kaolin 1	956	1747
Kaolin 2	870	975
Cubic PCC	365 / 1632*	338 / 1518*
Aragonite	952	1034
Wollastonite	976	1218
Clustered aragonite	1114	1186
Plastic 2	1083	1075
Plastic blend	1056	1045

* dispersed with 8000 g/mol maleic acid

Figure 72 shows an example of Kaolin 1 particles and figures 73 and 74 show the particle size distribution of kaolin 1 (5 mg/l). Parameters of particle analyses are showed in table X. Sample size was 956 particles in Feature and 1747 particles in Poikki-program.

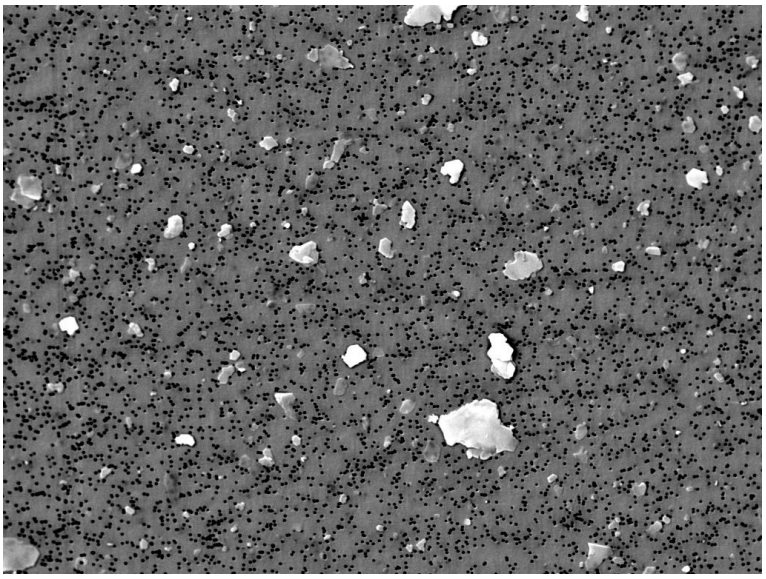

Figure 72. SEM image of kaolin 1 particles.

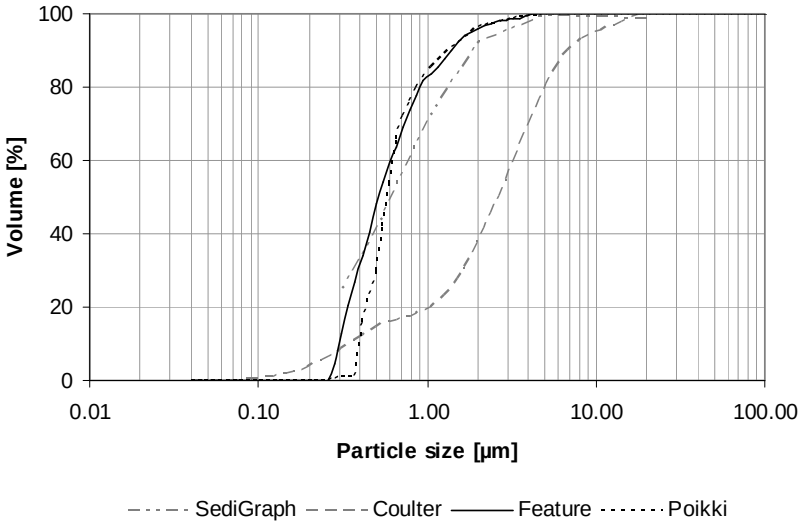

Figure 73. Cumulative basis particle size distribution of kaolin 1 measured by different methods.

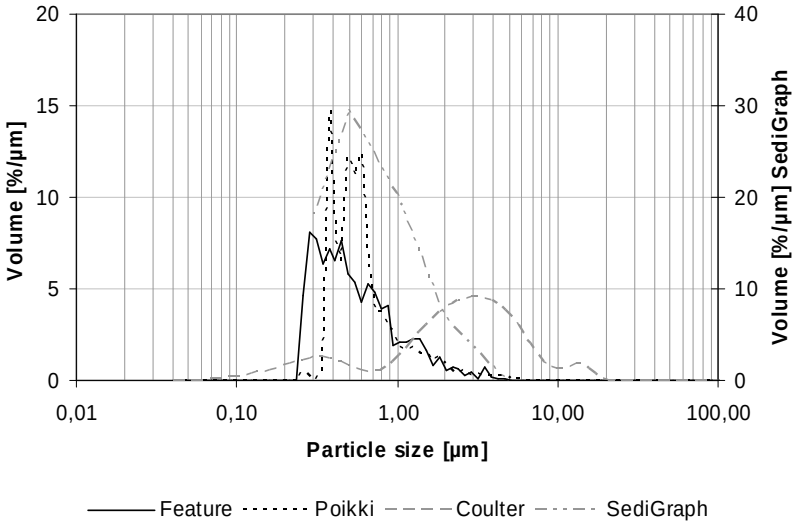

Figure 74. Frequency basis particle size distribution of kaolin 1 measured by different methods.

Table X: The parameters of kaolin 1 particle analyses.

Particle size	**SediGraph**	**Coulter**	**Feature**	**Poikki**
% < 0.1 µm	-	0.5	0.0	0.0
% < 0.3 µm	24.0	8.1	12.7	0.6
% < 0.5 µm	42.2	14.5	48.2	32.5
% < 1.0 µm	72.1	19.4	82.6	84.7
% < 2.0 µm	92.6	37.7	95.9	96.1
% < 5.0 µm	99.9	79.9	100.0	99.9
Mean [µm]	-	3.41	0.72	0.76
Median [µm]	0.6	2.63	0.51	0.58
Sd	-	3.19	0.59	0.58
Area, mean [μm^2]	-	-	0.68	0.61
Sd	-	-	1.61	1.34
Perimeter, mean [µm]	-	-	2.65	-
Sd	-	-	2.53	-
Length, mean [µm]	-	-	1.00	-
Sd	-	-	0.82	-
Breadth, mean [µm]	-	-	0.65	-
Sd	-	-	0.56	-
PSD, steepness				
d20/d50	41	40	65	78
d30/d70	38	41	53	68
Particle shape				
Aspect Ratio, mean	-	-	1.56	-
Sd	-	-	0.33	-
Shape factor, mean	-	-	1.28	1.12
Sd	-	-	0.43	0.07

As figures 73 and 74 and table X show, the results of particle analyses were very similar between the image analysis programs. Feature had analysed more small particles than Poikki-program as in case of platy talc pigment in test series I also. Mean particle size was slightly over 0.7 µm when median particle size was a little over 0.5 µm. The both steepness values of particle size distribution were higher when measured by Poikki-program. Aspect ratio and shape factor gave misleading values because the thickness of particles was not measured. The value of aspect ratio gave information only about the shape of largest area of the platy particle. Differences in the results of Coulter and image analyses were large, but the results of SediGraph and image analyses were very similar.

Figure 75 shows an example of kaolin 2 particles and figures 76 and 77 show the particle size distribution of kaolin 2 (15 mg/l). Table XI shows the parameters of particle analyses. Sample size was 870 particles in Feature and 975 particles in Poikki-program.

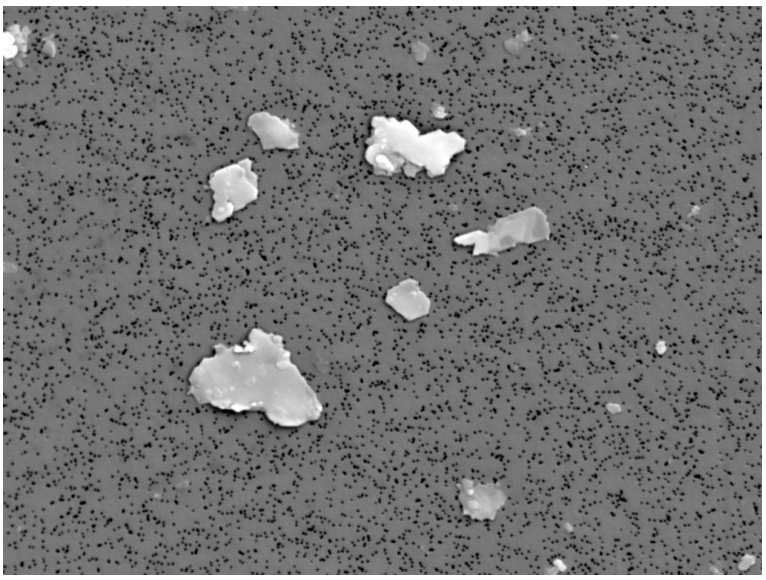

Figure 75. SEM image of kaolin 2 particles.

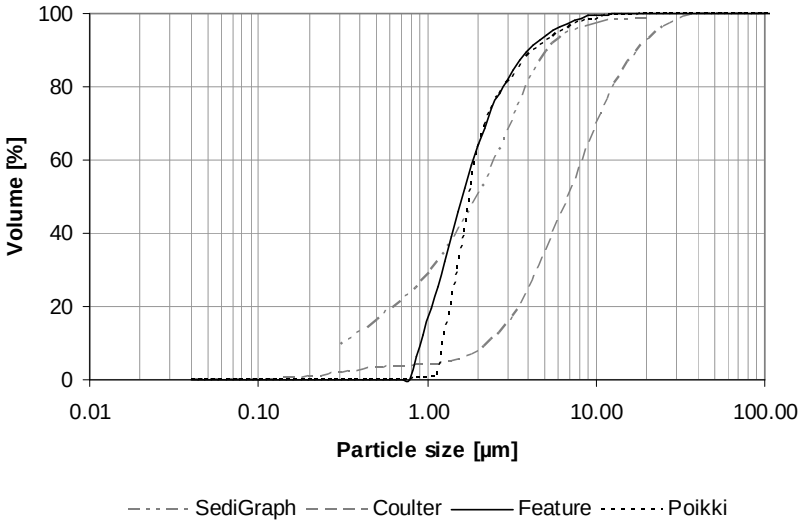

Figure 76. Cumulative basis particle size distribution of kaolin 2 measured by different methods.

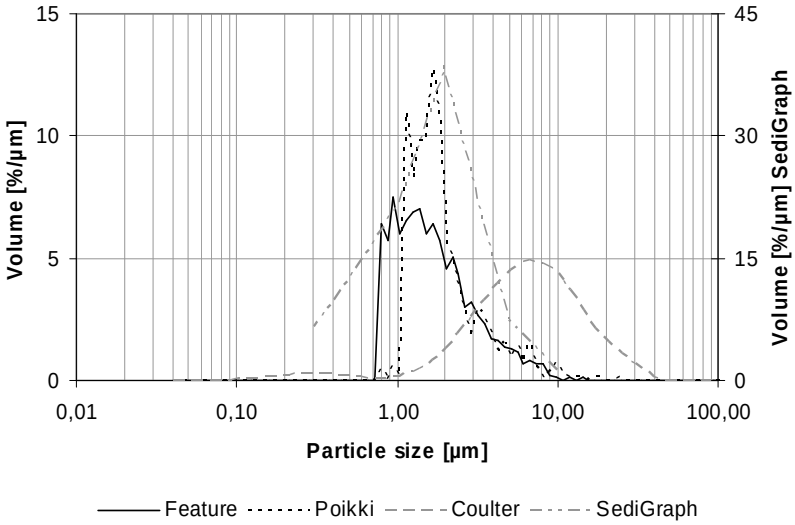

Figure 77. Frequency basis particle size distribution of kaolin 2 measured by different methods.

Table XI: The parameters of kaolin 2 particle analyses.

Particle size	**SediGraph**	**Coulter**	**Feature**	**Poikki**
% < 0.1 µm	-	0.1	0.0	0.0
% < 0.3 µm	10.1	1.8	0.0	0.0
% < 0.5 µm	16.8	3.2	0.0	0.0
% < 1.0 µm	29.7	4.0	15.9	0.6
% < 2.0 µm	51.5	7.8	64.0	63.2
% < 5.0 µm	90.2	34.4	93.8	92.3
Mean [µm]	-	8.69	2.13	2.42
Median [µm]	1.93	6.85	1.64	1.78
Sd	-	6.83	1.58	2.03
Area, mean [µm^2]	-	-	5.54	6.26
Sd	-	-	11.42	15.10
Perimeter, mean [µm]	-	-	7.76	-
Sd	-	-	7.04	-
Length, mean [µm]	-	-	2.93	-
Sd	-	-	2.28	-
Breadth, mean [µm]	-	-	1.93	-
Sd	-	-	1.45	-
PSD, steepness				
d20/d50	32	51	65	77
d30/d70	31	45	54	68
Particle shape				
Aspect Ratio, mean	-	-	1.52	-
Sd	-	-	0.29	-
Shape factor, mean	-	-	1.23	1.13
Sd	-	-	0.40	0.08

Figures 76 and 77 show that both image analysis programs gave very similar results also for kaolin 2. Mean particle size was over 2 µm and median particle size was about 1.7 µm. Steepness of particle size distribution was higher when measured by Poikki-program. According to pigment supplier the aspect ratio of kaolin 2 is about 40 and aspect ratio of kaolin 1 is about 25 which look reliable when particle sizes are compared and if the thickness of particles is almost the same. As in case of kaolin 1, SediGraph's results were very similar to results of image analyses also with kaolin 2. According to results of particle analyses of these two kaolin pigments, it seems that SediGraph is better suited to platy pigments than Coulter.

Figure 78 shows an example of cubic PCC particles and figures 79 and 80 show the particle size distribution of cubic PCC (15 mg/l). The parameters of particle analyses are showed in table XII. Sample size was 1632 particles in Feature and 1518 particles in Poikki-program. This PCC had only cubic particles because nano PCC had too small particle size (~40 nm) and was left out of analyses. Preparation and especially separation of individual nanoparticles was too difficult.

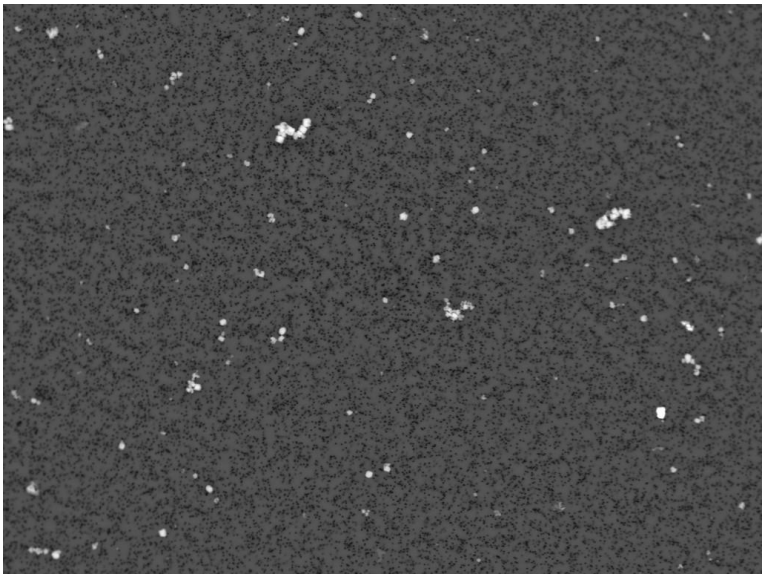

Figure 78. SEM image of cubic PCC particles.

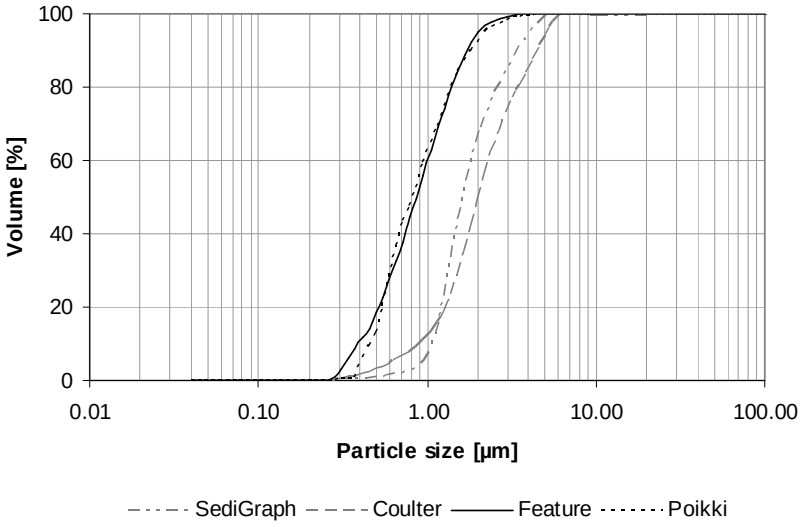

Figure 79. Cumulative basis particle size distribution of cubic PCC measured by different methods (dispersed with 8000 g/mol maleic acid in image analyses).

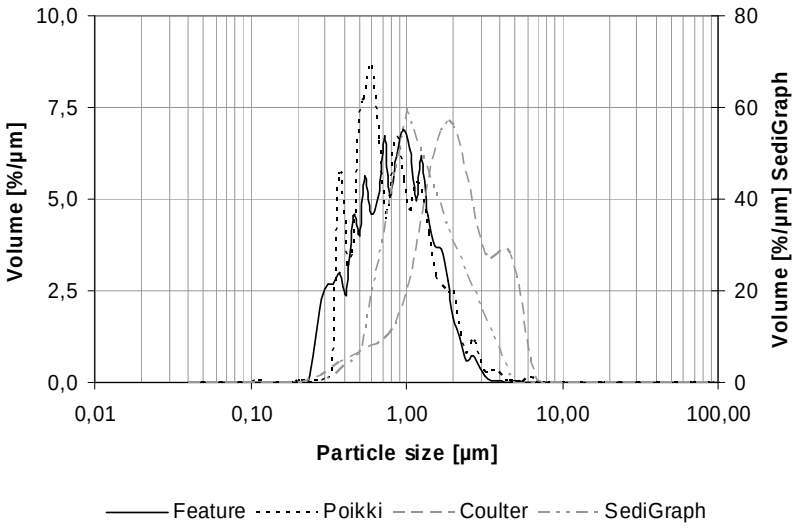

Figure 80. Frequency basis particle size distribution of cubic PCC measured by different methods (dispersed with 8000 g/mol maleic acid in image analyses).

Table XII: The parameters of cubic PCC particle analyses (dispersed with 8000 g/mol maleic acid in image analyses).

Particle size	**SediGraph**	**Coulter**	**Feature**	**Poikki**
% < 0.1 µm	-	0.0	0.0	0.0
% < 0.3 µm	0.7	0.3	3.3	0.3
% < 0.5 µm	1.4	3.1	18.6	14.3
% < 1.0 µm	8.0	12.0	59.2	62.3
% < 2.0 µm	68.4	48.9	94.5	92.4
% < 50 µm	100.0	93.8	99.9	99.9
Mean [µm]	-	2.37	0.99	1.01
Median [µm]	1.7	2.03	0.87	0.82
Sd	-	1.35	0.56	0.64
Area, mean [μm^2]	-	-	1.01	0.96
Sd	-	-	1.34	1.28
Perimeter, mean [µm]	-	-	3.50	-
Sd	-	-	2.43	-
Length, mean [µm]	-	-	1.28	-
Sd	-	-	0.79	-
Breadth, mean [µm]	-	-	0.91	-
Sd	-	-	0.51	-
PSD, steepness				
d20/d50	71	63	59	66
d30/d70	63	56	53	53
Particle shape				
Aspect Ratio, mean	-	-	1.41	-
Sd	-	-	0.23	-
Shape factor, mean	-	-	1.22	1.13
Sd	-	-	0.33	0.09

Image analyses of cubic PCC were made from dispersed sample because of larger number of particles in one field (image). The mean particle size was almost 1 µm by both programs and the median particle size was near of 0.85 µm. The particle size distribution was very similar between the image analysis programs and steepness d30/d70 was just the same; 53. Aspect ratio was quite high for square (cubic) particles but shape factor was near of square particles. The differences in the results of all analysing methods were surprise because of simple shape of PCC particles.

Figure 81 shows an example of aragonite particles and figures 82 and 83 show the particle size distribution of aragonite (100 mg/l) and table XIII shows the parameters of particle analyses. Sample size was 952 particles in Feature and 1034 particles in Poikki-program.

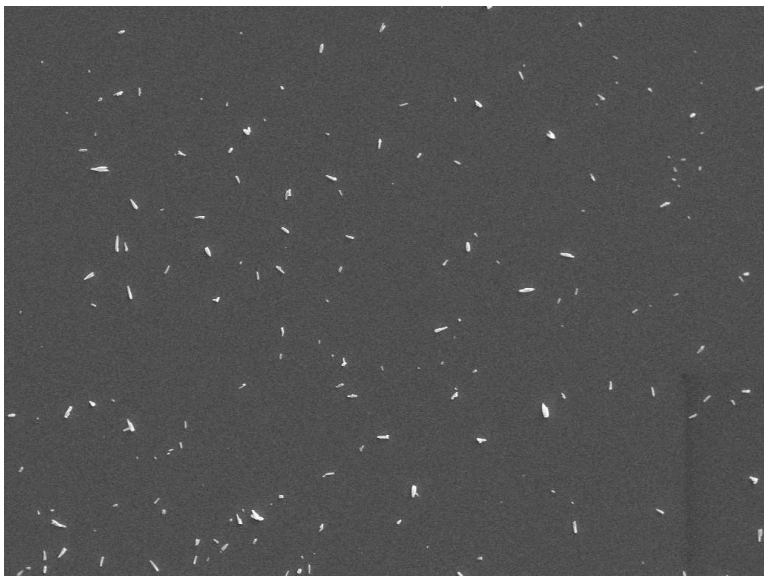

Figure 81. SEM image of aragonite particles.

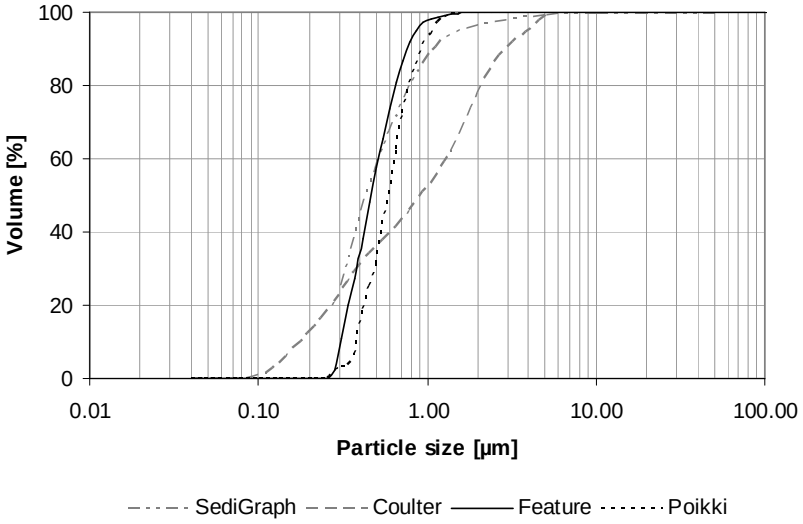

Figure 82. Cumulative basis particle size distribution of aragonite measured by different methods.

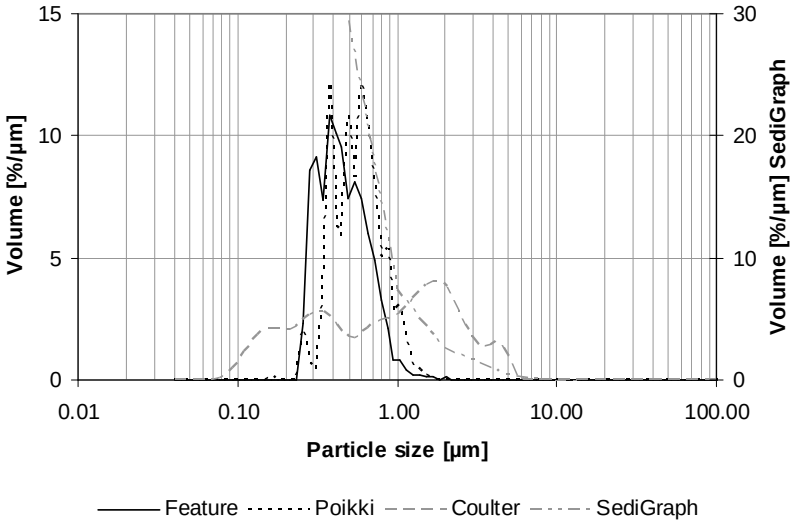

Figure 83. Frequency basis particle size distribution of aragonite measured by different methods.

Table XIII: The parameters of aragonite particle analyses.

Particle size	**SediGraph**	**Coulter**	**Feature**	**Poikki**
% < 0.1 µm	-	0.6	0.0	0.0
% < 0.3 µm	24.5	22.6	10.9	2.6
% < 0.5 µm	59.6	36.2	57.9	33.3
% < 1.0 µm	89.2	52.1	97.6	92.4
% < 2.0 µm	96.7	77.7	99.9	100.0
% < 5.0 µm	99.4	98.7	100.0	100.0
Mean [µm]	-	1.29	0.51	0.63
Median [µm]	0.44	0.92	0.46	0.59
Sd	-	1.19	0.20	0.23
Area, mean [µm^2]	-	-	0.23	0.30
Sd	-	-	0.23	0.17
Perimeter, mean [µm]	-	-	1.92	-
Sd	-	-	0.95	-
Length, mean [µm]	-	-	0.83	-
Sd	-	-	0.40	-
Breadth, mean [µm]	-	-	0.39	-
Sd	-	-	0.17	-
PSD, steepness				
d20/d50	60	30	72	76
d30/d70	49	23	66	67
Particle shape				
Aspect Ratio, mean	-	-	2.14	-
	-	-	0.68	-
Shape factor, mean	-	-	1.39	1.14
	-	-	0.36	0.07

The mean particle size of aragonite was about 0.5 µm by Feature and slightly over 0.6 µm by Poikki-program. The median particle size had also deviation; Feature: 0.46 µm and Poikki: 0.59 µm. The particle size distribution was still very similar between the programs; steepness had only one and four unit margins. For needle-like aragonite the aspect ratio and the shape factor were quite good. For particle which size is 2x4 pixels the aspect ratio is 2 and the shape factor is 1.43. According to SEM images (figure 49) aragonite particles should have higher aspect ratio. SediGraph and Coulter gave different results; median particle size by SediGraph (0.44 µm) was almost the same as in image analyses but median particle size by Coulter was twice as high.

Figure 84 shows an example of wollastonite particles and figures 85 and 86 show the particle size distribution of wollastonite (15 mg/l) and table XIV shows the parameters of particle analyses. Sample size was 976 particles in Feature and 1218 particles in Poikki-program.

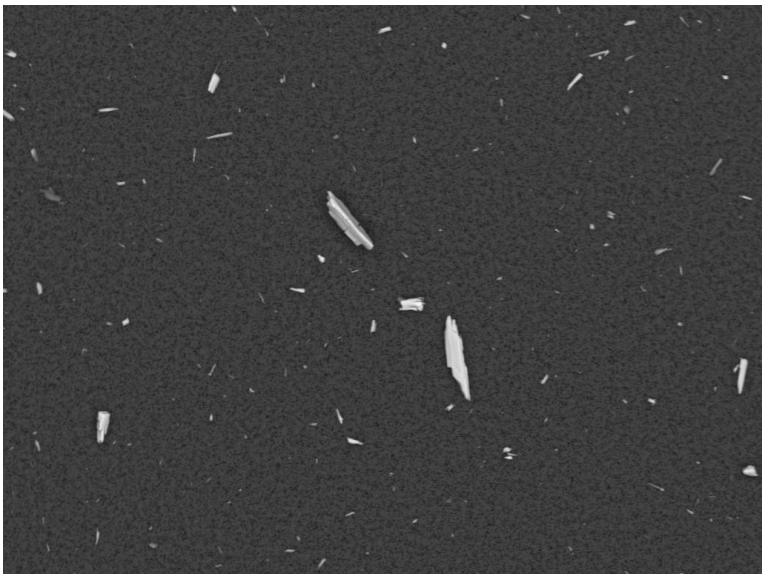

Figure 84. SEM image of wollastonite particles.

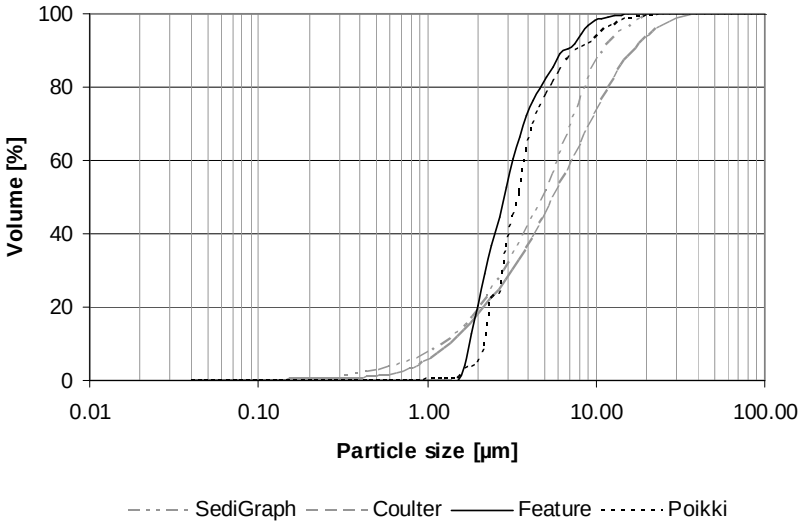

Figure 85. Cumulative basis particle size distribution of wollastonite measured by different methods.

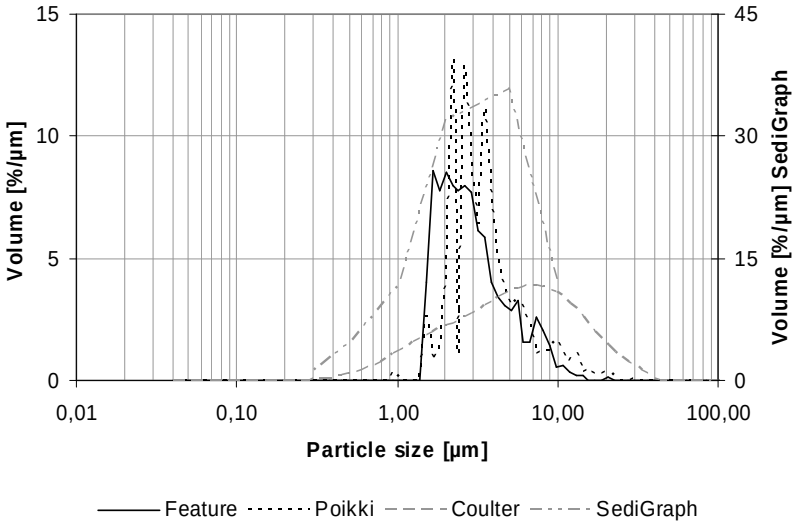

Figure 86. Frequency basis particle size distribution of wollastonite measured by different methods.

Table XIV: The parameters of wollastonite particle analyses.

Particle size	**SediGraph**	**Coulter**	**Feature**	**Poikki**
% < 0.1 µm	-	0.1	0.0	0.0
% < 0.3 µm	1.7	0.4	0.0	0.0
% < 0.5 µm	3.1	1.0	0.0	0.0
% < 1.0 µm	8.0	5.3	0.0	0.0
% < 2.0 µm	19.8	17.5	19.0	5.2
% < 5.0 µm	52.0	45.3	82.2	77.4
Mean [µm]	-	7.66	3.57	4.36
Median [µm]	4.8	5.64	2.79	3.45
Sd	-	6.81	2.20	3.12
Area, mean [μm^2]	-	-	13.79	14.76
Sd	-	-	22.46	20.16
Perimeter, mean [µm]	-	-	13.82	-
Sd	-	-	10.29	-
Length, mean [µm]	-	-	5.95	-
Sd	-	-	4.47	-
Breadth, mean [µm]	-	-	2.66	-
Sd	-	-	1.52	-
PSD, steepness				
d20/d50	42	39	72	68
d30/d70	39	35	61	63
Particle shape				
Aspect Ratio, mean	-	-	2.19	-
Sd	-	-	0.91	-
Shape factor, mean	-	-	1.42	1.16
Sd	-	-	0.48	0.11

The particle size of wollastonite had much deviation between the all methods. The mean particle size varied between 3.57 µm (Feature) and 7.66 µm (Coulter) when the median particle size varied between 2.79 µm (Feature) and 5.64 µm (Coulter). The particle size distribution was quite similar between the image analysis programs; steepness values had only a little deviation. Differences in particle size distribution were also quite small between SediGraph and Coulter, but they differed from particle size distribution by image analysis programs. Aspect ratio and shape factor were typical for wollastonite which has more deviation in particle shape than totally needle-like aragonite. Represented values of aspect ratio were mean values and therefore looked quite low. The aspect ratio depends on particle size especially in case of needle-like particles. Figure 87 shows the correlation between particle size and aspect ratio.

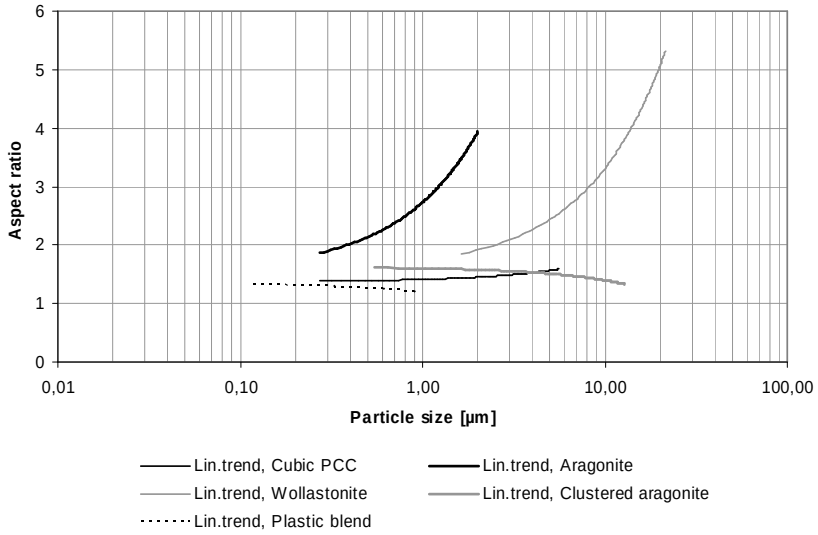

Figure 87. The correlation between particle size and aspect ratio when particle shape differs. Lines are linear trendlines of scatter plot.

The real aspect ratio of aragonite varied between 1 and 5 and the real aspect ratio of wollastonite varied between 1 and 7.5. The real aspect ratio of clustered aragonite varied between 1 and 5. These values are more reliable than only mean value. The real aspect ratio of cubic PCC and plastic blend varied only little (1-2.5) which means that aspect ratio does not depend on particle size as strongly. Figures 88 and 89 show the correlation between shape factor and particle size.

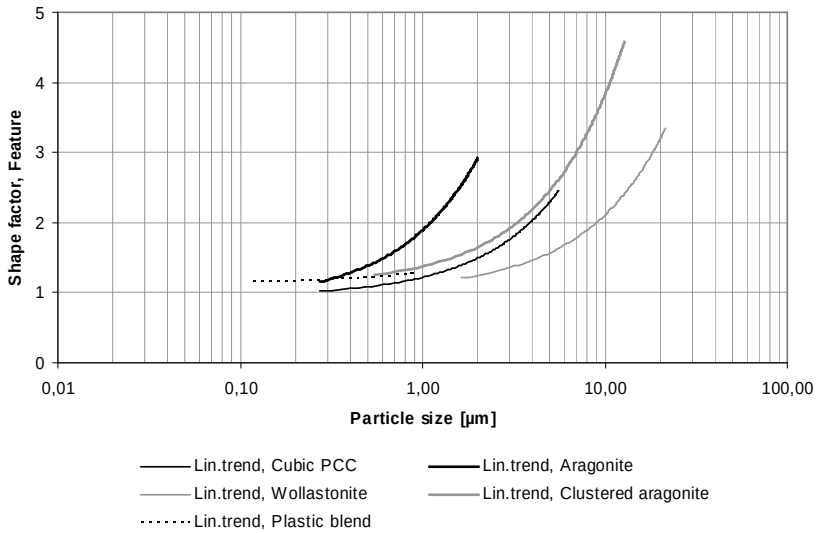

Figure 88. The correlation between particle size and shape factor when particle shape differs. Analysed by Feature. Lines are linear trendlines of scatter plot.

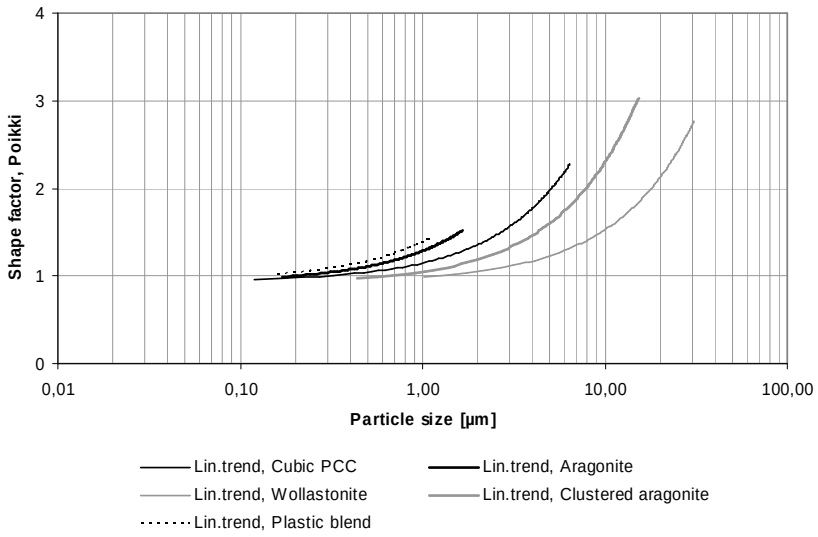

Figure 89. The correlation between particle size and shape factor when particle shape differs. Analysed by Poikki-program. Lines are linear trendlines of scatter plot.

The real shape factor depended on particle size the most in case of clustered aragonite (1-6.5) and the less in case of plastic pigments (1-3.5). Shape factors had a little difference between the image analysis programs; shape factor values from Feature were higher than from Poikki-program. Differences may be caused by image processing. Figures 90-92 show an example in which original SEM image and thresholded image were different from calculated image in Poikki-program.

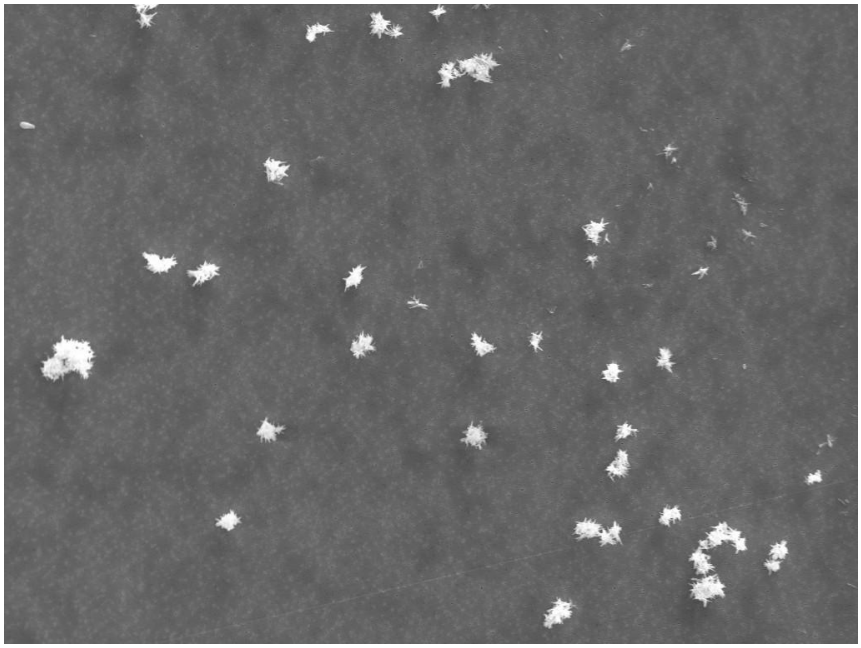

Figure 90. Original SEM image for Poikki-analysis. Clustered aragonite, 750x SE.

Figure 91. Thresholded binary image from Poikki-program.

Figure 92. Calculated image from Poikki-program.

Figure 93 shows an example of clustered aragonite particles and figures 94 and 95 show the particle size distribution of clustered aragonite (150 mg/l) and table XV shows the parameters of particle analysis. Sample size was 1114 particles in Feature and 1186 particles in Poikki-program.

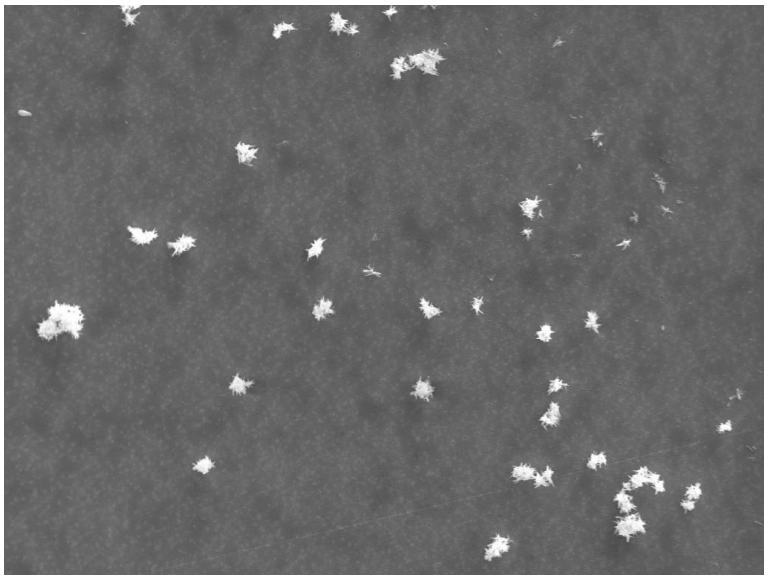

Figure 93. SEM image of clustered aragonite particles.

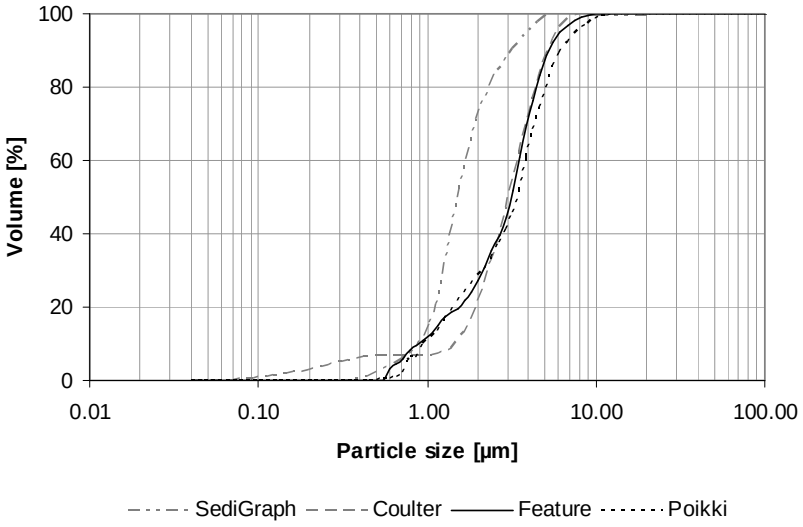

Figure 94. Cumulative basis particle size distribution of clustered aragonite measured by different methods.

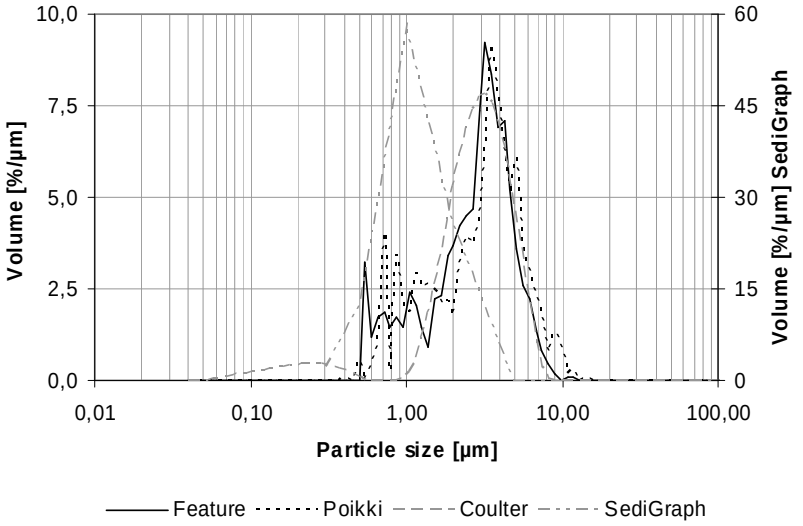

Figure 95. Frequency basis particle size distribution of clustered aragonite measured by different methods.

Table XV: The parameters of clustered aragonite particle analyses.

Particle size	**SediGraph**	**Coulter**	**Feature**	**Poikki**
% < 0.1 µm	-	0.7	0.0	0.0
% < 0.3 µm	0.1	4.9	0.0	0.0
% < 0.5 µm	2.6	6.7	0.0	0.1
% < 1.0 µm	15.3	6.8	11.9	10.2
% < 2.0 µm	73.9	20.9	27.4	28.4
% < 5.0 µm	100.0	87.6	87.7	78.8
Mean [µm]	-	3.16	3.15	3.54
Median [µm]	1.61	3.03	3.11	3.42
Sd	-	1.53	1.71	2.16
Area, mean [μm^2]	-	-	10.10	9.51
Sd	-	-	10.80	9.80
Perimeter, mean [µm]	-	-	14.51	-
Sd	-	-	10.04	-
Length, mean [µm]	-	-	4.60	-
Sd	-	-	2.66	-
Breadth, mean [µm]	-	-	3.06	-
Sd	-	-	1.70	-
PSD, steepness				
d20/d50	68	65	50	42
d30/d70	65	60	55	50
Particle shape				
Aspect Ratio, mean	-	-	1.55	-
Sd	-	-	0.39	-
Shape factor, mean	-	-	1.96	1.34
Sd	-	-	0.72	0.14

The particle size and particle size distribution had quite much deviation between the programs. The mean particle size varied between 3.15 µm (Feature) and 3.54 µm (Poikki) when the median particle size varied between 3.11 µm (Feature) and 3.42 µm (Poikki). d20/d50 steepness had even eight unit margin between the programs. The results from SediGraph had high differences from other analysing methods. Coulter's and Feature's results were almost similar. Aspect ratio and shape factor were typical for irregular particles, but especially the shape factor could be much higher as figure 96 shows.

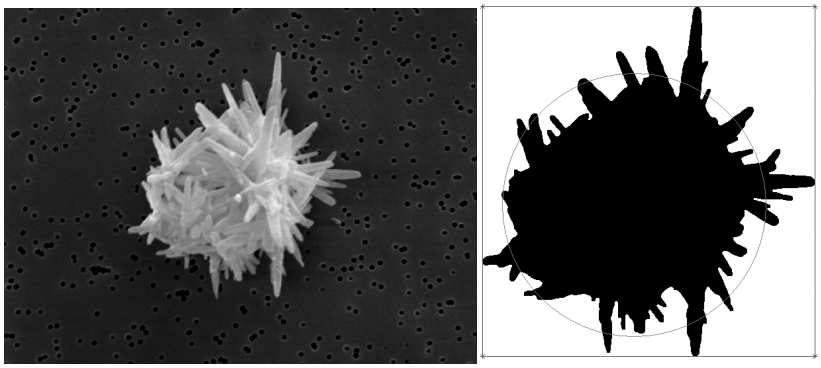

Figure 96. Individual particle of clustered aragonite. Left: SEM image, 7500x SE, right: analysed grey scale profile of the same particle.

The aspect ratio of analysed particle was about one which was specified in image processing program with the lines of right figure. The shape factor, 8.33, was specified by Poikki-program. When the magnification is high enough the shapes can be specified more exactly than with lower magnifications. Magnification in image analysis of clustered aragonite was only 750 which explains low values of the shape factor (1.96 in Feature and 1.34 in Poikki).

Figure 97 shows an example of plastic 2 particles and figures 98 and 99 show the particle size distribution of spherical plastic 2 (1 mg/l) and table XVI show the parameters of particle analyses. Sample size was 1083 particles in Feature and 1075 particles in Poikki-program.

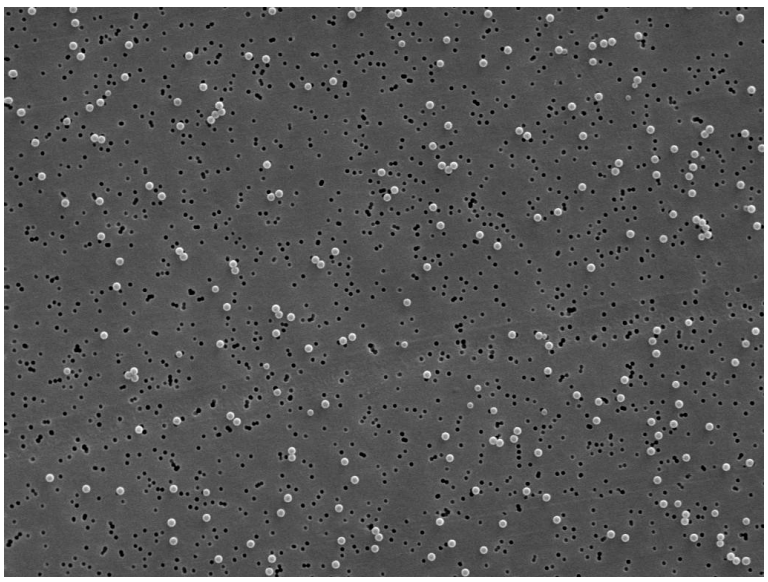

Figure 97. SEM image of plastic 2 particles.

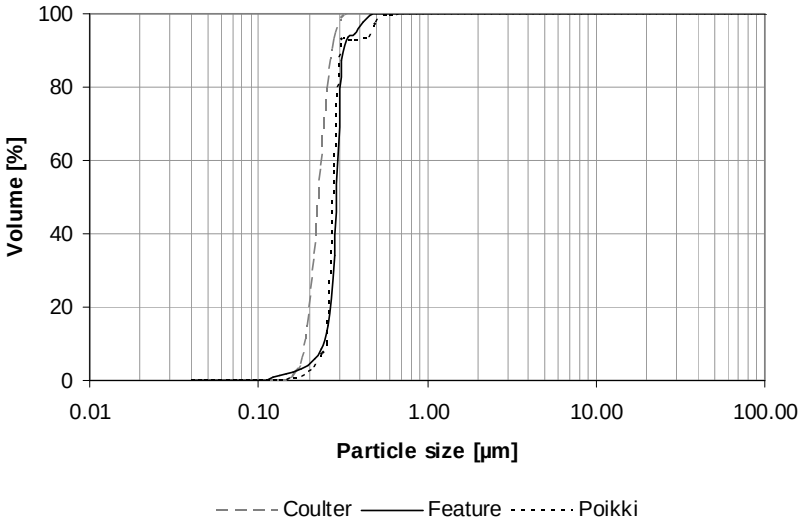

Figure 98. Cumulative basis particle size distribution of plastic 2 measured by different methods.

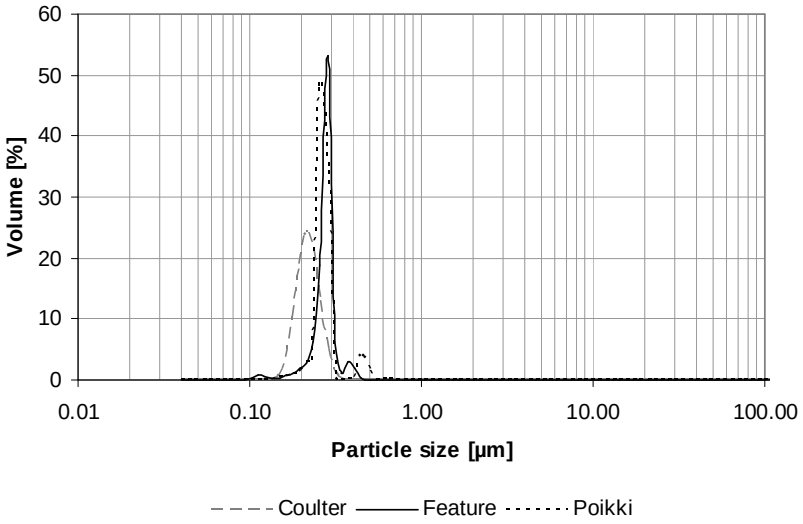

Figure 99. Frequency basis particle size distribution of plastic 2 measured by different methods.

Table XVI: The parameters of plastic 2 particle analyses.

Particle size	**Coulter**	**Feature**	**Poikki**
% < 0.1 µm	0.0	0.0	0.0
% < 0.3 µm	96.4	68.6	92.2
% < 0.5 µm	100.0	99.8	98.0
% < 1.0 µm	100.0	100.0	100.0
% < 2.0 µm	100.0	100.0	100.0
% < 5.0 µm	100.0	100.0	100.0
Mean [µm]	0.23	0.29	0.29
Median [µm]	0.23	0.29	0.28
Sd	0.03	0.05	0.07
Area, mean [μm^2]	-	0.07	0.07
Sd	-	0.02	0.02
Perimeter, mean [µm]	-	0.97	-
Sd	-	0.23	-
Length, mean [µm]	-	0.34	-
Sd	-	0.08	-
Breadth, mean [µm]	-	0.28	-
Sd	-	0.04	-
PSD, steepness			
d20/d50	88	92	96
d30/d70	85	93	97
Particle shape			
Aspect Ratio, mean	-	1.24	-
Sd	-	0.21	-
Shape factor, mean	-	1.15	1.07
Sd	-	0.31	0.06

Both the mean and the median particle size of plastic 2 were very similar between the image analysis programs; 0.28-0.29 µm. Particle size distribution was also very similar. Particle size by Coulter was little smaller. Shape factor and especially the aspect ratio was little too high for spherical particle. The same character can be seen in table XVII which shows the parameters of particle analyses of plastic pigment blend (1 mg/l). Figure 100 shows an example of particles in plastic blend. The particle size distribution of plastic pigment blend is showed in figures 101 and 102. Sample size was 1056 particles in Feature and 1045 particles in Poikki-program.

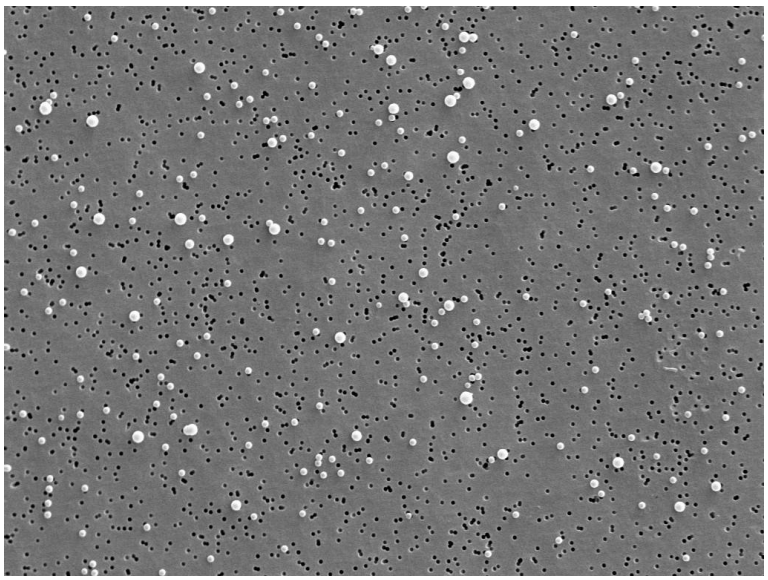

Figure 100. SEM image of particles in plastic blend.

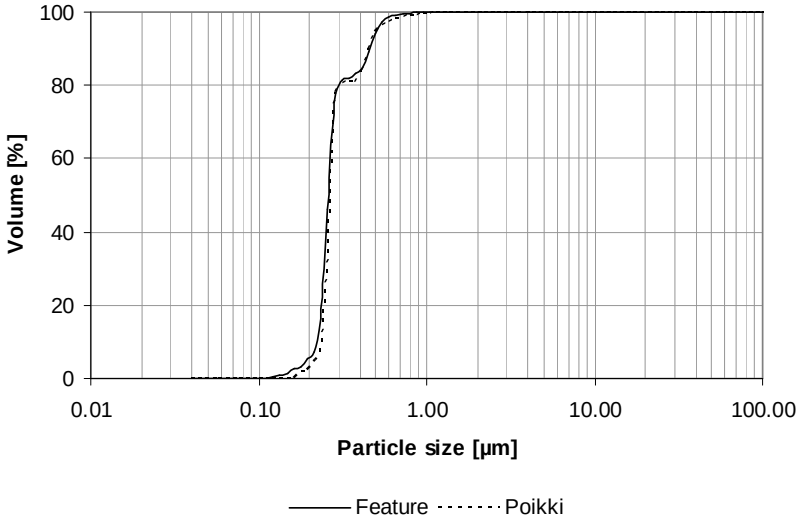

Figure 101. Cumulative basis particle size distribution of plastic pigment blend measured by image analysis.

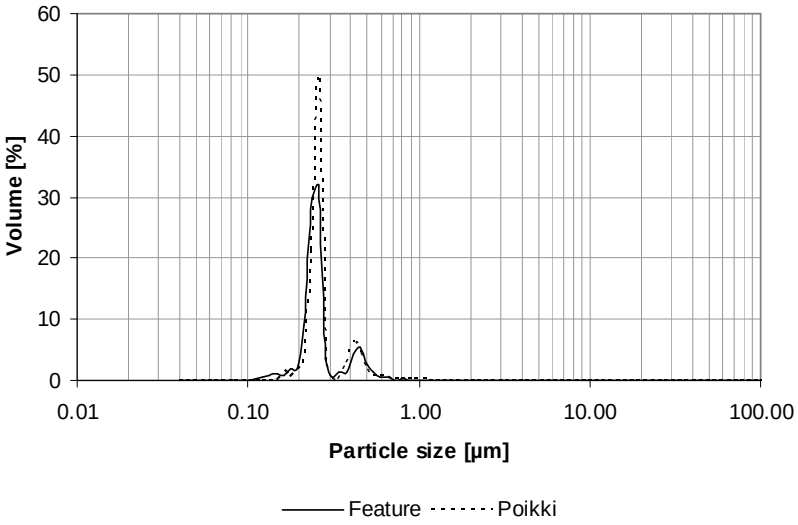

Figure 102. Frequency basis particle size distribution of plastic pigment blend measured by image analysis.

Table XVII: The parameters of plastic pigment blend particle analyses.

Particle size	**Feature**	**Poikki**
% < 0.1 µm	0.0	0.0
% < 0.3 µm	81.0	80.8
% < 0.5 µm	94.7	95.4
% < 1.0 µm	100.0	99.6
% < 2.0 µm	100.0	100.0
% < 5.0 µm	100.0	100.0
Mean [µm]	0.29	0.30
Median [µm]	0.26	0.26
Sd	0.10	0.11
Area, mean [μm^2]	0.07	0.08
Sd	0.07	0.07
Perimeter, mean [µm]	0.99	-
Sd	0.39	-
Length, mean [µm]	0.36	-
Sd	0.13	-
Breadth, mean [µm]	0.28	-
Sd	0.10	-
PSD, steepness		
d20/d50	93	96
d30/d70	90	93
Particle shape		
Aspect Ratio, mean	1.29	-
Sd	0.17	-
Shape factor, mean	1.18	1.08
Sd	0.21	0.05

The margins between the programs were very small also with plastic pigment blend. The mean particle size was 0.29-0.30 µm and the median particle size was 0.26 µm by the both programs. The particle size distribution had only little deviation. And as mentioned above the aspect ratio and the shape factor were little too high for spherical particles. The most important result of these analyses with plastic pigment blend were that the both image analysis programs gave two peaks in frequency basis particle size distribution and different particle sizes can be separated clearly.

12.2.4 3D-modelling of pigment particles

Examined wollastonite sample was imaged by SEM with 750x magnification and with tilt angles -5°, 0° and +5°. First target was the comparison of quality of the models which were created from two and three images. Figures 103 and 104 show the profiles of wollastonite particles.

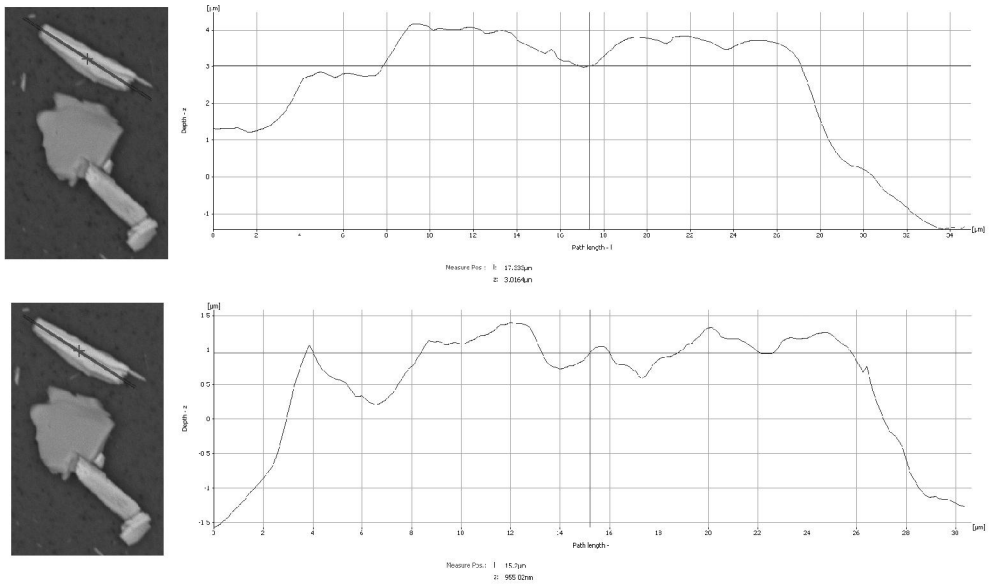

Figure 103. Profile I of wollastonite particle, 750x BSE. Up: modelled by two images, down: modelled by three images.

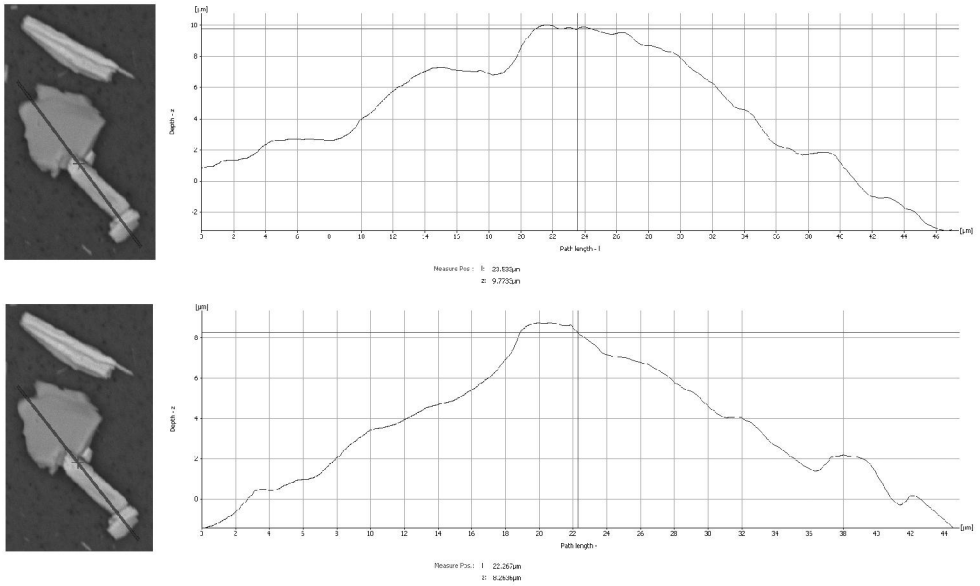

Figure 104. Profile II of wollastonite particles, 750x BSE. Up: modelled by two images, down: modelled by three images.

Figure 103 show that model by three images was more exact than model by two images. Differences between profiles in figure 104 are not as clear. Figures 105 and 106 show another profiles of wollastonite particles. Used magnification in these models was 2000x and tilt angles -8°, 0° and +8°.

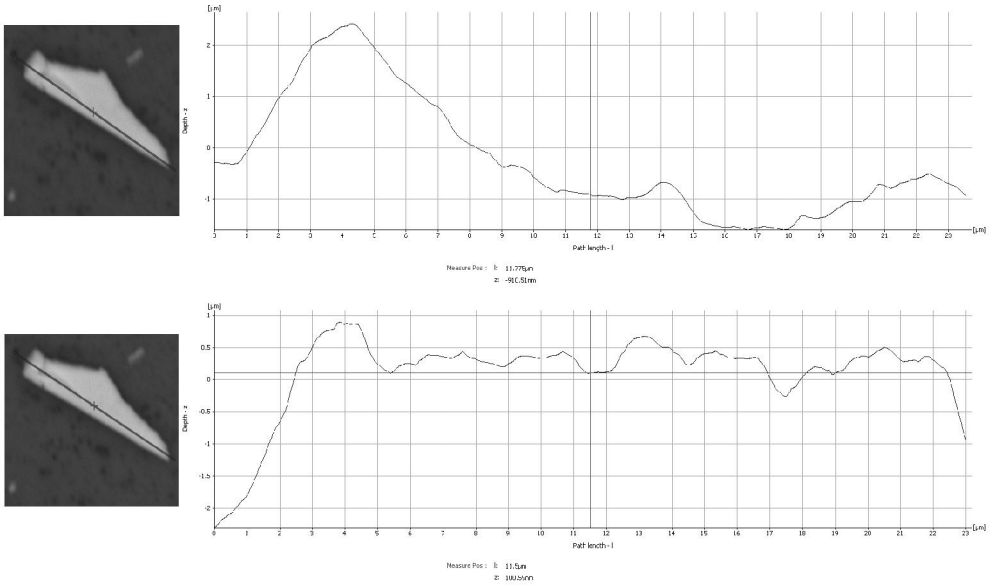

Figure 105. Profile III of wollastonite particle, 2000x BSE. Up: modelled by two images, down: modelled by three images.

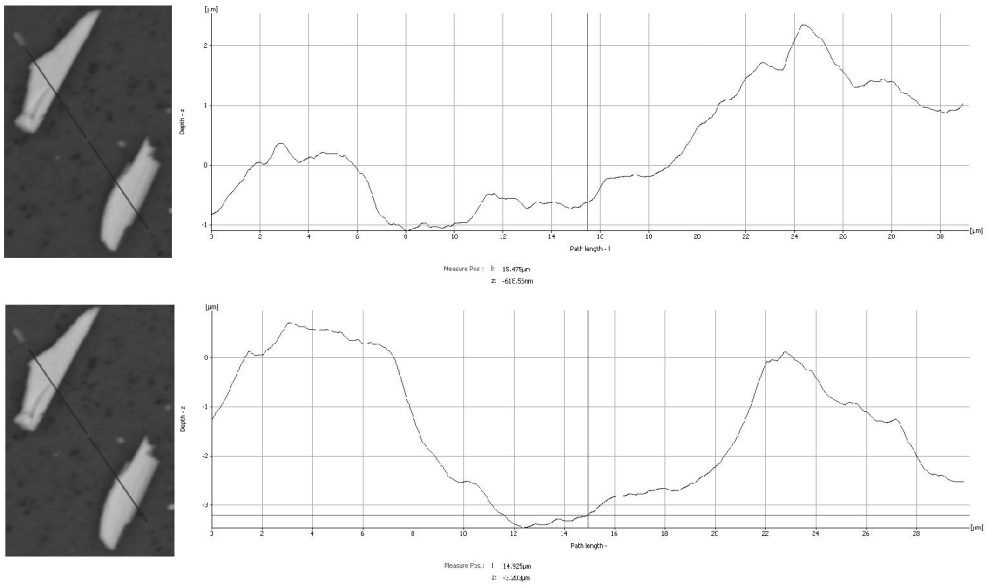

Figure 106. Profile IV of wollastonite particle, 2000x BSE. Up: modelled by two images, down: modelled by three images.

The better quality of models which base on three images can be noticed clearly also from figures 105 and 106. The shapes of particles are formed better than in models by two images. The duration of 3D-modelling which bases on three images was longer than modelling which bases on two images respectively. Tilt angles ± 8° gave also better profile than lower tilt angles ± 5°. Thickness of wollastonite particles was about 2-3 µm according to figures 103-106. The mean breadth (minimum Feret's diameter, corresponds to thickness) in Feature was 2.66 µm. The length of the particles in 3D-models was over 20 µm and in Feature (length) about 6 µm only. Aspect ratio of particles in 3D-models was between 11 and 15 and in Feature a little over 2. But these results are not reliable neither comparable because in 3D-models were only few particles and in Feature analysis 976 particles.

Figure 107 shows the profile of needle-like aragonite particle.

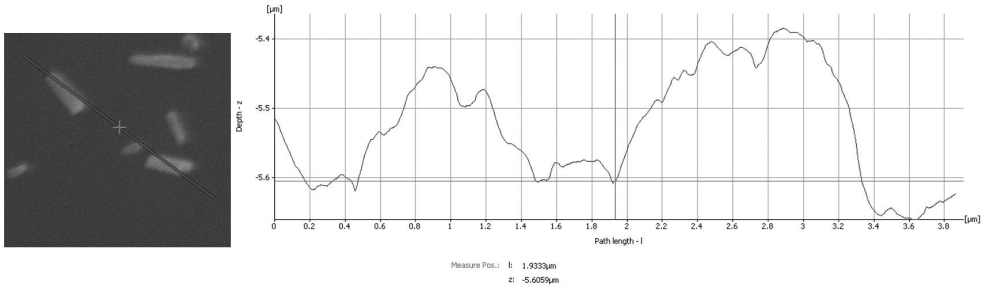

Figure 107. Profile of aragonite particle, 9000x SE, modelled by three images.

Aragonite particles were much smaller than wollastonite particles as showed in chapter 12.2.3. Therefore the accuracy model was lower. The thickness of aragonite particles was about 100-200 nm according to the 3D-model. In Feature the mean breadth of the particles was 0.39 µm (corresponds to thickness). The aspect ratio of aragonite is about 5.5 if the mean particle length is from Feature and the thickness of the particles is from MeX. That is much higher than aspect ratio from Feature; 2.14.

Platy kaolins were also used for 3D-models. Tilt angles were -7°, 0° and +7° in both cases. Magnifications were 7500x (kaolin 1) and 4000x (kaolin 2). All 3D-models bases on three images. Figures 108-110 show three profiles of kaolin 1 particles.

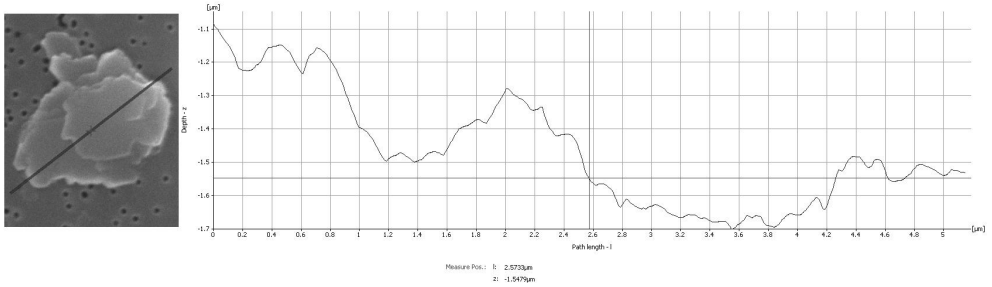

Figure 108. Profile I of kaolin 1 particles, 7500x SE, modelled by three images.

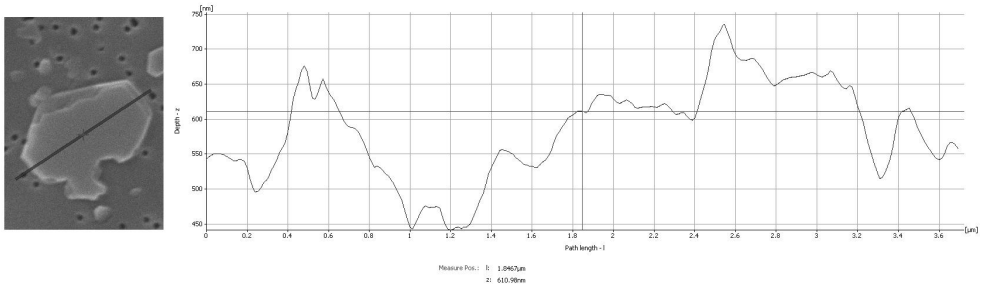

Figure 109. Profile II of kaolin 1 particles, 7500x SE, modelled by three images.

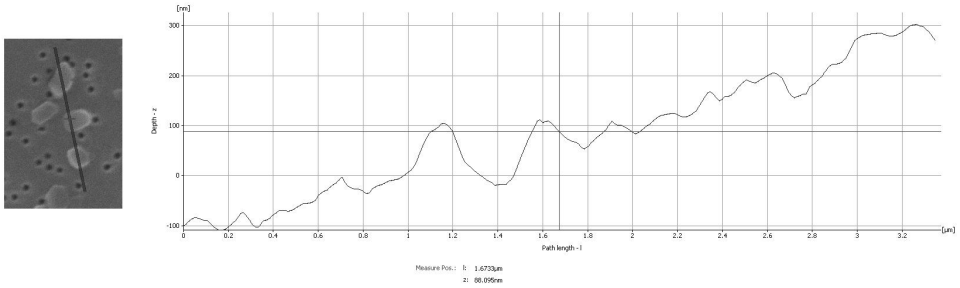

Figure 110. Profile III of kaolin 1 particles, 7500x SE, modelled by three images.

According to figures 108-110, kaolin 1 particles were too platy for exact 3D-modelling. An inexact value for particle thickness was about 100 nm. The mean particle size in Feature was 0.72 µm. If these values are used, the aspect ratio is about 7. Aspect ratio should be 25 according to pigment supplier.

Figures 111 and 112 show two profiles of kaolin 2 particles.

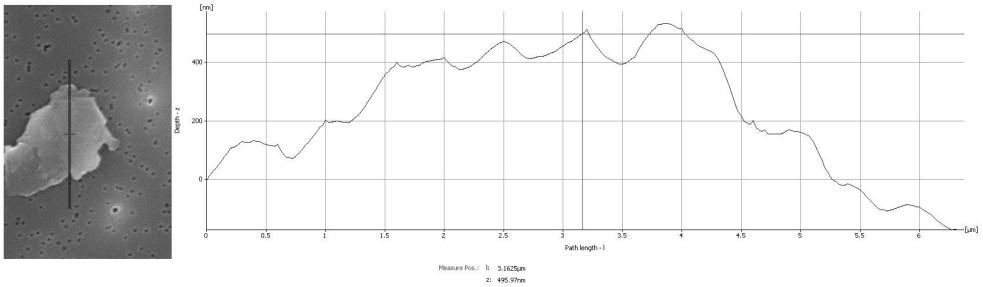

Figure 111. Profile I of kaolin 2 particle, 4000x SE, modelled by three images.

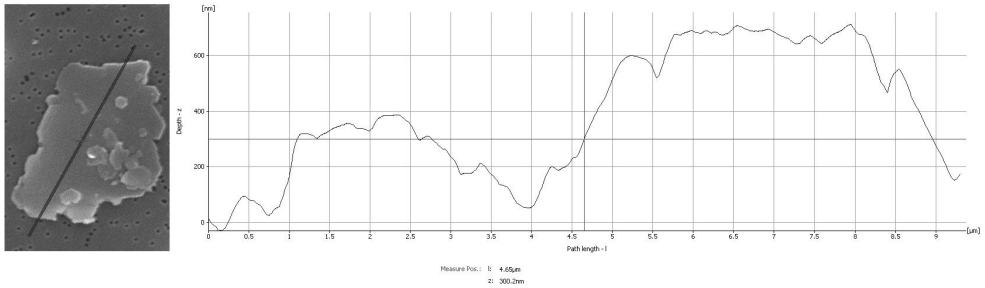

Figure 112. Profile II of kaolin 2 particle, 4000x SE, modelled by three images.

Kaolin 2 particles were also too flat for exact 3D-models. An inexact value for particle thickness was about 300-400 nm. If thickness is compared to the mean particle size in Feature, the aspect ratio is about 6 when it should be 40 according to supplier.

13 Conclusions

The main objective was development and testing of particle characterisation by image analysis method based on scanning electron microscope images. The most desired characters were particle shape (2D and 3D) and particle size (mean particle size and particle size distribution). Other objectives were finding out the effect of particle shape to laser diffraction (Coulter) and sedimentation (SediGraph) based particle size measurements and comparison of different measurement techniques. According to the results of these two test series; objectives were fulfilled but some further measures are needed.

Sample preparation was the most difficult step of image analysis because the sample concentration depends on the particle size and optimising of the concentration can be done by testing only. When optimal concentration was found, the analyses were very easy. Sample preparation was made by filtration in the most cases, but for clustered and aggregated particles spraying was better method. Spraying method can be developed further and it requires standardisation of the stages.

Sample scanning requires experience especially with very small pigment particles. Sharp image in SEM was one requirement for successful image analysis. The results of image analysis were reliable when image was sharp and conditions in SEM were stable. The most difficult step in image analyses was thresholding of the image. It has to be made exactly and carefully because it has high influence to the values of measured particle properties. INCA Feature was better program for image analyses because it has more settings, larger number of parameters in results and possibility to use EDS. Data processing can be done in spreadsheet program where can be standard calculation model for the results. Appendix IV includes more detailed working instruction for image analysis. MeX 3D-modelling program can be used with larger (thickness~1 µm) particles but creation of 3D-models needs still more experience and development.

The results from image analyses corresponded very well to either the results of sedimentation or to the results of laser diffraction. The values of aspect ratio and shape factor defined well the shape of the particles especially when high magnification was used. Still, the optimal magnification for these analysed

pigments may be higher than used. If the shape parameters are exact, they can be used more efficiently. Anyway, shape factor and aspect ratio should be used together for better comprehension of particle shape. Especially the diagrams where the shape parameters are plotted as function of particle size are very useful. Use of higher magnification enables the analysing of smaller particles also. The resolution of SEM is high enough for particles with diameter 100 nm and below, but sample preparation is more difficult. Imaging of nanoparticles by SEM requires experience also.

Image analysis is as suitable method for particle characterisation as sedimentation or laser diffraction. The advantages of image analysis are good repeatability, reliable results, large number of different parameters of particles, shape parameters and possibilities to 3D-modelling and use of chemical classification (EDS). The disadvantages are a little difficult optimising of the sample concentration, two-dimensional imaging (platy particles) and large number of test points if detailed parameters of particle shape are needed (requires high magnification).

14 Further measures

One objective of further measures could be better and more exact measurement of particle shape. More detailed image requires higher magnification when each particle consists of higher number of pixels than particles in these test series. Optimal magnification could be calculated so that particle which size is about 200 nm (or even 100 nm) can be analysed with details. Unfortunately this increases the number of required images. When the shape parameters are measured more exact, they could be used to definition of degree of clustering. This is very important indicator when different grades of precipitated calcium carbonate are compared.

Another objective could be 3D-modelling; it requires much more examination especially about imaging by SEM. Different acceleration voltages, spot sizes, detectors, tilt angles etc. could be examined. Small and platy particles (thickness < 1 µm) are the most difficult in 3D-modelling also.

References

1. Lehtinen E., Coating pigments – general, in E. Lehtinen, ed., *Pigment Coating and Surface Sizing of Paper*, Fapet Oy, Jyväskylä, 2000, p. 61-67.

2. Krogerus B., Fillers and pigments, in L. Neimo, ed., *Papermaking Chemistry*, Fapet Oy, Jyväskylä, 2000, p. 117-119.

3. Velho J.L., *Mineral fillers for paper. Why, what, how*, TECNICELPA, Tomar, Portugal, 2003, p. 1-7.

4. Drage G., Tamms O., Kaolin, in E. Lehtinen, ed., *Pigment Coating and Surface Sizing of Paper*, Fapet Oy, Jyväskylä, 2000, p. 69-92.

5. Eklund D., Lindström T., *Paper chemistry – an introduction*, DT Paper Science Publications, Grankulla, 1991, p. 242-264.

6. Likitalo M., Talc, in E. Lehtinen, ed., *Pigment Coating and Surface Sizing of Paper*, Fapet Oy, Jyväskylä, 2000, p. 107–119.

7. Huggenberger L., Manfred A., Köster H.-H., Ground calcium carbonate, in E. Lehtinen, ed., *Pigment Coating and Surface Sizing of Paper*, Fapet Oy, Jyväskylä, 2000, p. 95-105.

8. Imppola O., Precipitated calcium carbonate – PCC, in E. Lehtinen, ed., *Pigment Coating and Surface Sizing of Paper*, Fapet Oy, Jyväskylä, 2000, p. 141-151.

9. Alatalo M., Heikkilä K., Titanium dioxide, in E. Lehtinen, ed., *Pigment Coating and Surface Sizing of Paper*, Fapet Oy, Jyväskylä, 2000, p. 121-138.

10. Sokka T., *Päällystyspastan raaka-aineet*, lecture notes in Finnish, Lappeenranta University of Technology, Department of Chemical Technology, 2007, p.18-23.

11. Brown J.T., Kotoye F.O., Synthetic plastic pigments, in E. Lehtinen, ed., *Pigment Coating and Surface Sizing of Paper*, Fapet Oy, Jyväskylä, 2000, p. 178.

12. Kerker M., Light Scattering, *Ind. Eng. Chem.* **60**(1968), 10, 30-46.

13. Xu R., *Particle Characterization: Light Scattering Methods*, Kluwer Academic Publishers, Hingham, Massachusetts, USA, 2000, p. 12-82.

14. Brittain H.G., Particle-size distribution IV: Determination by laser-light scattering, *Pharmaceutical Technology* **27**(2003), 10, 102-104.

15. Kippax P., Measuring particle size using modern laser diffraction techniques. *Paint & Coating Industry* **21**(2005), 8, 42-47.

16. Young H.D., Freedman R.A., *University physics with modern physics*, 10th ed., Addison Wesley Longman, Inc., San Francisco, 2000, p. 1165-1169.

17. Li M., Patchigolla K., Wilkinson D., Measuring size distribution of organic crystals of different shapes using different technologies, *Part. Part. Syst. Charact.* **23**(2006), 138-144.

18. *Chemical Engineering*, Vol 2, Particle Technology and Separation Process, Backhurst J.R., Coulson J.M., Harker J.H., Richardson J.F., eds., 4th ed., Pergamon Press, Oxford, 1991, p. 1-13.

19. Xu R., Di Guida O.A., Comparison of sizing small particles using different technologies, *Powder Technology* **132**(2003), 145-153.

20. VTT, Prowledge Oy, KnowPap 9.0, Learning Environment for Papermaking and Automation, LUT intranet, referenced 13.2.2008, available: LUT intranet, demands user name.

21. Biagini E., Narducci P., Tognotti L., Size and structural characterization of lignin-cellulosic fuels after the rapid devolatilization, *Fuel* **87**(2008), 177-186.

22. Lieberman A., Fine Particle Characterization Methods in Liquid Suspension, in J.K. Beddow, ed., *Particle Characterization in Technology*, Vol 1, CRC Press Inc., Boca Raton, Florida, 1984, p.187-232.

23. Kati Turku, Paperikemia, course material in Finnish, LUT intranet, referenced 15.2.2008, available: LUT intranet, demands user name.

24. Nikki M., Nutbeem C., Imerys Oy, internal report, 2008.

25. Anon., Micromeritics Instrument Corp., Sedigraph™ III 5120, product data sheet, available on the internet: http://www.importecnical.com/images/PDF/MicromeriticsSEDIGRAPH5120.pdf, referenced 26.2.2008.

26. Strickland M.L., Characterizing Particles, *Ceramic Industry* **156**(2006), 2, 12-17.

27. Kinsman S., Particle Size Instrumentation – COULTER® Counter, in J.K. Beddow, ed., *Particle Characterization in Technology*, Vol 1, CRC Press Inc., Boca Raton, Florida, 1984, p.184.

28. Anon., Beckman Coulter, company's product introduction, available on the internet: http://www.beckmancoulter.com/coultercounter, referenced 12.3.2008.

29. Carr R., Smith J., Nelson P., Hole P., Malloy A., Weld A., Warren J., The real-time visualisation and size analysis of nanoparticles in liquids – nanoparticle tracking analysis, *Journal of Nanoparticle Research* (2008) unpublished.

30. Anon., NanoSight: An Introduction-CD-ROM, Ver 2.8, NanoSight Ltd.

31. Goodhew P.J., Humphreys F.J., *Electron Microscopy and Analysis*, 2nd ed., Taylor & Francis, London, 1988.

32. Lyman C.E., Newbury D.E., Goldstein J.I., Williams D.B., Romig A.D. Jr., Armstrong J.T., Echlin P., Fiori C.E., Joy D.C., Lifshin E., Peters K-R., *Scanning Electron Microscopy, X-Ray Microanalysis and Analytical Electron Microscopy, A Laboratory Workbook*, Plenum Press, New York, 1990.

33. Banerjee S, Conners T.E., *Surface Analysis of Paper*, CRC Press, Boca Raton, 1995, p. 41-59.

34. Niemistö A., Quantitative image analysis methods for applications in biomedical microscopy, Tampere University of Technology, Publication 632, Tampere, 2006, p. 16-28.

35. Gy P.M., *Sampling for analytical purposes*, John Wiley & Sons Ltd, Chichester, 1998.

36. Webb P.A., Orr C., *Modern methods of particle characterization*, Micromeritics Instrument Corp., available on the internet: http://www.micromeritics.com/applications/articles.aspx, referenced 31.3.2008.

37. Neijssen W., Roussel L., High-Resolution, Three-Dimensional Imaging for Analyzing Coating Fast and Easier than Ever, *Paint & Coating Industry* **23**(2007), 8, 78-79.

38. Kaur L., McCarthy O.J., Singh H., Singh J., Physico-chemical, rheological and structural properties of fractionated potato starches, *Journal of food engineering* **82**(2007), 383-394.

39. Xu Y., Particle Size Analyses of Porous Silica and Hybrid Silica Chromatographic Support Particles: Comparison of Flow/Hyperlayer Field-Flow Fractionation with Scanning Electron Microscopy, Electrical Sensing Zone and Static Light Scattering, *Journal of Chromatography A* (2007), doi:10.1016/j.chroma.2008.01.051.

40. Huffman G.P., Chen Y., Shah N., Huggins F.E., Linak W.P., Miller C.A., Investigation of primary fine particulate matter from coal combustion by computer-controlled scanning electron microscopy, *Fuel Processing Technology* **85**(2004), 743-761.

41. Turner S., Sieber J.R., Vetter T.W., Zeisler R., Marlow A.F., Moreno-Ramirez M.G., Davis M.E., Kennedy G.J., Borghard W.G., Yang S., Navrotsky A., Toby B.H., Kelly J.F., Fletcher R.A., Windsor E.S., Verkouteren J.R., Leigh S.D., Characterization of chemical properties, unit cell parameters and particle size distribution of three zeolite reference materials: RM 8850 – zeolite Y, RM 8851 – zeolite A and RM 8852 – ammonium ZSM-5 zeolite, *Microporous and Mesoporous Materials* **107**(2008), 252-267.

42. Linnala M., Partikkelikokoanalyysi, laboratory work of advanced special studies in paper technology, in Finnish, Lappeenranta University of Technology, Department of Chemical Technology, 2007.

43. Shi B., Wu Z., Inyang H., Chen J., Wang B., Preparation of soil specimens for SEM analysis using freeze-cut-drying, *Bull. Eng. Geol. Env.* **58**(1999), 1-7.

44. Laininen P., *Todennäköisyyslasku ja tilastomatematiikka*, in Finnish, 10th ed., Otatieto Oy, Espoo, 1995, p. 157–166.

45. Anon., *Tilastomatematiikan perusteet*, lecture notes in Finnish, Lappeenranta University of Technology, Department of Information Technology, 2004, p. 40-56.

46. Anon., Alicona Imaging Corporation, company's product introduction, available on the internet: http://www.alicona.com/englisch/main-navigation/products/mex/

47. Anon., Oxford Instruments, company's product introduction, available on the internet: http://www.oxford-instruments.com/wps/wcm/connect/Oxford+Instruments/Products/Microanalysis/INCAFeature/INCAFeature, referenced 22.9.2008.

Appendices

APPENDIX I	Data table of the particle analyses of test series I
APPENDIX II	SEM images of ultrasound bath comparison
APPENDIX III	Results of the shape analyses of test series II
APPENDIX IV	Working instruction for image analysis

Table I: Parameters of image analyses of plastic 1 and talc pigments.

Particle size	**Plastic 1**		**Talc**	
	Feature	**Poikki**	**Feature**	**Poikki**
% < 0.1 µm	0.0	0.0	0.0	0.0
% < 0.3 µm	0.2	4.6	0.0	0.0
% < 0.5 µm	61.9	65.4	8.7	0.6
% < 1.0 µm	100.0	95.1	46.5	47.7
% < 2.0 µm	100.0	100.0	80.1	76.3
% < 5.0 µm	100.0	100.0	97.8	96.8
Mean [µm]	0.49	0.55	1.42	1.60
Median [µm]	0.49	0.48	1.06	1.05
Sd	0.04	0.23	1.14	1.35
Area, mean [μm^2]	0.19	0.24	2.61	2.57
Sd	0.03	0.18	5.51	5.16
Perimeter, mean [µm]	1.53	-	5.15	-
Sd	0.14	-	4.63	-
Length, mean [µm]	0.53	-	2.00	-
Sd	0.05	-	1.66	-
Breadth, mean [µm]	0.48	-	1.24	-
Sd	0.04	-	1.03	-
PSD, steepness				
Steepness, d20/d50	93	92	59	72
d30/d70	92	87	47	51
Particle shape				
Aspect ratio, mean	1.11	-	1.61	-
Sd	0.04	-	0.42	-
Shape factor, mean	1.00	1.11	1.23	1.16
Sd	0.03	0.22	0.30	0.10

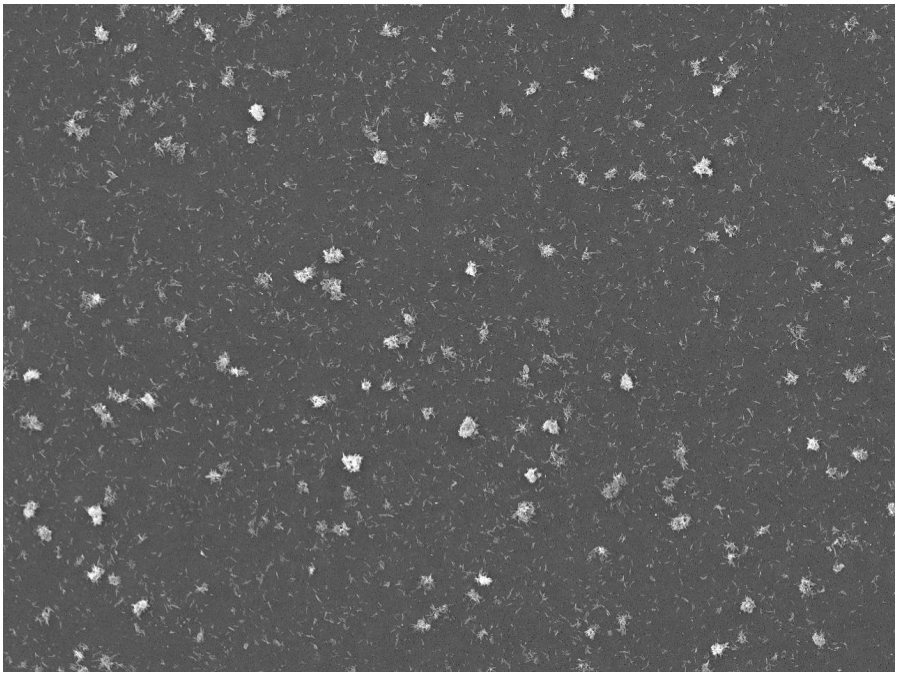

Figure 1. SEM image of clustered aragonite, 25 mg/l filtrated, no ultrasound, 500x SE.

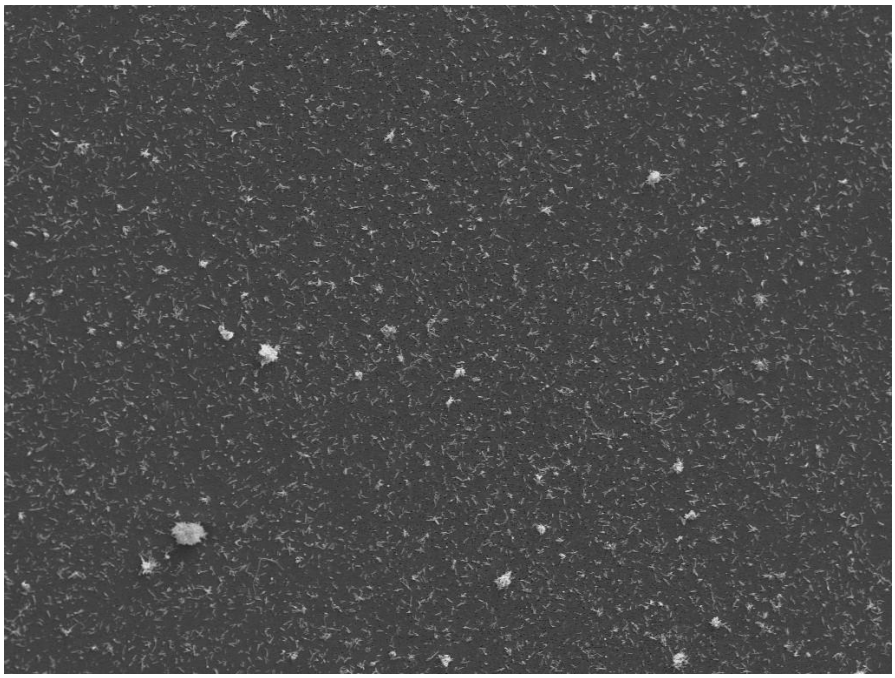

Figure 2. SEM image of clustered aragonite, 25 mg/l filtrated, ultrasound m03 10min, 500x SE.

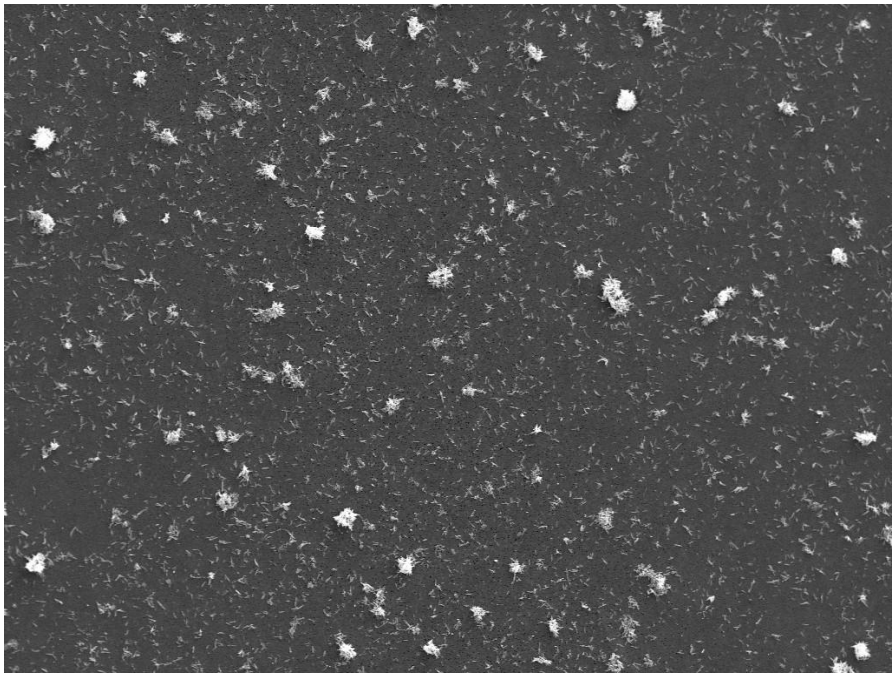

Figure 3. SEM image of clustered aragonite, 25 mg/l filtrated, ultrasound "old" 10min, 500x SE.

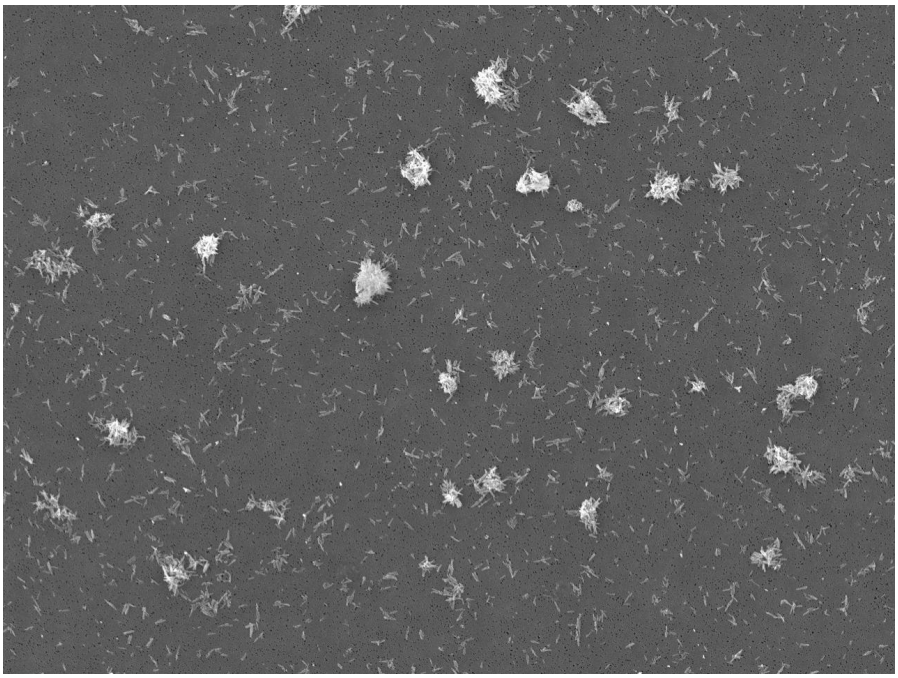

Figure 4. SEM image of clustered aragonite, 25 mg/l filtrated, no ultrasound, 1000x SE.

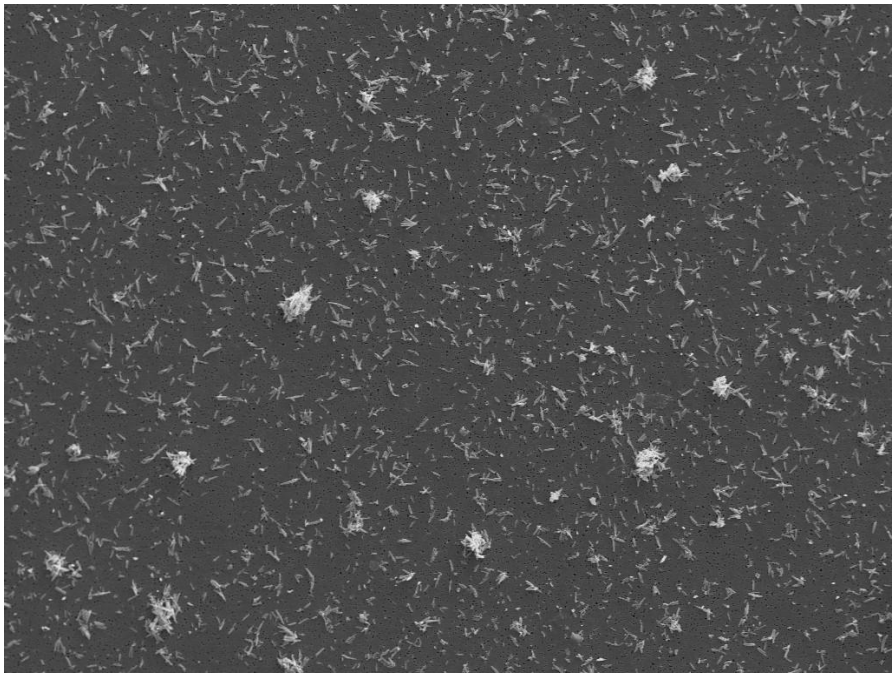

Figure 5. SEM image of clustered aragonite, 25 mg/l filtrated, ultrasound m03 10min, 1000x SE.

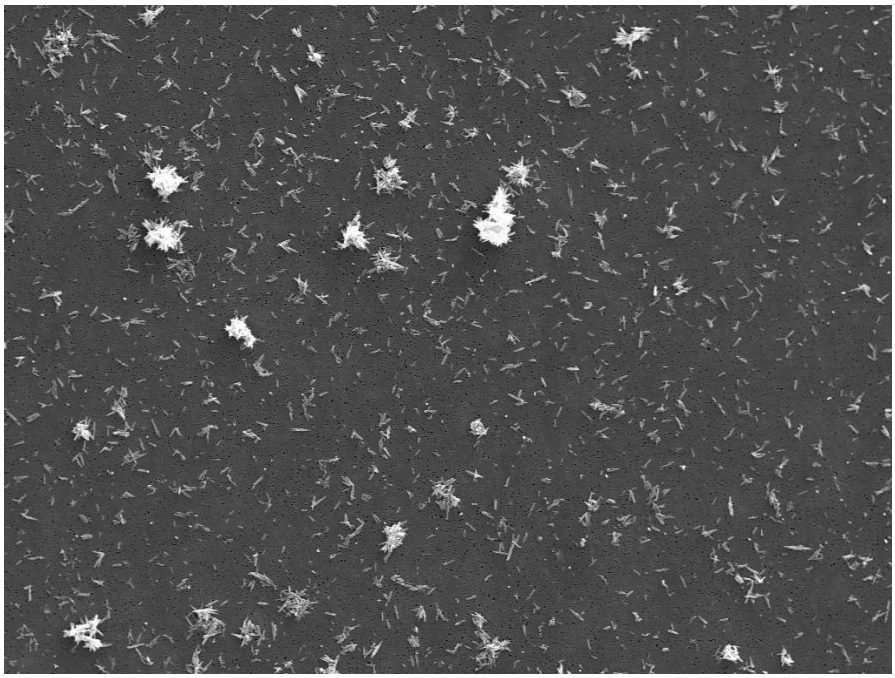

Figure 6. SEM image of clustered aragonite, 25 mg/l filtrated, ultrasound "old" 10min, 1000x SE.

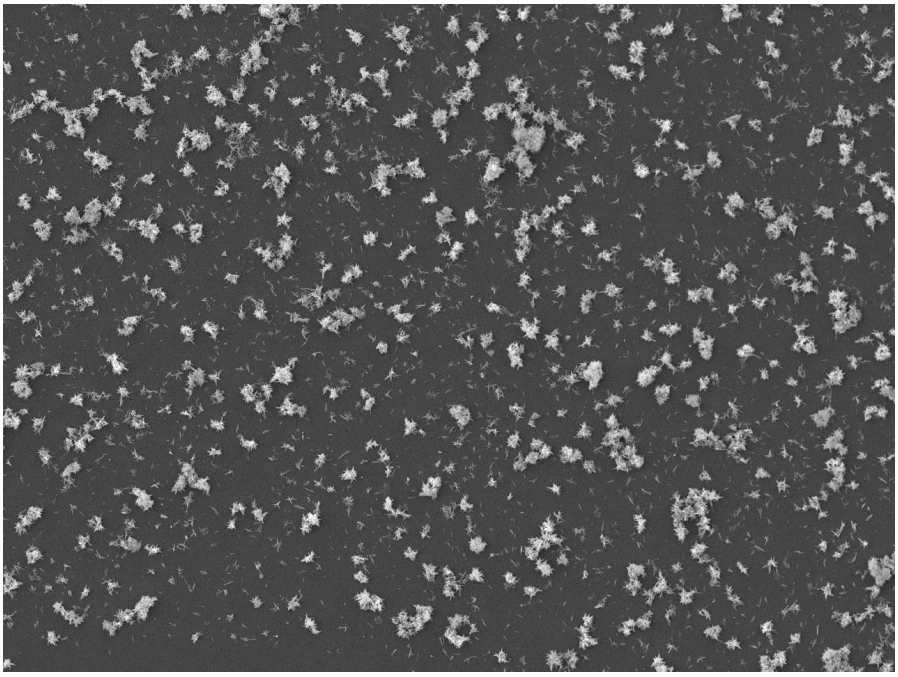

Figure 7. SEM image of clustered aragonite, 50 mg/l filtrated, no ultrasound, 500x SE.

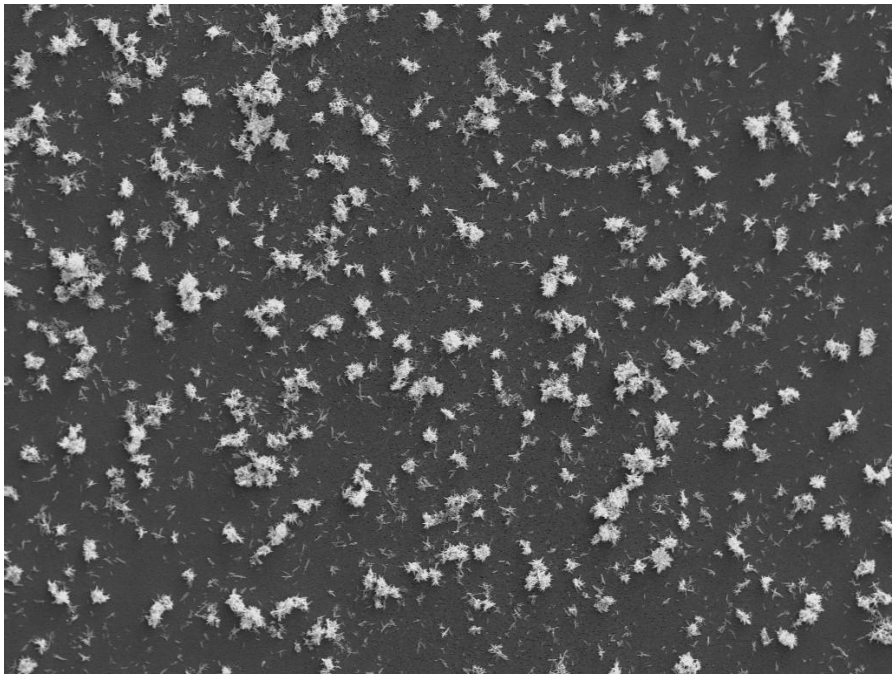

Figure 8. SEM image of clustered aragonite, 50 mg/l filtrated, ultrasound m03 10min, 500x SE.

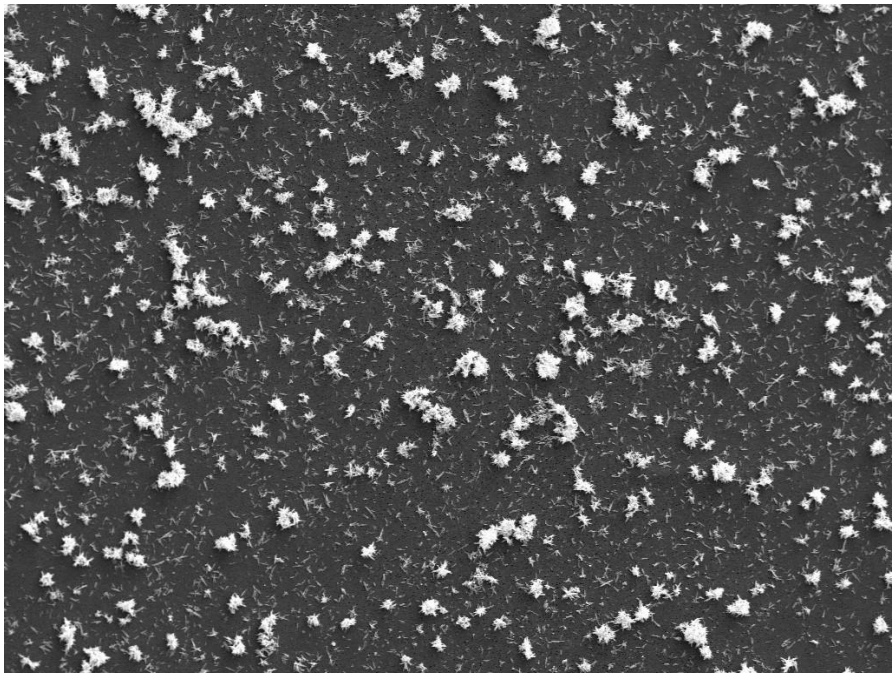

Figure 9. SEM image of clustered aragonite, 50 mg/l filtrated, ultrasound "old" 10min, 500x SE.

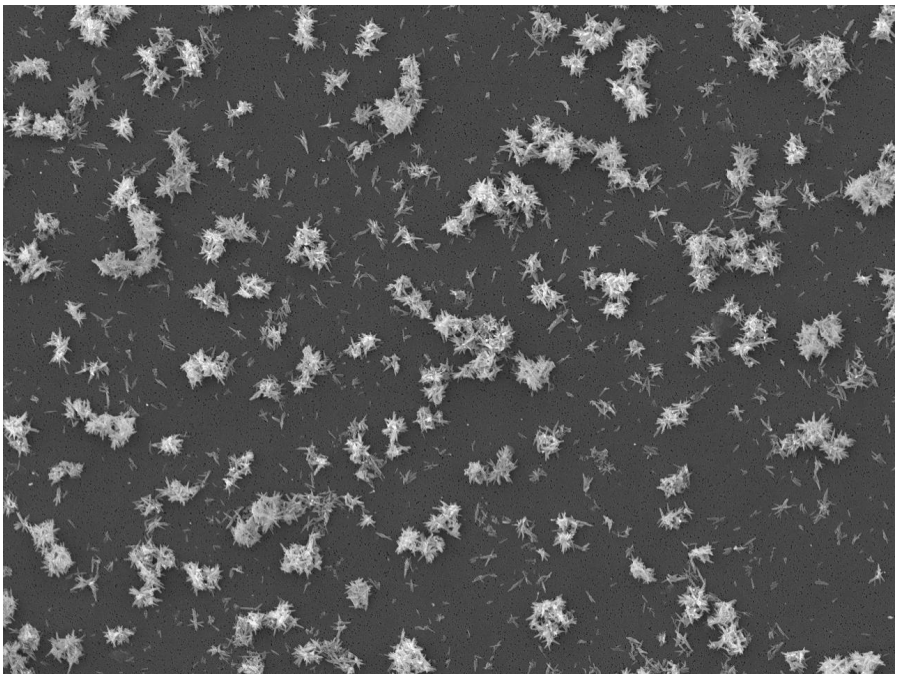

Figure 10. SEM image of clustered aragonite, 50 mg/l filtrated, no ultrasound, 1000x SE.

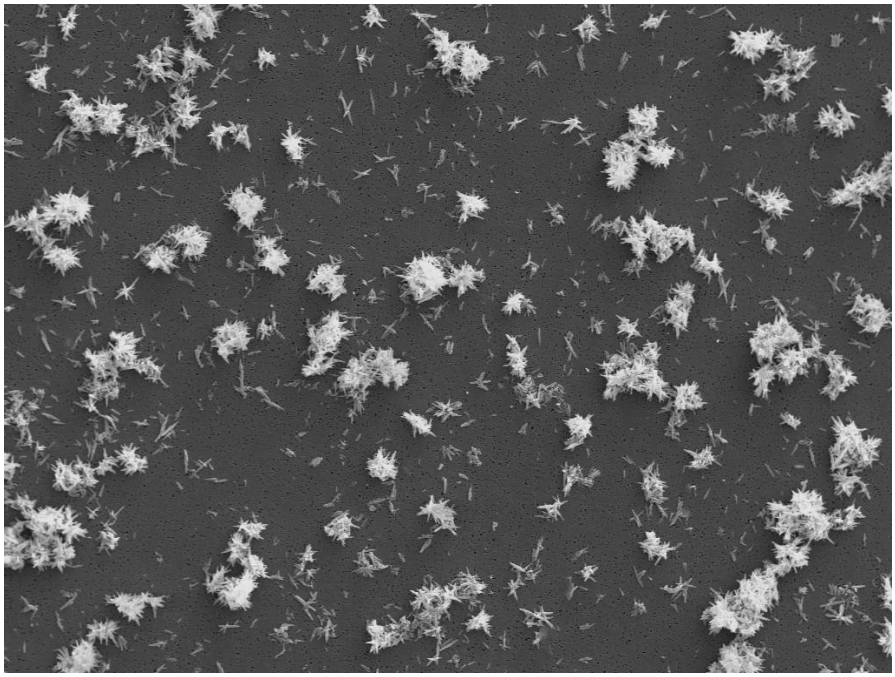

Figure 11. SEM image of clustered aragonite, 50 mg/l filtrated, ultrasound m03 10min, 1000x SE.

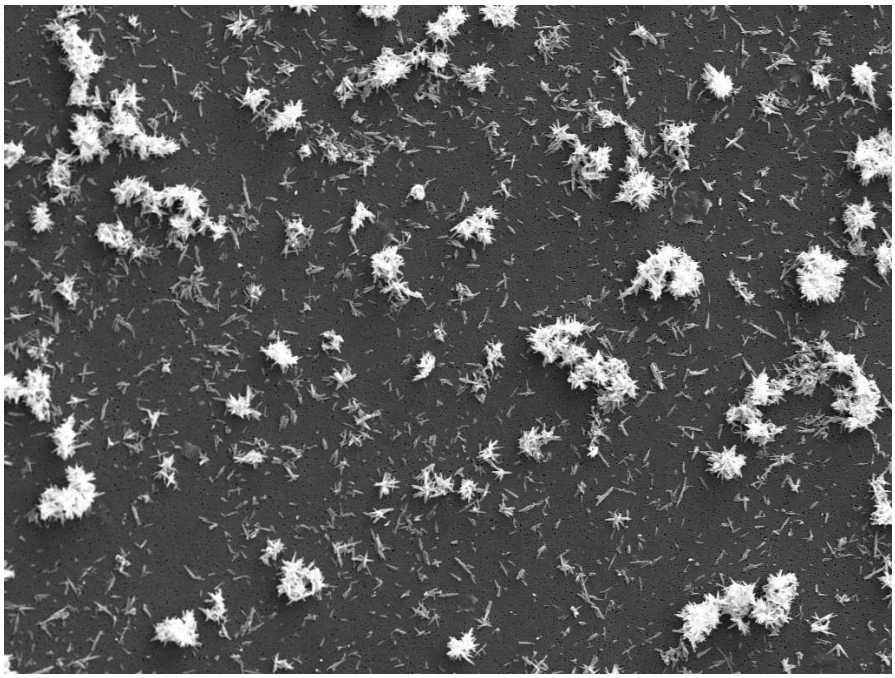

Figure 12. SEM image of clustered aragonite, 50 mg/l filtrated, ultrasound "old" 10min, 1000x SE.

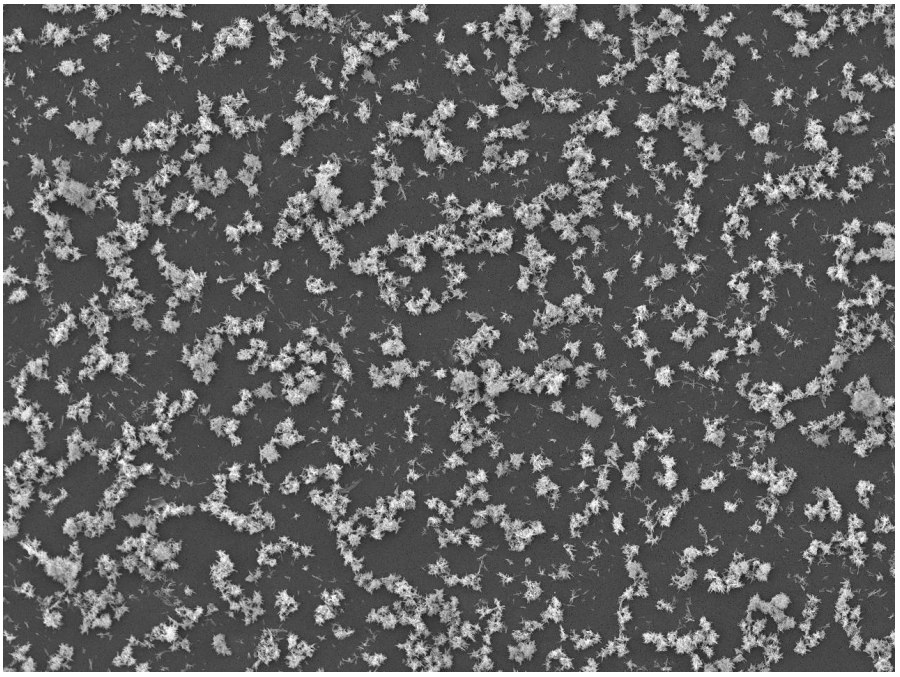

Figure 13. SEM image of clustered aragonite, 100 mg/l filtrated, no ultrasound, 500x SE.

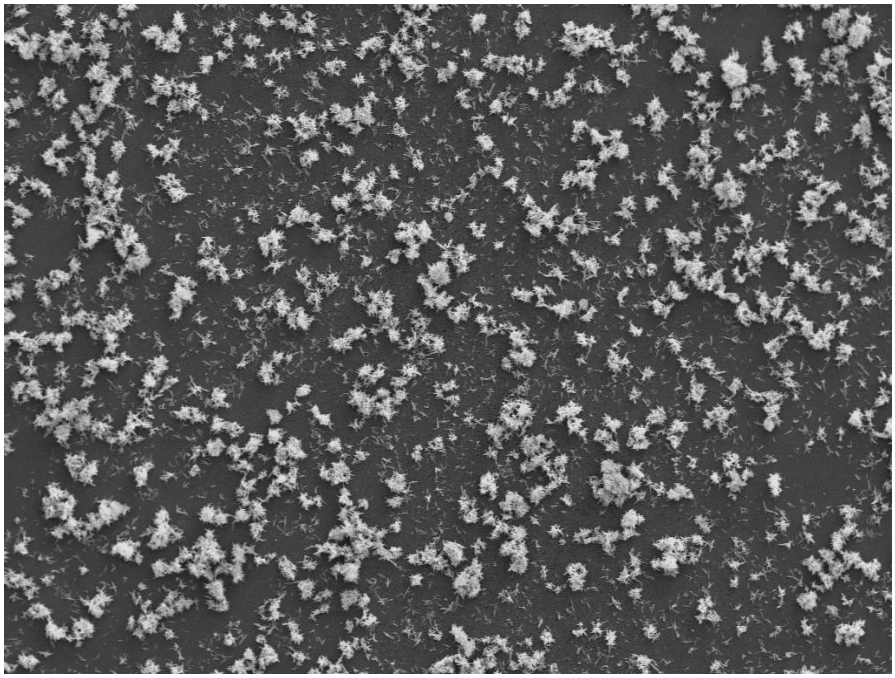

Figure 14. SEM image of clustered aragonite, 100 mg/l filtrated, ultrasound m03 10min, 500x SE.

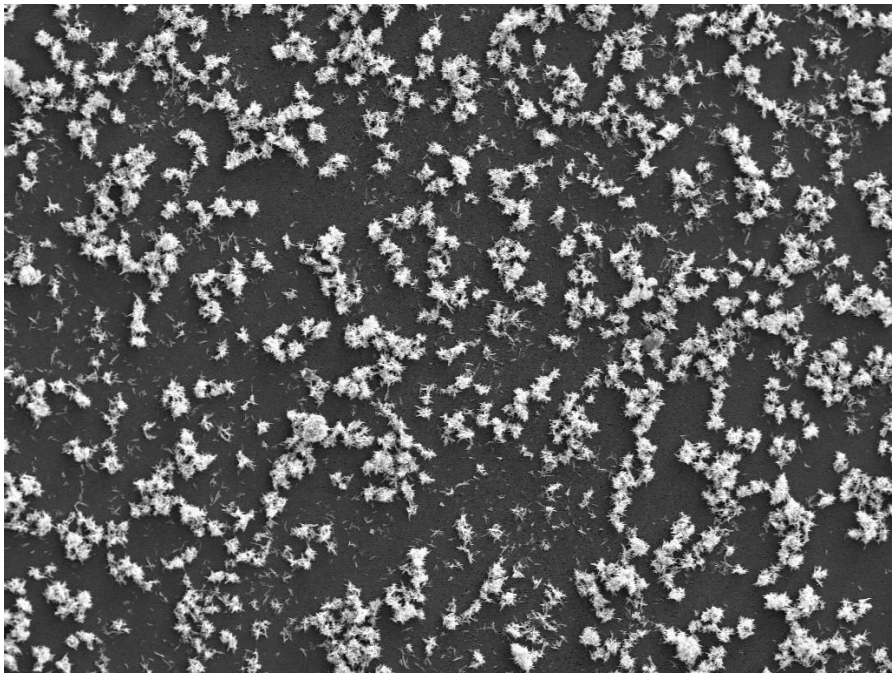

Figure 15. SEM image of clustered aragonite, 100 mg/l filtrated, ultrasound "old" 10min, 500x SE.

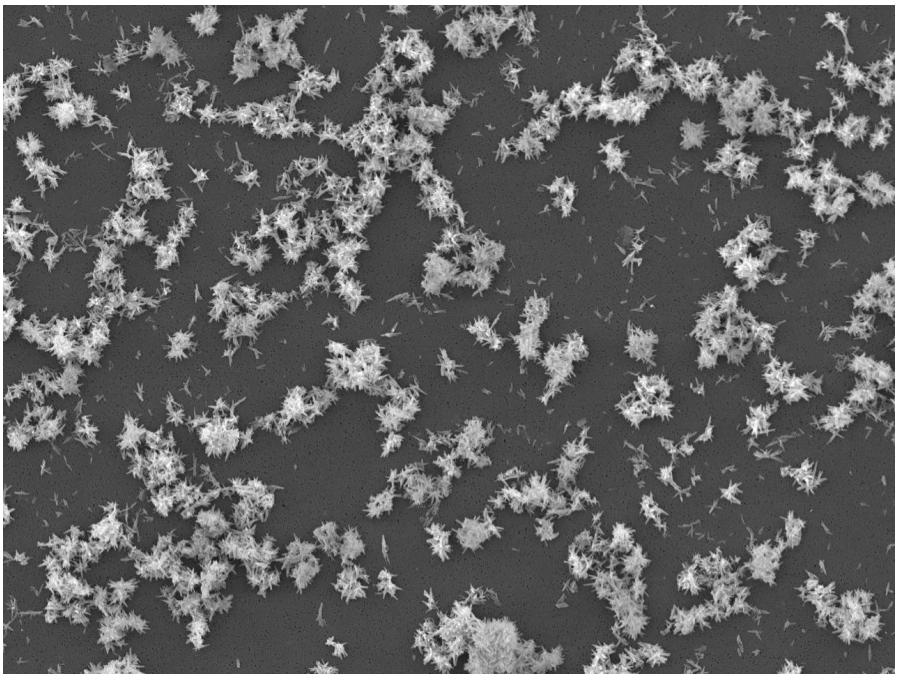

Figure 16. SEM image of clustered aragonite, 100 mg/l filtrated, no ultrasound, 1000x SE.

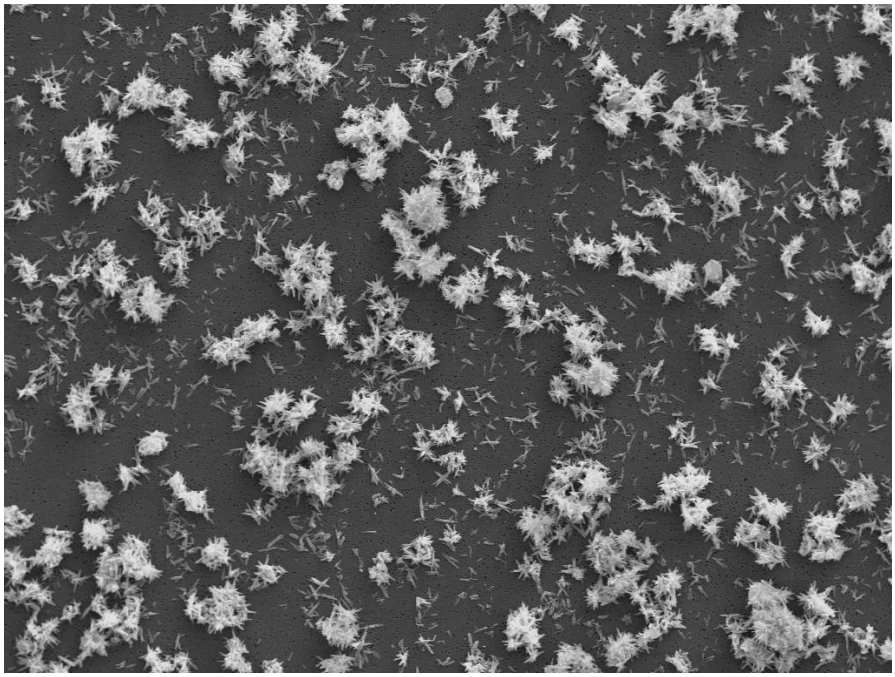

Figure 17. SEM image of clustered aragonite, 100 mg/l filtrated, ultrasound m03 10min, 1000x SE.

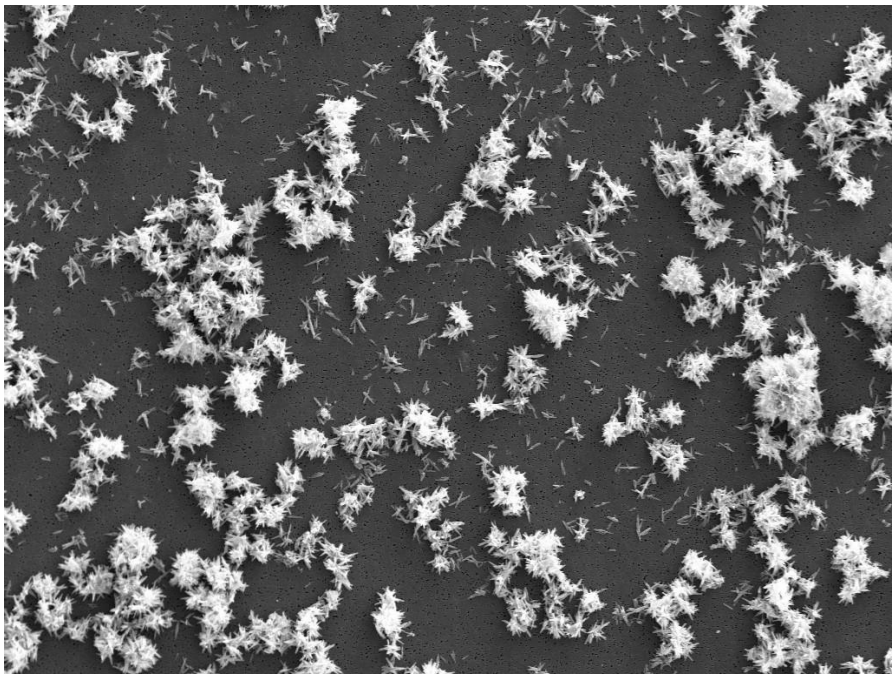

Figure 18. SEM image of clustered aragonite, 100 mg/l filtrated, ultrasound "old" 10min, 1000x SE.

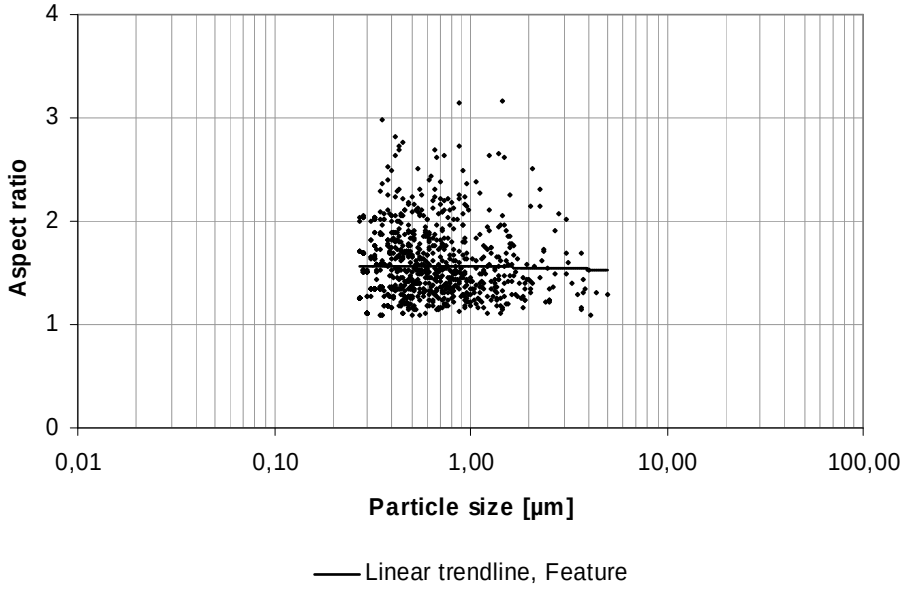

Figure 1. The correlation between aspect ratio and particle size of kaolin 1 particles.

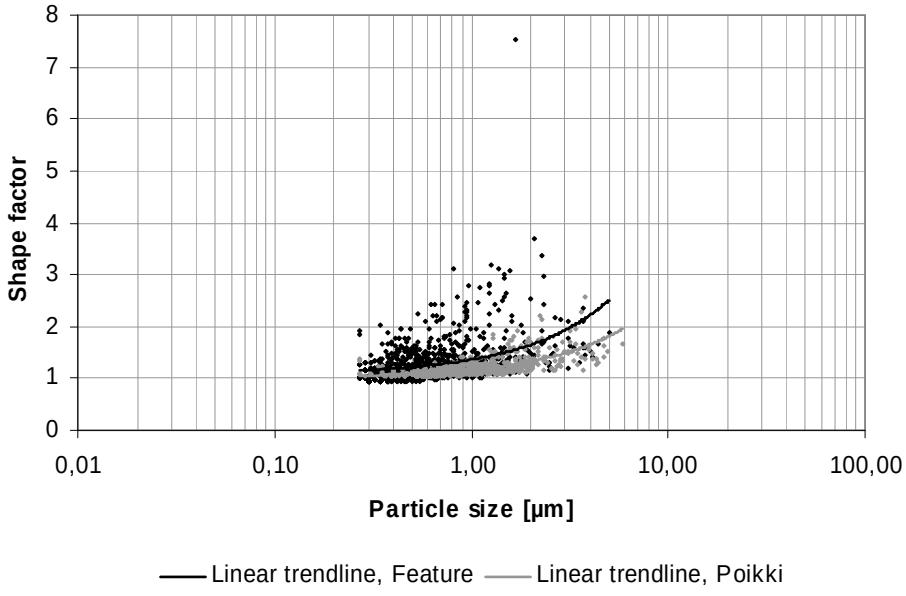

Figure 2. The correlation between shape factor and particle size of kaolin 1 particles.

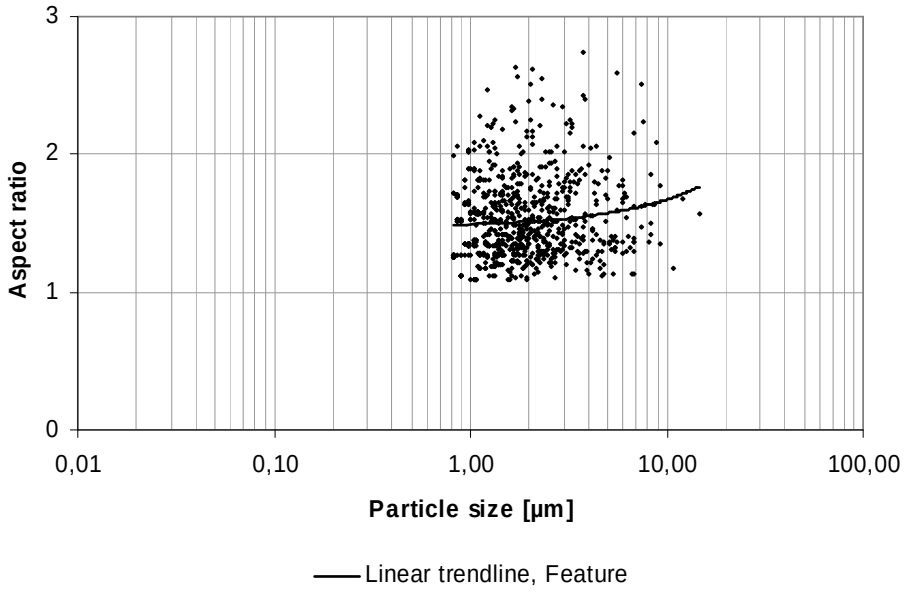

Figure 3. The correlation between aspect ratio and particle size of kaolin 2 particles.

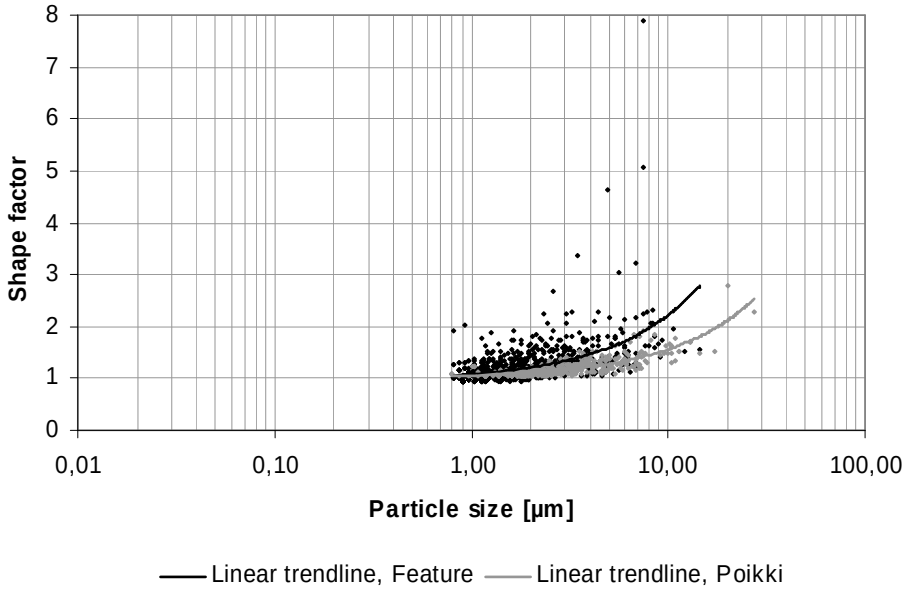

Figure 4. The correlation between shape factor and particle size of kaolin 2 particles.

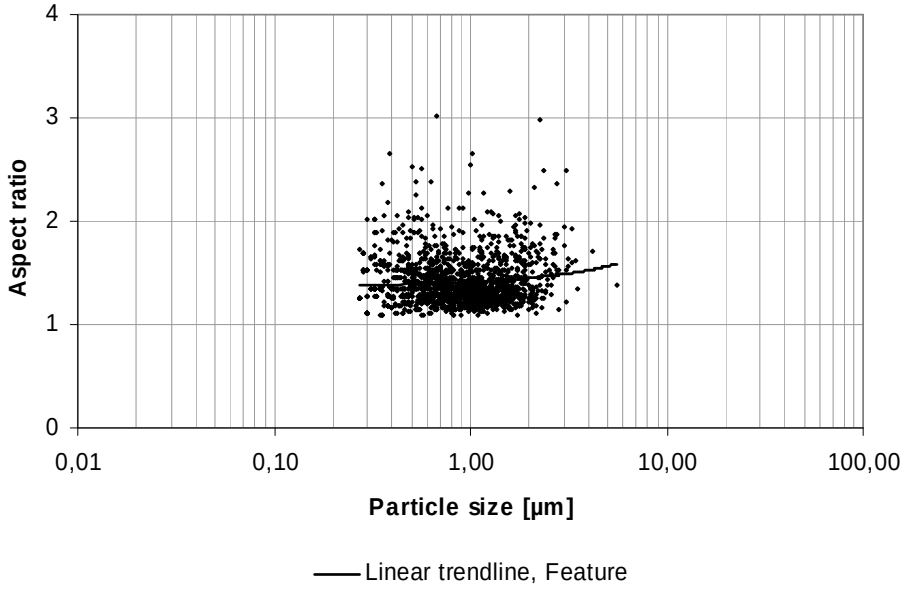

Figure 5. The correlation between aspect ratio and particle size of cubic PCC particles.

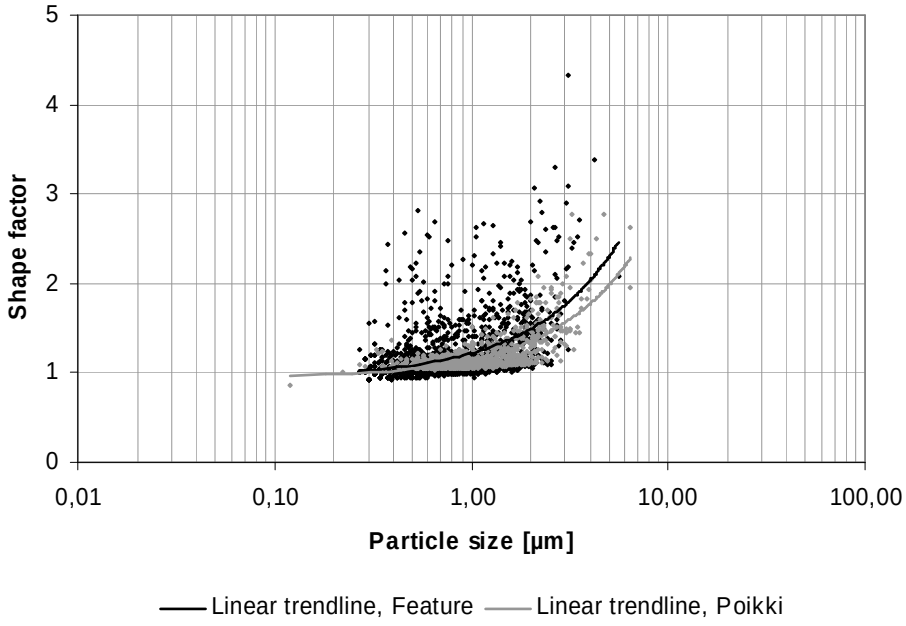

Figure 6. The correlation between shape factor and particle size of cubic PCC particles.

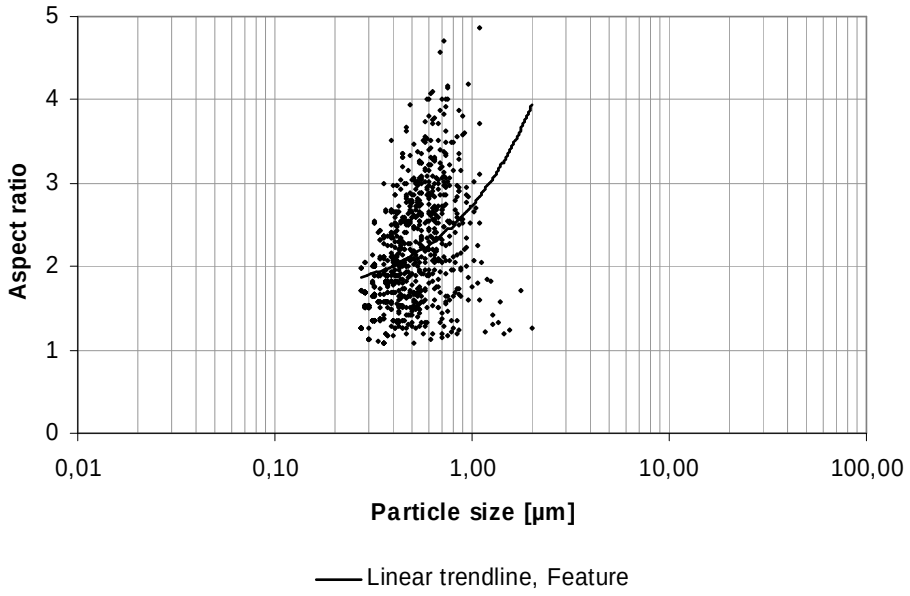

Figure 7. The correlation between aspect ratio and particle size of aragonite particles.

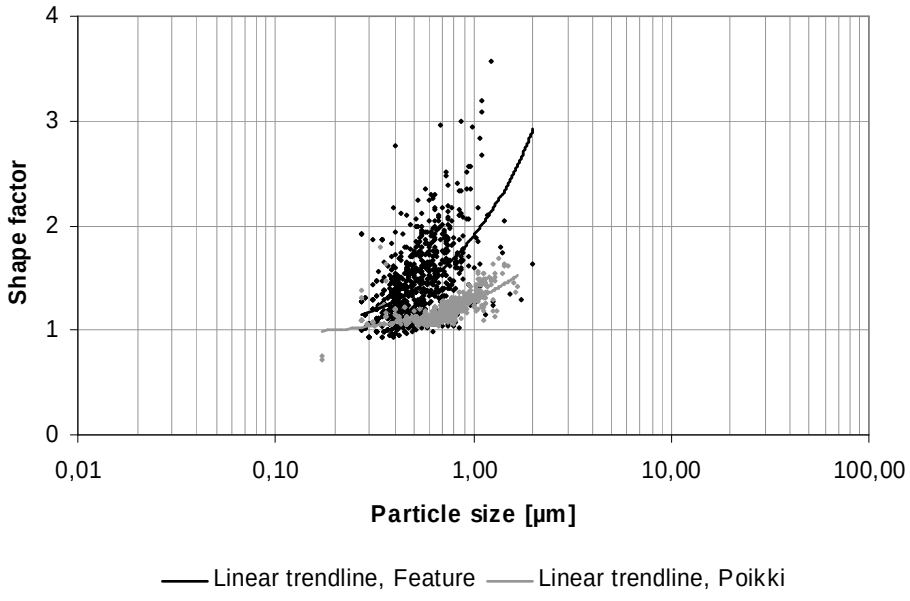

Figure 8. The correlation between shape factor and particle size of aragonite particles.

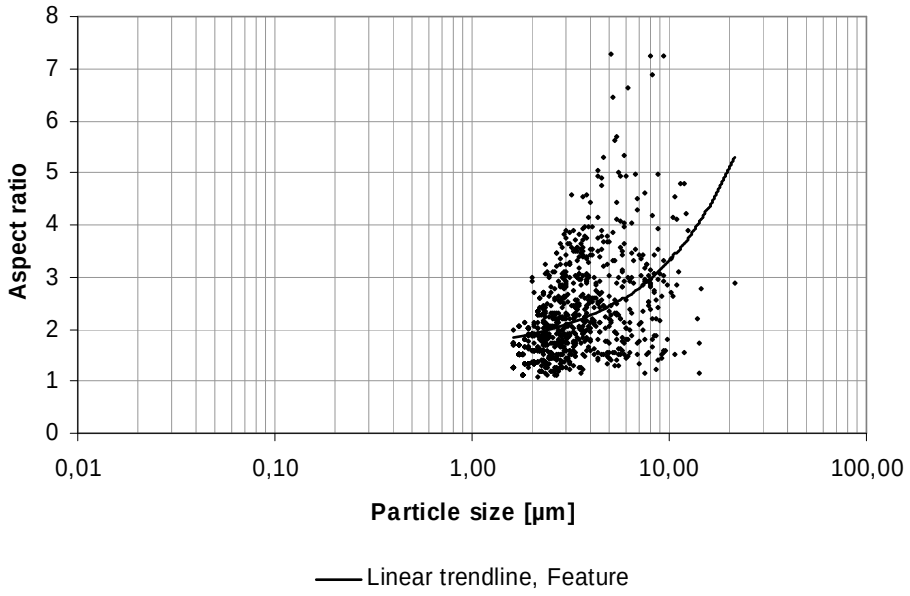

Figure 9. The correlation between aspect ratio and particle size of wollastonite particles.

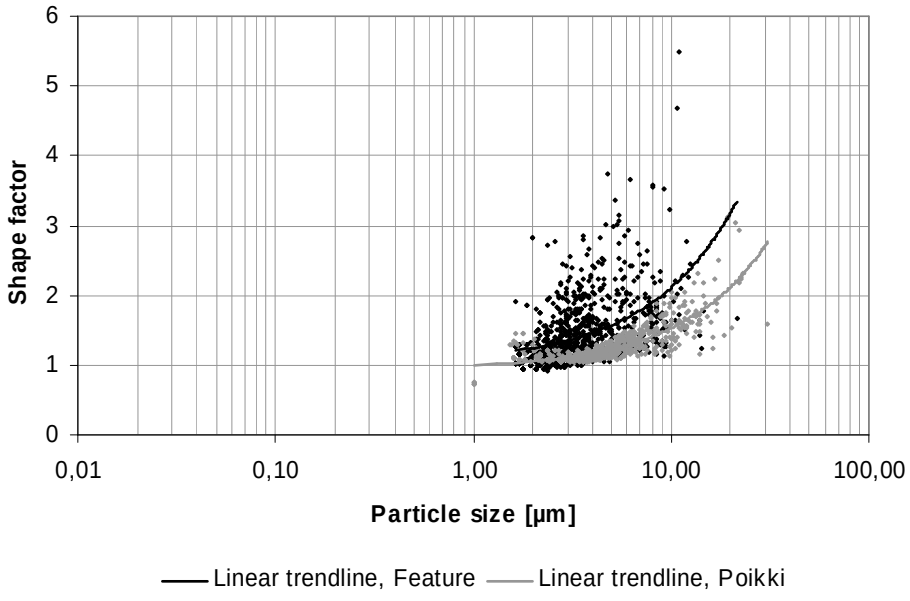

Figure 10. The correlation between shape factor and particle size of wollastonite particles.

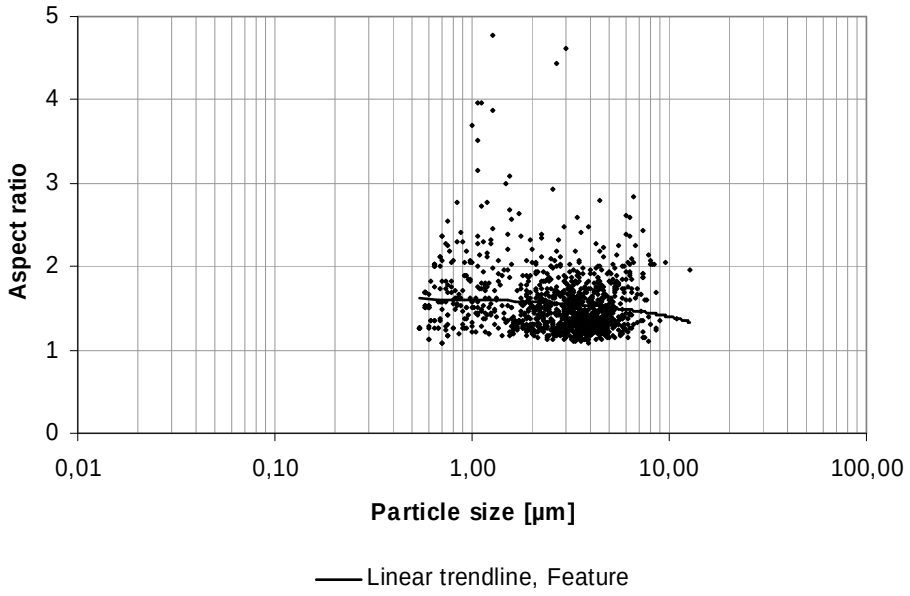

Figure 11. The correlation between aspect ratio and particle size of clustered aragonite particles.

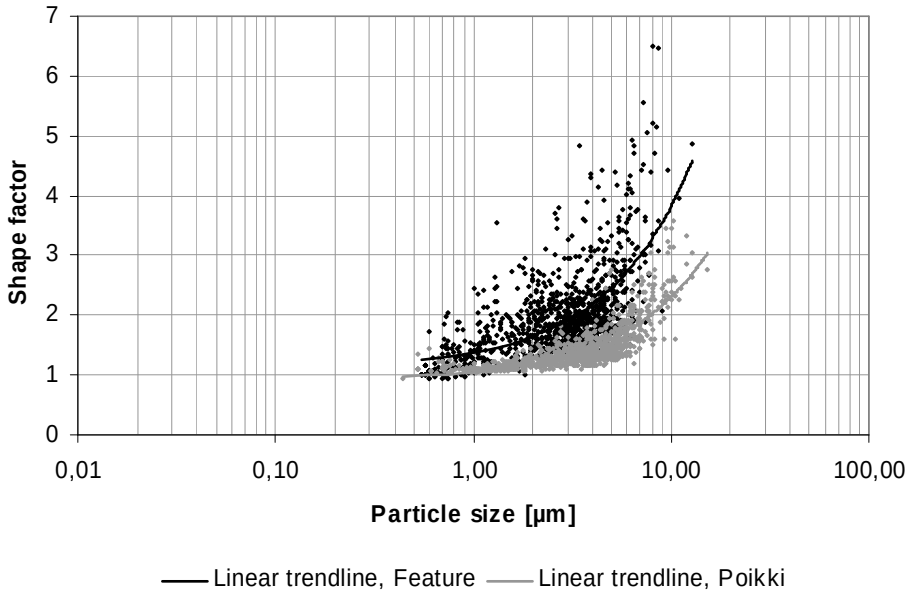

Figure 12. The correlation between shape factor and particle size of clustered aragonite particles.

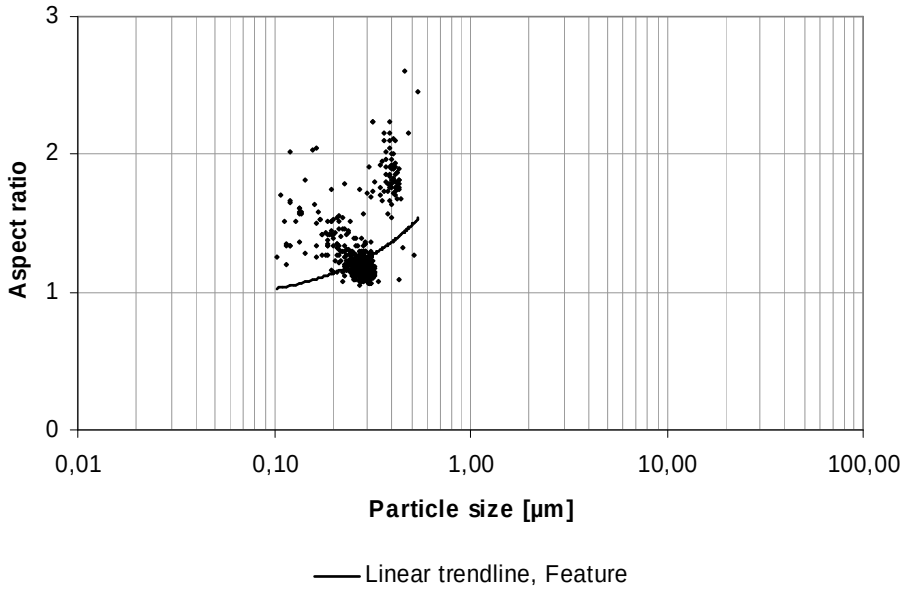

Figure 13. The correlation between aspect ratio and particle size of plastic 2 particles.

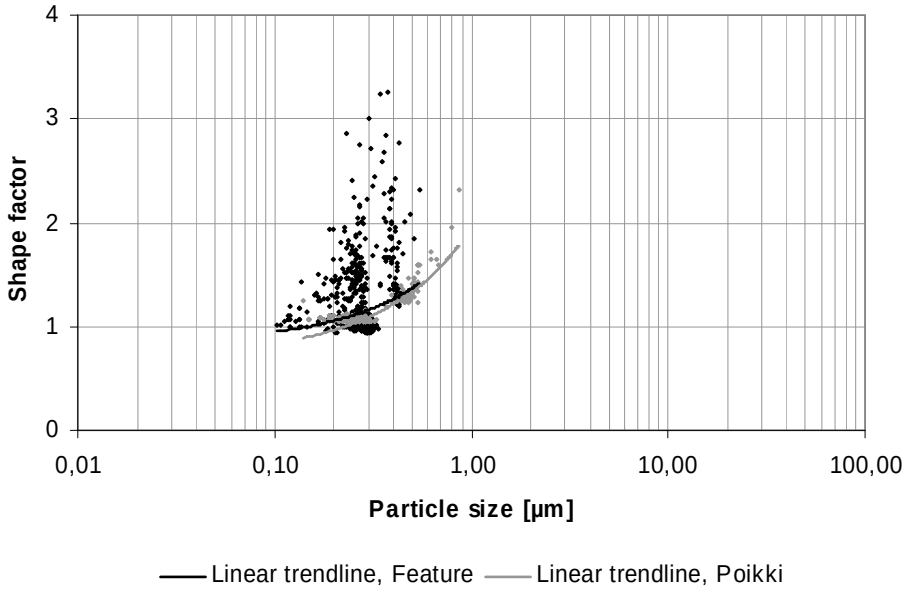

Figure 14. The correlation between shape factor and particle size of plastic 2 particles.

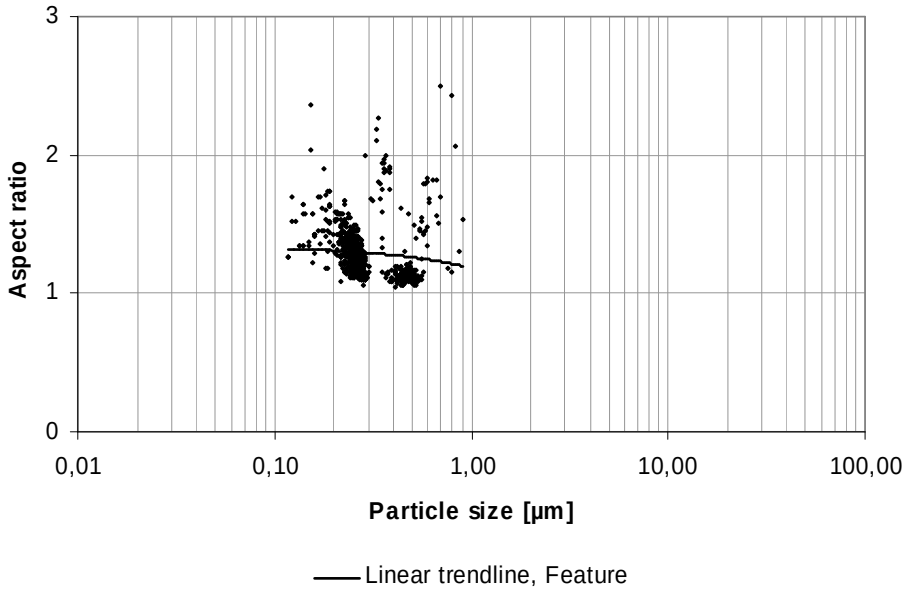

Figure 15. The correlation between aspect ratio and particle size of plastic blend particles.

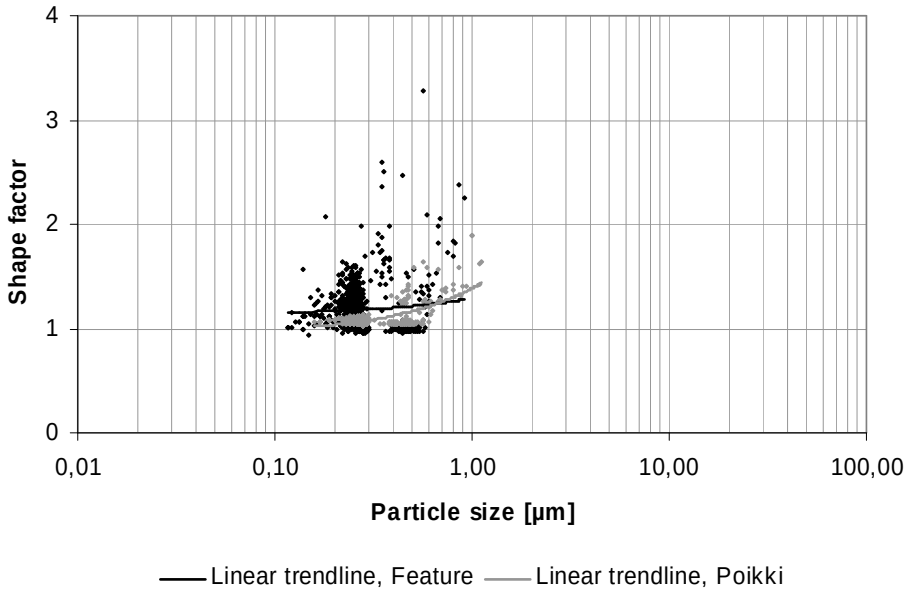

Figure 16. The correlation between shape factor and particle size of plastic blend particles.

DETERMINATION OF PARTICLE SIZE AND SHAPE BY IMAGE ANALYSIS

1
Suitability of the method

Method is suitable for determination of particle properties of both coating and filler pigments. The only limitation is particle size; sample preparation is difficult if particle size is too small (<100 nm). Particles have to be one by one in scanning electron microscope images.

2
Definitions and abbreviations

SEM=Scanning Electron Microscope
EDS=Energy Dispersive X-ray Spectroscopy
SE=Secondary Electrons
BSE=Backscattered Electrons

3
Measurement principles

Pigment sample is prepared even by filtration or by air brush. Sample is imaged by SEM from which image is transferred on-line to INCA Feature image analysis program. Defined area of the sample is analysed by Feature and results are exported to Microsoft Excel for processing.

4
Reagents and materials

Pigment slurry, purified water and ethanol.

5
Laboratory hardware and equipments

Sample preparation: aspirator bottle, Millipore-filtration equipments, membrane filter (polycarbonate, pore size ≤ 0.2 µm), pipette, air brush. For sample coating: sputter coater or carbon evaporator.
Image analysis: SEM, INCA Feature-program, spreadsheet program.

6
Execution of work

The method can be divided into two parts: sample preparation and image analysis.

Sample preparation: Sample preparation starts by dilution of pigment slurry to needed concentration. Initial value can base on table I which shows different particle properties. Particle size (ECD) is measured by SediGraph.

Table I: Sample concentrations for different pigment types.

pigment	shape	ECD, [µm]	c, [mg/l]
kaolin	platy	0.60 µm	5
kaolin	platy	1.93 µm	5
PCC	cubic	1.70 µm	15
aragonite	needle	0.44 µm	7
clust. aragonite	irregular	1.61 µm	150*
wollastonite	stick/needle	4.80 µm	15
plastic	sphere	0.26 µm	1
plastic	sphere	0.45 µm	3

* Preparation by air brush (concentration about ten times as high as in filtration)

Three parallel samples in different concentrations are needed if pigment is unknown (one above and one below of initial value). Optimal concentration can be found only by visualisation with SEM.

Diluted sample solutions are filtrated onto the membrane filter by Millipore filtration equipments. Sample volume is 5 ml in filtration. Preparation by air brush is made from 20 cm distance when vacuum is on. Sample volume in spraying is 0.5 ml and concentration is about ten times as high as the values in the table I. The maximum pore size of the filters is 0.2 µm; the smaller the better.

After the filter is dried, a small piece of it is cut onto the stub which is coated with carbon tape. Sample is coated with gold or gold-palladium-mixture if EDS is not needed. This enables the best image quality in SEM. If chemical classification is needed, sample has to be coated with carbon.

Image analysis: Before image analysis, sample has to be visualised to assure the number and location of particles. If particles are aggregated or the number of particles is too small, sample concentration or preparation technique has to be changed.

Image analysis requires sharp and stable image, so the set-ups of SEM have to be set carefully. Acceleration voltage can be 15 kV with all pigments but spot size and magnification depend on particle size. Magnification affects to the number of particles in one image and to the accuracy on details. If particles are clustered and exact shape is needed, magnification can be few thousands. This increases the number of required images. Used detector (SE or BSE) depends on pigment material and it does not affect to execution of image analysis.

Recommended type of analysing area is ”line” which is defined by two points; start and end. Points can be chosen by moving the sample with controllers of SEM. These two points have to be chosen so that any empty area did not include in analysing area. When the sample is moved, the number of images and also the number of particles can be estimated. Total number of particles should be 1500 at minimum.

The most critical detection set-ups are "First Pass Image" and "Second Pass Image" which should be 10 µs (FPI) and 80 µs (SPI). Minimum particle size can be limited to 6-10 pixels. This reduces the interference from filter pores. Needed filter in grey image processing is ”median” and in binary image processing "erode", "dilate", "hole fill" and "remove edge touching". Filters can be also deleted and increased if needed.

The most critical operation of the whole image analysis is thresholding. Different grey tones are separated from filtered (median) grey image. Threshold should be set so that details are sharp but image does not include interference. Success of thresholding depends significantly on the set-ups of SEM, especially on brightness and contrast.

When optimal threshold value is found, measurement can be started. After the each pigment is measured, results can be investigated and exported to Microsoft Excel. Needed particle size distributions and statistical parameters can be defined easier in Excel.

7
Calculating and reporting of results

Results are exported from INCA Feature to Microsoft Excel.

8
References and literature

Further information about image analysis in pigment particle characterisation is presented in Master's Thesis "Characterisation of pigment particles by scanning electron microscope and image analysis programs" (Mikko Linnala, Lappeenranta University of Technology, 2008).